REFERENCE ONLY

UNIVERSITY OF LONDON THESIS

Degree	Year	Name of Author
PhD	2006	BINIONS, R.

COPYRIGHT

This is a thesis accepted for a Higher Degree of the University of London. It is an unpublished typescript and the copyright is held by the author. All persons consulting the thesis must read and abide by the Copyright Declaration below.

COPYRIGHT DECLARATION

I recognise that the copyright of the above-described thesis rests with the author and that no quotation from it or information derived from it may be published without the prior written consent of the author.

LOAN

Theses may not be lent to individuals, but the University Library may lend a copy to approved libraries within the United Kingdom, for consultation solely on the premises of those libraries. Application should be made to: The Theses Section, University of London Library, Senate House, Malet Street, London WC1E 7HU.

REPRODUCTON

University of London theses may not be reproduced without explicit written permission from the University of London Library. Enquiries should be addressed to the Theses Section of the Library. Regulations concerning reproduction vary according to the date of acceptance of the thesis and are listed below as guidelines.

A. Before 1962. Permission granted only upon the prior written consent of the author. (The University Library will provide addresses where possible).

B. 1962 - 1974. In many cases the author has agreed to permit copying upon completion of a Copyright Declaration.

C. 1975 - 1988. Most theses may be copied upon completion of a Copyright Declaration.

D. 1989 onwards. Most theses may be copied.

This thesis comes within category D.

☑ This copy has been deposited in the Library of UCL

☐ This copy has been deposited in the University of London Library, Senate House, Malet Street, London WC1E 7HU.

P:\Office\Standard forms\Copyright - thesis.doc

CHEMICAL VAPOUR DEPOSITION OF METAL OXIDES AND PHOSPHIDES

by

Russell Binions

A thesis submitted to the University of London in partial fulfilment of the requirements for the degree of Doctor of Philosophy

University College London

2005

UMI Number: U591853

All rights reserved

INFORMATION TO ALL USERS
The quality of this reproduction is dependent upon the quality of the copy submitted.

In the unlikely event that the author did not send a complete manuscript
and there are missing pages, these will be noted. Also, if material had to be removed,
a note will indicate the deletion.

UMI U591853
Published by ProQuest LLC 2013. Copyright in the Dissertation held by the Author.
Microform Edition © ProQuest LLC.
All rights reserved. This work is protected against
unauthorized copying under Title 17, United States Code.

ProQuest LLC
789 East Eisenhower Parkway
P.O. Box 1346
Ann Arbor, MI 48106-1346

Most scientists tend to understand little more *about* science than fish about hydrodynamics.

Imre Lakatos [1]

Abstract.

This thesis investigates the deposition of thin films of main group metal phosphide and main group metal oxide compounds on glass substrates by the use of dual source atmospheric pressure chemical vapour deposition. Binary phosphide systems with tin, germanium, silicon, antimony, copper or boron have been examined. Binary oxide systems of gallium, antimony, tin or niobium have also been investigated. Additionally these systems were deposited on gas sensor substrates and evaluated as metal oxide semiconductor gas sensors. Halides were used as the metal precursor, R_xPH_{3-x} (R = Cyc^{hex} or Phenyl) were used as phosphorous precursors and either methanol or ethyl acetate were used as oxygen precursors. These coatings showed good uniformity and coverage and the films were adherent passing the Scotch tape test. The tin phosphide films were opaque in appearance with some signs of birefringence due to differential thickness effects. Germanium phosphide and the gallium, antimony, niobium and tin oxide systems were all transparent, once again birefringence was observed. The films produced from the antimony phosphide and silicon phosphide systems were opaque, grey and metallic. Additional work was conducted on the deposition on a variety of alkali metal and alkaline earth metal fluorides on glass substrates using aerosol assisted chemical vapour deposition. In all cases the films were very powdery and were easily wiped off of the substrate. A number of depositions were carried out combining the aerosol and atmospheric pressure methodologies. A tin oxide film was produced from the atmospheric pressure chemical vapour deposition reaction of tin tetrachloride and ethyl acetate. The film contained tungsten, which was introduced into the reaction using a polyoxometalate delivered via aerosol assisted chemical vapour deposition.

Films were analysed using Raman microscopy, X-ray diffraction, scanning electron microscopy, energy dispersive analysis of X-rays, electron probe microanalysis, X-ray photoelectron spectroscopy and ultra violet and visible spectroscopy.

Acknowledgments.

First and foremost I would like to thank my supervisors Prof. Ivan Parkin and Dr. Claire Carmalt; not least because without them putting some faith in me right at the start, this work may never have occurred. I would also like to thank Pilkington glass for the provision of a CASE award and in particular the online coatings group who have always been available for informative and interesting discussion. The CVD apparatus was built and maintained courtesy of Mr. David Knapp, Mr. David Morphett and Mr. Joe Nolan.

Many people helped with film analysis notably; Mr. Rob Palgrave, Mr Shane O'Neill and Miss Emily Peters for conducting XPS experiments at various times. Mr. Kevin Reeves is thanked for help with all things electron microscope related, Dr Steve Firth for assistance with Raman spectroscopy. Dr. Keith Pratt, Dr. Graham Shaw, Mr Simon Nesbitt and Mr. Dominic Mann are thanked for help with setting up, running and understanding gas-sensing experiments.

I would also like to thank everyone whom I have meet in room 310 over the last few years, your influence cannot be underestimated, special mentions must go to Miss Sobia Ashraf for the seemingly endless supply of tea and Dr. Christopher Blackman for all the assistance and advice during the course of this work.

Contents.

Page

Abstract. 2

Acknowledgements. 4

Contents. 5

List of figures, tables and equations. 10

List of Abbreviations. 16

Chapter 1 - Introduction. 17

1.1 Aim and purpose. 17

1.2 Electronic considerations. 17

1.2.1 Band theory. 17

1.2.2 Charge carriers in semiconductors. 21

1.2.3 Semiconductors. 21

1.2.4 Compound semiconductors. 23

1.2.5 Direct and indirect semiconductors. 24

1.3 Film deposition. 25

1.3.1 Physical vapour deposition. 25

1.3.1.1 Evaporation and sublimation. 25

1.3.1.2 Molecular beam Epitaxy. 25

1.3.1.3 Sputtering. 26

1.3.2 Chemical vapour deposition. 26

1.3.3 The CVD process. 27

1.3.3.1 Kinetics – mass transport. 30

1.3.3.2 Thermodynamics – heat transport. 32

1.3.3.3 Film growth. 33

1.3.3.4 Precursors. 34

1.3.4 Types of CVD. 36

1.3.4.1 Photo assisted CVD. 36

1.3.4.2 Plasma enhanced CVD. 36

1.3.4.3 Aerosol assisted CVD. 37

1.3.5 Applications of CVD. 37

1.4 Gas sensing. 38

1.4.1 Metal oxide semiconductor gas sensors. 38

Chapter 2 – Experimental. 40

2.1 Atmospheric pressure chemical vapour deposition. 40

2.2 Aerosol assisted chemical vapour deposition. 44

2.3 Analysis. 46

2.3.1 X-Ray diffraction. 46

2.3.2 Raman spectroscopy. 46

2.3.3 Energy dispersive X-ray analysis. 46

2.3.4 Scanning electron microscopy. 47

2.3.5 X-Ray photoelectron spectroscopy. 47

2.3.6 Transmittance / Reflectance Spectroscopy. 48

2.3.7 Adhesion tests. 48

2.3.8 Ultraviolet / visible spectroscopy. 48

2.4 Gas sensing. 48

Chapter 3 – Main group metal phosphides. 50

3.1 Introduction. 50

3.1.1 Tin Phosphide. 52

3.1.2 Germanium phosphide. 52

3.1.3 Copper phosphide. 53

3.1.4 Silicon phosphide. 53

3.1.5 Antimony phosphide. 53

3.1.6 Boron phosphide. 54

3.2 Experimental details. 54

3.3 Results and discussion. 55

3.3.1 Tin phosphide and germanium phosphide. 55

3.3.1.1 Tin phosphide and germanium phosphide results. 55

3.3.1.2 Discussion. 67

3.3.2 Copper phosphide. 70

3.3.2.1 Copper phosphide results. 70

3.3.2.2 Discussion. 75

3.3.3 Silicon phosphide. 77

3.3.3.1 Silicon phosphide results and discussion. 77

3.3.3.2 Summary. 82

3.3.4 Antimony phosphide. 83

3.3.4.1 Antimony phosphide results. 83

3.3.4.2 Discussion. 87

3.3.5 Boron phosphide. 87

3.4 Conclusions. 88

Chapter 4 – Main group metal oxides. 90

4.1 Introduction. 90

4.1.1 Gallium oxide. 90

4.1.2 Tin oxide. 91

4.1.3 Antimony oxide. 91

4.1.4 Niobium oxide. 92

4.2 Results. 93

4.3 Discussion. 107

4.4 Conclusion. 110

Chapter 5 – Gas sensing. 111

5.1 Introduction. 111

5.1.1 Gallium oxide. 112

5.1.2 Antimony oxide. 112

5.1.3 Niobium oxide. 113

5.1.4 Tin oxide. 113

5.2 Results. 113

5.2.1 Gallium oxide. 114

5.2.2 Antimony oxide. 119

5.2.3 Niobium oxide. 122

5.2.4 Tin oxide. 125

5.3 Discussion. 128

5.4 Conclusion. 133

Chapter 6 – Aerosol assisted chemical vapour deposition. 134

6.1 Introduction. 134

6.2 Results. 135

6.3 Discussion. 139

6.4 Conclusion. 141

Chapter 7 - AACVD + APCVD. 142

7.1 Results and discussion. 143

7.2 Conclusion. 148

Chapter 8 – Conclusions. 149

8.1 Overall conclusions. 149

8.2 Future work. 153

Bibliography. 154

References. 156

List of Figures, Tables and Equations.

		Page
Chapter 1 - Introduction.		17
Figure 1.1	Orbital diagram schematically showing the derivation of band theory *via* cumulative addition of atomic/molecular orbitals.	18
Figure 1.2	Density of states representation of a half filled band.	19
Figure 1.3	Density of states diagrams illustrating the differences between a semimetal, semiconductor and insulator.	20
Equation 1.1	The Boltzman distribution formula.	20
Figure 1.4	Intrinsic and extrinsic semiconductors.	23
Figure 1.5	Direct and indirect semiconductors.	24
Figure 1.6	Conformal and non-conformal film growth.	28
Figure 1.7	The processes in CVD.	29
Figure 1.8	The three main types of film growth.	29
Equation 1.2	Flux.	30
Equation 1.3	The Reynolds number.	31
Equation 1.4	Growth rate.	33
Figure 1.9	Structure of titanium isoproproxide.	35
Equation 1.5	Example of a dual source CVD reaction.	35
Chapter 2 - Experimental.		40
Figure 2.1	Schematic of an APCVD rig.	40
Figure 2.2	Schematic of a CVD reaction chamber.	41
Figure 2.3	Photograph of an APCVD rig.	42

Figure 2.4 Schematic of a bubbler. 42

Figure 2.5 Schematic of an AACVD rig. 45

Figure 2.6 Photograph of an AACVD rig. 45

Figure 2.7 SEM micrograph of a blank gas sensor substrate. 49

Chapter 3 – Main group metal phosphides. 50

Table 3.1 Table of reaction conditions and microanalytical results for the tin phosphide system. 56

Table 3.2 Table of reaction conditions and microanalytical results for the germanium phosphide system. 57

Figure 3.1 Raman pattern of a tin phosphide thin film. 59

Figure 3.2 Raman pattern of a germanium phosphide thin film. 59

Figure 3.3 EDXA area maps of a sample of tin phosphide. 60

Figure 3.4 SEM images of tin phosphide and germanium phosphide. 61

Figure 3.5 SEM images of tin phosphide films made with various precursors. 62

Figure 3.6 The vapour – liquid – solid growth mechanism. 62

Figure 3.7 SEM image of a very thin film of germanium phosphide. 63

Figure 3.8 Transmission and reflectance data for thin films of tin phosphide and germanium phosphide. 64

Figure 3.9 XPS peaks for a tin phosphide sample. 65

Figure 3.10 XPS peaks for a germanium phosphide sample. 67

Table 3.3 Table of reaction conditions and microanalytical results for the copper phosphide system. 71

Figure 3.11 SEM images of copper phosphide samples. 72

Figure 3.12 XPS peaks for a copper phosphide sample. 74

Figure 3.13 XRD pattern of Cu_3P. 75

Table 3.4 Table of reaction conditions and microanalytical results for the silicon phosphide system. 78

Figure 3.14 SEM image of a silicon phosphide sample. 79

Figure 3.15 XPS peaks for a silicon phosphide sample. 81

Figure 3.16 XRD of a silicon phosphide sample. 82

Table 3.5 Table of reaction conditions and microanalytical results for the antimony phosphide system. 84

Figure 3.17 SEM image of an antimony (phosphide?) sample. 85

Figure 3.18 XRD pattern of antimony metal. 86

Figure 3.19 XPS peaks for a sample of antimony phosphide. 86

Table 3.6 Table of reaction conditions and microanalytical results for the boron phosphide system. 88

Chapter 4 – Main group metal oxides. 90

Table 4.1 Table of reaction conditions and microanalytical results for the gallium oxide system. 93

Table 4.2 Table of reaction conditions and microanalytical results for the tin oxide system. 94

Table 4.3 Table of reaction conditions and microanalytical results for the niobium oxide system. 95

Table 4.4 Table of reaction conditions and microanalytical results for the antimony oxide system. 96

Figure 4.1 SEM images of various metal oxide thin films. 98

Figure 4.2 Raman pattern of a tin oxide sample. 99

Figure 4.3 XPS peaks for a sample of gallium oxide. 100

Figure 4.4 XPS peaks for a sample of tin oxide. 101

Figure 4.5 XPS peaks for a sample of antimony oxide. 102

Figure 4.6 XPS peaks for a sample of niobium oxide. 103

Figure 4.7 Transmission and reflectance data of metal oxide thin films. 104

Figure 4.8 Tauc plots of gallium oxide and tin oxide thin films. 105

Figure 4.9 XRD of a tin oxide sample. 106

Chapter 5 – Gas sensing. 111

Figure 5.1 Gas response of a CVD produced gallium oxide sensor. 115

Table 5.1 Gas responses of gallium oxide sensors. 116

Figure 5.2 Gas response of a screen-printed gallium oxide sensor. 117

Figure 5.3 The effect of humidity on the gas response of a CVD produced gallium oxide sensor. 118

Figure 5.4 Gas response of a CVD produced antimony oxide sensor. 119

Table 5.2 Gas responses of antimony oxide sensors. 120

Figure 5.5 Gas response of a screen-printed antimony oxide sensor. 121

Figure 5.6 The effect of humidity on the gas response of a CVD produced antimony oxide sensor. 121

Figure 5.7 Gas response of a CVD produced niobium oxide sensor. 122

Table 5.3 Gas responses of niobium oxide sensors. 123

Figure 5.8 Gas response of a screen-printed niobium oxide sensor. 124

Figure 5.9 The effect of humidity on the gas response of a screen-print produced niobium oxide sensor. 125

Figure 5.10 Gas response of a CVD produced tin oxide sensor. 126

Figure 5.11 Gas response of a screen-printed tin oxide sensor. 126

Table 5.4 Gas responses of tin oxide sensors. 127

Figure 5.12 The effect of humidity on the gas response of a CVD produced tin oxide sensor. 128

Figure 5.13 SEM images of CVD produced metal oxide sensors. 129

Figure 5.14 SEM images of screen-print produced metal oxide sensors. 131

Chapter 6 – Aerosol assisted chemical vapour deposition. 134

Table 6.1 Table of reaction conditions for the sodium fluoride system. 136

Figure 6.1 SEM image of a sodium fluoride thin film. 137

Table 6.2 Table of optical properties and microanalytical results for metal fluoride thin films. 138

Figure 6.2 XRD of sodium fluoride. 138

Figure 6.3 XPS peaks for a sample of sodium fluoride. 140

Chapter 7 – AACVD + APCVD. 142

Figure 7.1 Experimental set up of combined AA/AP CVD system. 142

Figure 7.2 Structural representation of the anion of $[^{n}Bu_4N]_2[W_6O_{19}]$, $[W_6O_{19}]^{2-}$. 143

Table 7.1 Table of experimental conditions and microanalytical results for the combined AA/AP CVD system. 144

Figure 7.3 SEM image of a thin film produced using the combined AA/AP CVD methodology. 144

Figure 7.4 XRD pattern of a thin film produced using the combined AA/AP CVD methodology. 145

Figure 7.5 XPS peaks of tin, tungsten and oxygen for a thin film produced using the combined AA/AP methodology. 147

List of Abbreviations

CVD	Chemical vapour deposition.
APCVD	Atmospheric pressure chemical vapour deposition.
AACVD	Aerosol assisted chemical vapour deposition.
PACVD	Photo assisted chemical vapour deposition.
PECVD	Plasma enhanced chemical vapour deposition.
MOCVD	Metal organic chemical vapour deposition.
PVD	Physical vapour deposition
AA/AP CVD	Combined aerosol assisted and atmospheric pressure chemical vapour deposition.
EDXA	Energy dispersive X-ray analysis.
EPMA	Electron probe microanalysis.
SEM	Scanning electron microscopy.
XRD	X-ray diffraction.
XPS	X-ray photoelectron spectroscopy.
Vis	Visible.
UV	Ultra violet.
Re	Reynolds number.
Kn	Knudsen number.
T_c	Critical temperature.
E_f	Fermi energy.
$N_{(e)}$	Density of states.
E_g	Band gap energy.
^{n}Butyl	Normal butyl.

Chapter 1 - Introduction

1.1 Aim and Purpose

The aim of this work was to investigate the deposition of novel main group metal phosphide and oxide materials on a variety of different substrates (Chapters 3 & 4 respectively). As these materials are semiconductors it is important to have an understanding of semiconductor properties and what causes them. It also advantageous to have an understanding of chemical vapour deposition, related techniques and thin film deposition in general. Metal oxide semiconductors provide a resistance change with varying surrounding gas composition; this is the basis of metal oxide semiconductor gas sensors that are evaluated in chapter 5. In this chapter band theory, semiconductors, film deposition and simple gas sensing theory are discussed.

1.2 Electronic Considerations

1.2.1 Band Theory

As a consequence of quantum theory and the combination of atomic orbitals, molecules have discreet quantised energy levels called molecular orbitals. These molecular orbitals may be bonding, non-bonding or anti-bonding; they may or may not be occupied with electrons. In a solid many similar molecules are bought and packed together (Figure 1.1). As such the molecular orbitals combine and rather than producing an extensive degenerate energy level they produce a "band".

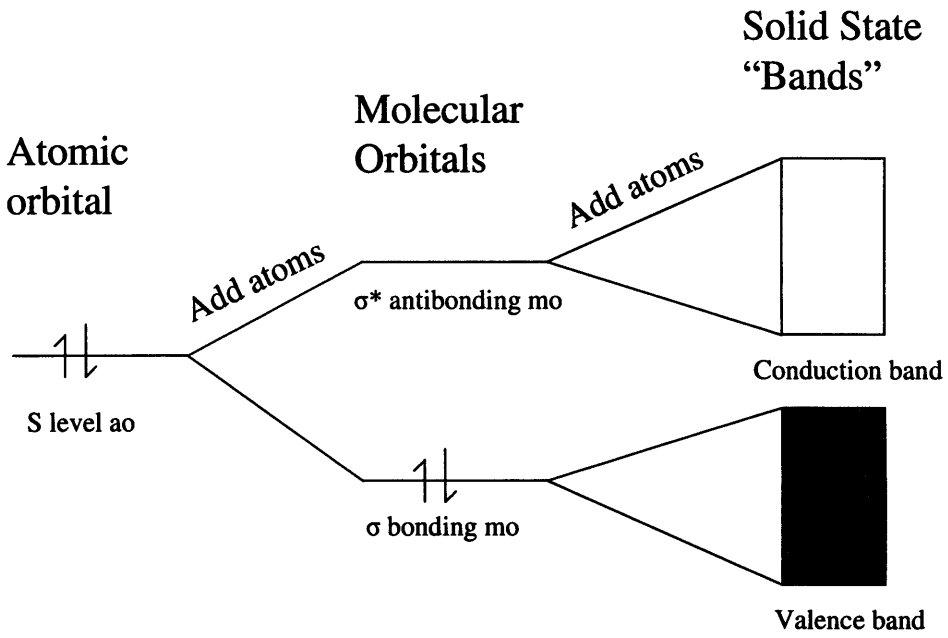

Figure 1.1. Orbital diagram schematically showing the derivation of band theory *via* cumulative addition of atomic/molecular orbitals.

This non-degeneracy is a consequence of the Pauli exclusion principle, which states that no two electrons may have the same set of quantum numbers associated with them.[2] Hence these molecular orbitals in a solid must all be slightly perturbed in order for the molecules to pack in a solid. As such a band is a collection of similar energy molecular orbitals, and the band structure of a material corresponds (broadly) to the molecular orbital energy levels of the constituent molecules. This can lead to filled or unfilled bands. The bands in some cases may overlap or be partially filled. The Pauli exclusion principle also governs the filling of bands, as each energy level can only contain two electrons and these must have opposing spin quantum numbers. Hence a band may contain 2N electrons where N is the number of energy levels in a band.

For example a metal such as lithium contains only one 2s electron. So the 2s band in lithium metal will contain only N electrons (one for every 2s level). Figure 1.2 shows the band picture for a metal where one energy level contains N electrons and is therefore half full. Other metals such as magnesium or calcium have filled s levels so we might expect them to be insulators as their electrons are immobile. However, the next energy level up, the p band, overlaps with the s band giving the effect of a partially filled band.

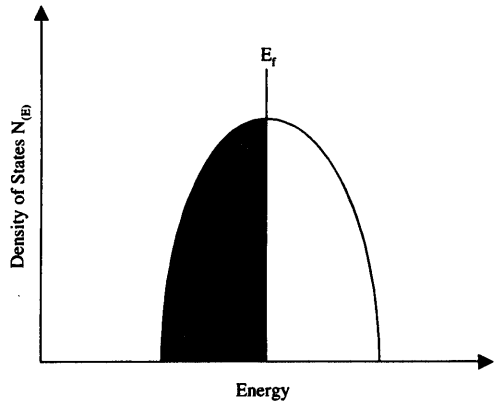

Figure 1.2. Density of states representation of a half filled band.

The highest filled energy level at absolute zero is known as the Fermi level; the energy of this level is called the Fermi energy and is denoted E_f. The definition of a metallic conductor is when E_f falls where $N_{(E)}$ (the density of states) is greater than zero. Superconductors are identical to metallic conductors with the exception that for a superconductor the resistance of the material is zero. Superconductivity is only observed at low temperatures (~10 – 80 K) and at temperatures above a critical temperature (T_c) this effect disappears and the material behaves like a metallic conductor. This happens because of lattice vibrations caused by elevated temperature. These lattice vibrations hinder the motion of electrons. This effect is observed in all

superconductors and the increase of resistivity with temperature is seen with all metallic conductors.

The same effect is not observed in semimetals, semiconductors or insulators (Figure 1.3) because E_f lies where $N_{(E)}$ is equal to zero. The effect of heating these systems is to reduce resistivity.

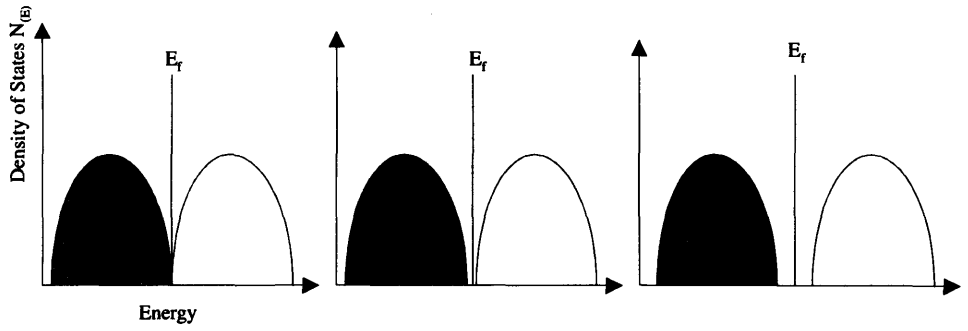

Figure 1.3. Density of states diagrams illustrating the differences between a semimetal, semiconductor and insulator.

The reason for this reduction is that thermal energy may allow the redistribution of electrons about the bands according to the Boltzman distribution law (Equation 1.1).

$$Nj = Ne^{-\beta\varepsilon i}/\Sigma e^{-\beta\varepsilon j}$$

Equation 1.1. The Boltzman distribution formula where N = number of states, β = 1/kT (k = Boltzman constant, T = thermodynamic temperature) and εi = the energy of state i.

So that the highest filled energy bands may be higher than E_f and some electronic conductivity will be allowed.

1.2.2 Charge Carriers in Semiconductors

In insulators and semiconductors at absolute zero the valence band is completely filled and the conduction band is completely empty. Neither full nor empty bands are able to carry any current so a semiconductor behaves like an insulator at absolute zero. In order for electron conduction to be possible, electrons have to be excited into the conduction band. This could be achieved by thermal excitation or doping the semiconductor material. Doping is achieved by replacing one of the atoms of the semiconductor with another atom, which has one or more electrons than the constituent atoms. This leads either to an excess of electrons or an absence of electrons in the valence band. An absence of an electron in the valence band is called a "hole". At absolute zero no hole states are observed since the valence band is fully occupied. Holes have corresponding properties to electrons. The effective mass of a hole is equal to the negative effective mass of an electron. The charge of a hole is the equal opposite of an electron; i.e. +e. The velocity of the hole is considered equal to the velocity of a mobile electron. In addition to this the energy of a hole is equal but opposite to that of an electron.

1.2.3 Semiconductors

If an electron is promoted from the valence band to the conduction band by light, thermal energy or similar, then it leaves a vacancy or hole behind. This hole has the appearance of behaving like a positron. Some interesting properties result from this, for example this hole may recombine with an electron re-entering the valence band leading to an emission of electromagnetic radiation or a phonon. The energy of this emission corresponds to the energy gap between the valence and conduction band. A

phonon is a mechanical vibration of energy hv, and related to sound waves in the same way that photons relate to electromagnetic radiation. The hole may also migrate through the semiconductor material. This may occur because the hole has properties like a positron but is in fact the absence of an electron. Electrons in the valence band will want to move towards this positive charge as an electron does so it creates a hole from where it came whilst filling where the hole was before. In this way holes migrate. Intrinsic conduction is when the number of holes is equal to the number of promoted electrons. In this case the Fermi level lies in the middle of the band gap. Pure silicon and germanium are such semiconductor materials.

Extra atoms such as impurities or atoms deliberately doped into the material can lead to an excess of electrons or holes. Semiconductors of this type are called extrinsic semiconductors. For example if silicon is doped with phosphorus, then there will be an excess of electrons as phosphorus has five valence shell electrons compared to silicon's four. This spare electron has to go into the conduction band. This type of semiconductor is denoted n-type because the majority charge carrier is negatively charged. The opposite is true if silicon is doped with an element such as gallium, which has only three valence shell electrons. In this case there will be a deficit of electrons and so there will be hole in the valence band. Holes are considered to be positive charge carriers hence this type of semiconductor is denoted p-type.

The addition of dopants also leads to donor or acceptor levels being introduced into the band picture of the material (Figure 1.4). This occurs because dopants have different molecular orbitals to that of the host material.

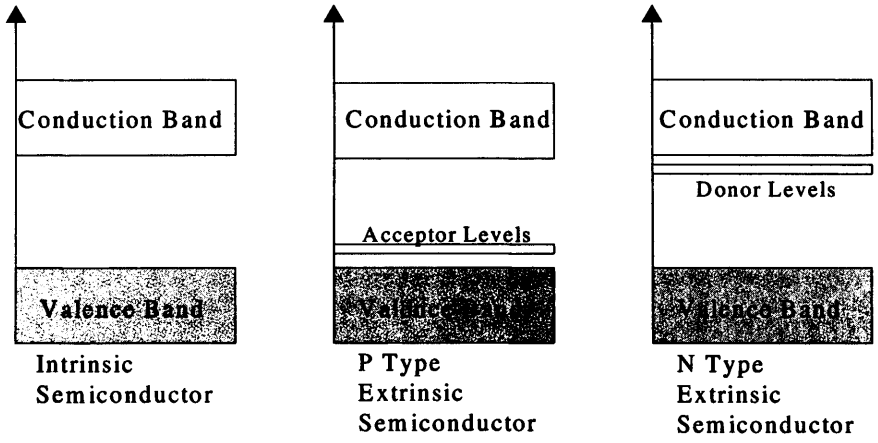

Figure 1.4. The difference between intrinsic and extrinsic semiconductors.

It is possible for a semiconductor to contain both p-type and n-type dopants. Semiconductors of this type are called compensated semiconductors.

1.2.4 Compound Semiconductors

A large number of compounds exhibit semiconductor behaviour. Binary compounds of groups 13 and 15 (III-V), groups 2 and 16 (II-VI) and groups 1 and 17 (I-VII) are expected to be semiconductors. However, only the III-V and II-VI materials are semiconductors, whereas I-VII compounds are insulators. This is because the bonds in this type of material are very ionic in character. II-VI materials are more ionic in character than III-V materials and II-VI materials have a larger band gap as a result. These materials may be expected to show intrinsic behaviour but do not, because crystal defects behave in the same way as dopant atoms. Cation deficiencies lead to n-type behaviour and anion deficiencies lead to p-type behaviour. Ternary and quaternary compounds can also be made. The choice and relative proportions of the elements used

in these compounds to some degree allows us to tune the properties of the semiconductor.

1.2.5 Direct and Indirect Semiconductors

Intrinsic and extrinsic descriptions of semiconductors only describe allowed and disallowed states. They do not describe the associated transitions.

Direct transitions occur when no perturbation of the wave vector of the system is necessary. The wave vector of the system is a measure of the momentum of the system. These transitions typically occur when the band gap is small where the lowest energy point of the conduction band is directly above the highest energy point of the conduction band on a wave vector versus energy plot (Figure 1.5).

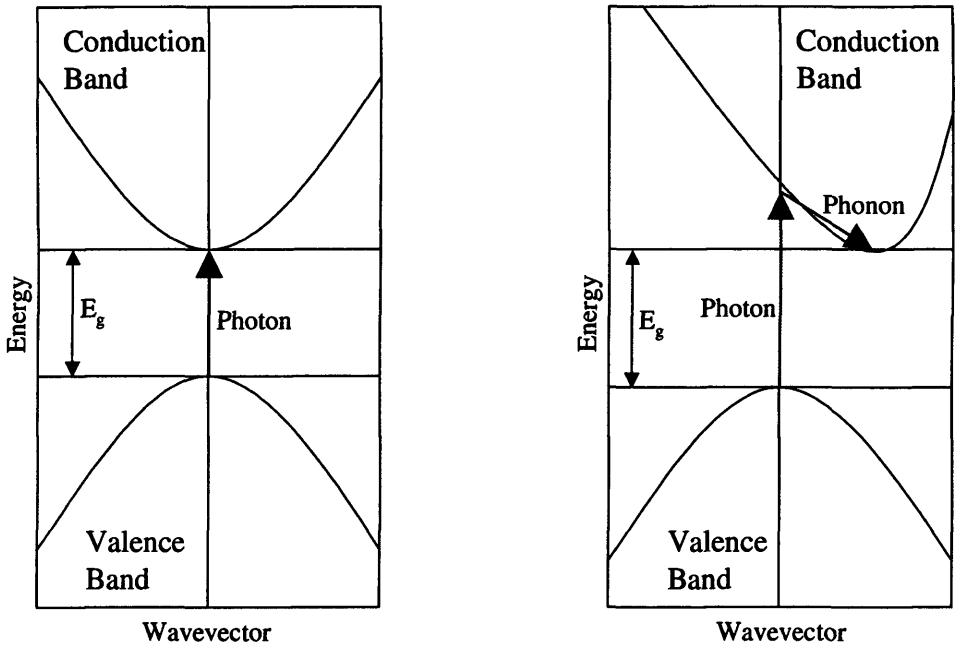

Figure 1.5. The difference between direct (left) and indirect (right) transitions in semiconductor materials.

Indirect transitions occur when perturbation of the wave vector is necessary because the momentum of an electron being promoted is altered. This perturbation occurs in the wave vector through phonons.

1.3 Film Deposition

There are many different methods to deposit films and there are a variety of ways in which the deposited film may interact with the target substrate. Films may be epitaxial, polycrystalline or amorphous. The type of film obtained depends on the conditions used for the production and the nature of the substrate. Film deposition often requires additional energy, for example from a heated substrate or by activation of the precursor species.

1.3.1 Physical Vapour Deposition

1.3.1.1 Evaporation and Sublimation

The easiest way to grow a film is by vaporising a pure material and allowing the vapour phase molecules to deposit on a cooler surface. Different ways of evaporating a material lead to alternative methods that all work on the same principle. Examples include vacuum deposition, flash evaporation and electron bombardment.[3]

1.3.1.2 Molecular Beam Epitaxy

This technique involves the production of an epitaxial film, which is to say a film that is crystalline and ordered in a coherent way that matches the substrate surface.

To enable this happen the process is done under ultrahigh vacuum and growth rates are slow (~1μm/hour).[4] The precursor is transported to the substrate as a molecular beam. This is achieved by heating the precursor in a pyrolytic boron nitride crucible. As the precursor is evaporated a small aperture controls the outlet of gaseous precursor molecules. This has the effect of creating a beam of molecules. The cell in which this happens is called a Knudsen cell. Multiple Knudsen cells can be used to create multi-component films or a single component but more uniform film.[3]

1.3.1.3 Sputtering

This method employs high-energy ions to bombard the surface of the precursor material. This causes atoms from the surface to be ejected in an ionised form. These ionised atoms are accelerated towards the substrate surface by an applied electric field, where the substrate forms part of one of the electrodes.[3,4]

1.3.2 Chemical Vapour Deposition

Chemical vapour deposition (CVD) is a process whereby thin solid film is synthesized from a gaseous phase by a chemical reaction. It is this reactive process that distinguishes CVD from a physical vapour deposition process such as those mentioned above. The main purpose of any CVD reaction is to produce a functionalised surface on a bulk material.

This may be a mechanical, magnetic, optical, electrical or chemical property, or even a combination of these, and a wide variety of films can be created from CVD reactions. There are important properties and characteristics that CVD reactions bring

to thin films that PVD methods cannot. Film thickness of CVD prepared films can vary within wide limits from single atomic layers to 100's of microns depending on the exact technique employed. Film adhesion is also important, and any useful film deposited will have to adhere to the substrate. The factors that determine film adhesion are not well-understood and not all CVD reactions produce adherent films. The use of interfacial barrier layers (deposited via CVD) can often overcome problems of substrate adhesion. Composition and purity can be controlled in CVD reactions, as can dopant levels. One of the most important things that can occur in CVD reactions is the production of conformal films (Figure 1.6). Unlike PVD methods, which are line of site, CVD features mobile, activated surface species.

1.3.3 The CVD Process

There are certain features which are always present in a CVD system: a source of gases or vapours, a reaction chamber and an exit for the exhaust gasses. Certain CVD systems require additional items such as a pump for low-pressure systems, lasers or plasma generators. Finally there must be a place for a target substrate for deposition to occur upon. There are a wide variety of processes which may take place in a CVD system. These are common to all CVD systems and are illustrated in Figure 1.7.

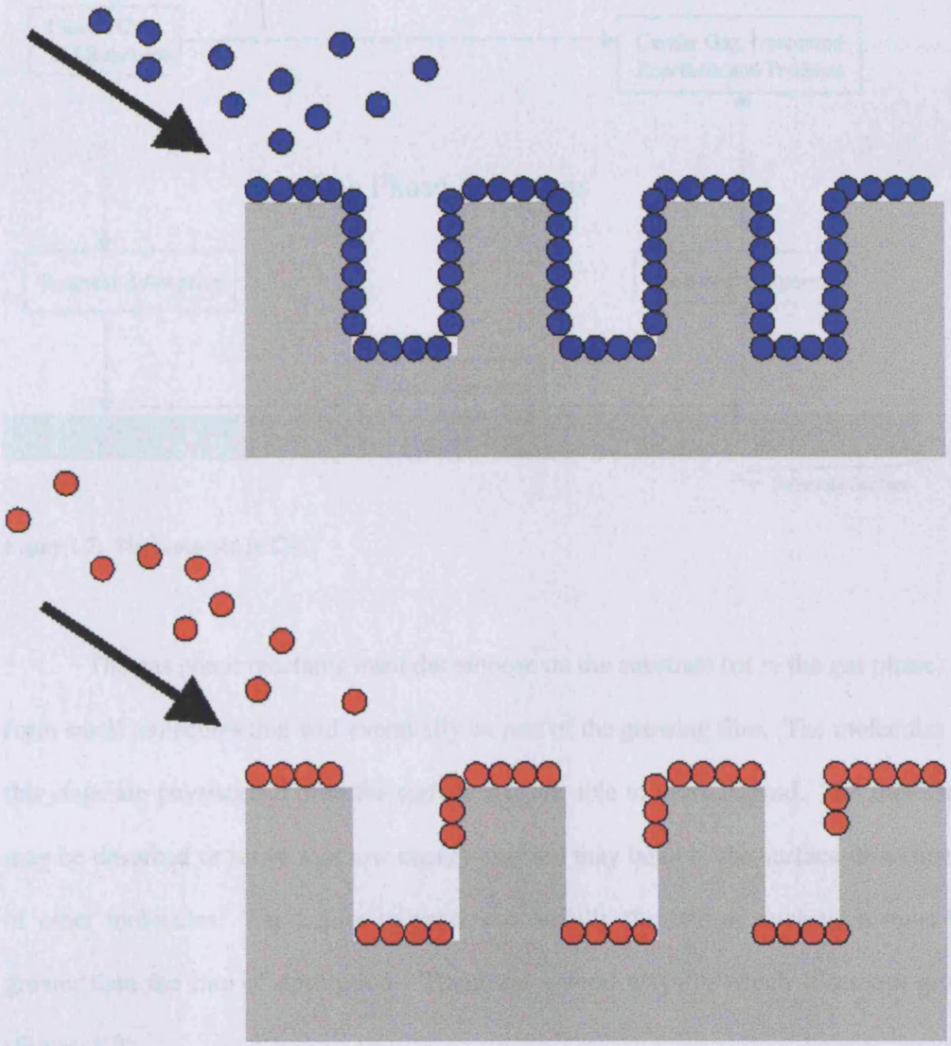

Figure 1.6. The top illustration indicates conformal film growth, the bottom non-conformal or "line of sight" film growth. The blue and red dots represent film precursor and the arrows indicate the direction of precursor flow.

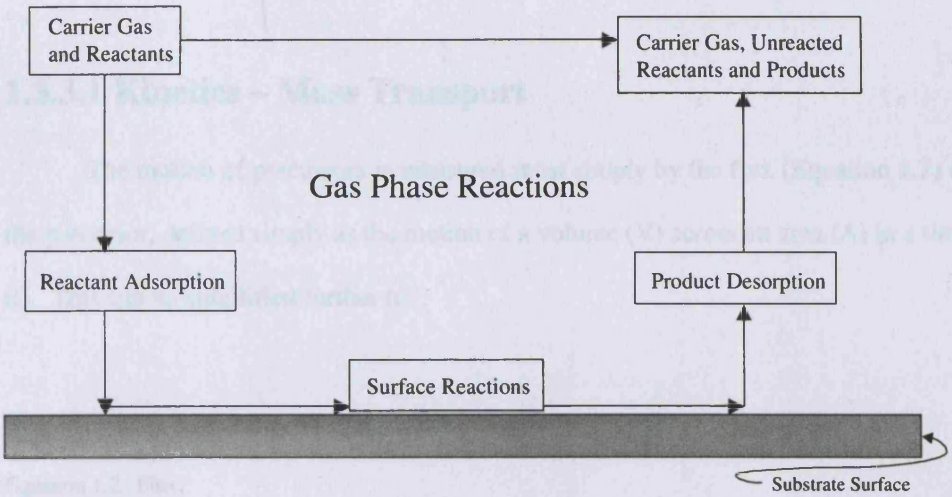

Figure 1.7. The processes in CVD

The gas phase reactants must decompose on the substrate (or in the gas phase) to form small molecules that will eventually be part of the growing film. The molecules at this stage are physisorbed onto the surface and are able to move around. The molecule may be desorbed or move to a low energy site and may bond to the surface or a cluster of other molecules. For a film to grow successfully the rate of nucleation must be greater than the rate of desorption. There are several ways in which films can grow (Figure 1.8).

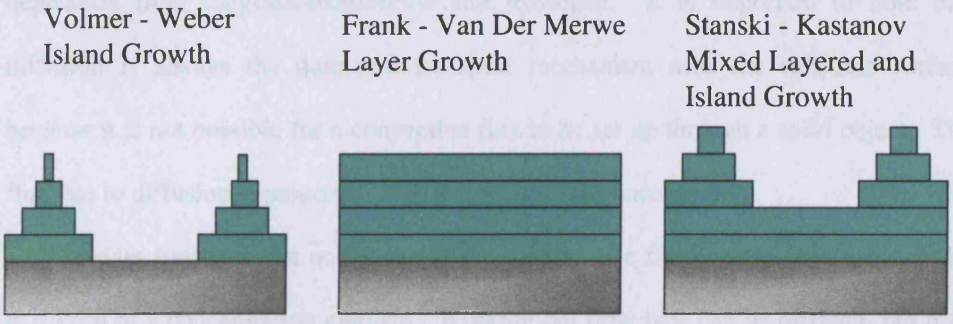

Figure 1.8. The three main types of film growth.

1.3.3.1 Kinetics – Mass Transport

The motion of precursors is measured most simply by the flux (Equation 1.2) of the precursor, defined simply as the motion of a volume (V) across an area (A) in a time (t). This can be simplified further to:

Flux = Density x Velocity

Equation 1.2. Flux.

The velocity is often just the overall velocity of a moving gas flow. Flux due to this overall motion of fluid is convection.

Diffusion is a more subtle mechanism but is just as important as convection. Diffusion results from the thermal motion of molecules. When molecules are evenly distributed diffusion tends to have no importance. However, where there is a concentration gradient the diffusive motion of molecules produces a net flux that reduces the gradient in concentration. Diffusion can also result from gradients in temperature (thermodiffusion) but this is usually unimportant in CVD except where there is a large difference in the molecular weights of precursors; e.g. tungsten deposition from tungstenhexafluoride and hydrogen. It is important to note that diffusion is always the dominant transport mechanism near the substrate surface because it is not possible for a convective flux to be set up through a solid object. The flux due to diffusion is proportional to the gradient in concentration.

Mass transport can occur due to the motion of a fluid or gas regardless of the existence of a concentration gradient. Working out flow type can be difficult, but may

be characterised with various measurements such as the Reynolds number (Equation 1.3).

$$Re = UL/v$$

Equation 1.3. The Reynolds number

where Re is the Reynolds number, U is the overall velocity of the flow through the reactor, L is the characteristic length of the reaction chamber and v is the kinematic viscosity defined as the viscosity of the system divided by the mass density of the system.

Where Re is large (Re>1000), momentum diffuses ineffectively and velocities vary greatly in the system; this would generally be described as turbulent flow. When Re is small (Re < 2), then momentum diffuses rapidly across the chamber and velocity varies in a simple manner; this would be describing laminar or creeping flow conditions. Most CVD reactors operate in the laminar flow region because turbulent flow conditions are not conducive to reproducibility.

The Reynolds number is unaffected by changes in pressure where there is constant molar flow. This is in essence because the viscosity is independent of pressure; it is determined by the product of the density and the mean free path; one being proportional to the pressure and the other inversely proportional. However, at low pressure where the mean free length is similar to the reactor dimensions molecules are just as likely to hit the walls of the reactor as they are each other. At this point the description of fluid flow becomes invalid. The validity of the fluid flow description may be calculated from the Knudsen number (Kn). This is the ratio of the system size to the mean free path of the gas molecules. If Kn >> 1 then our description of flow

conditions is still valid. If Kn << 1 then we must turn to computational methods to glean an insight to what's happening in the reactor. In reality however, things are much more complicated.

1.3.3.2 Thermodynamics – Heat Transport

Most CVD processes operate at some temperature other than room temperature. The vast majority of processes operate at elevated temperature. Heat transfer has three main facets. Conduction is the motion of heat through a stationary solid, liquid or gas. Conduction in a gas takes place by the same mechanisms as with mass transport. The main difference is that heat fluxes do not necessarily reduce to zero at a surface. Convection is the physical transfer of gasses or liquids containing energy. Radiative heat transfer dominates in a vacuum through the transfer of photons. The thermal conductivity varies a great deal between different materials, much more so than diffusion constants for common gasses. As such large temperature gradients may be set up near the substrate surface (and in hot walled reactors the walls), this will aid thermodiffusion.

When heat is added to a gas it expands and there is a change in density. This change in density creates a change in the body forces, which can lead to flow without any external force being applied. This natural convection is highly undesirable in CVD systems as it represents an uncontrolled gas flow. In most CVD systems it is insignificant as the applied flow velocity (forced convection) is usually much larger.

1.3.3.3 Film Growth

The growth of a thin film in CVD is achieved by exposing a suitably prepared substrate to the precursors in the reaction chamber. The resulting growth and microstructure of the film is determined by the surface diffusion and nucleation that take place at the growth interface. These are influenced by substrate temperature, reactor pressure, and gas phase composition.

Amorphous films tend to be created at lower temperatures and high growth rates where the surface diffusion is slow relative to the arrival rate of film precursors. At high temperatures and low growth rates where surface diffusion is fast relative to the incoming flux the adsorbed species are able to diffuse to step growth sites and produce a film replicating the substrate surface; this is known as an epitaxial layer. The intermediate case sees nucleation at many points on the surface and also surface diffusion to form "islands" of growth.

Growth rates depend on a number of factors such as substrate temperatures, reactor pressure and gas-phase composition. There are three main regimes to consider. At low temperatures, the growth rate is limited by chemical kinetics and increases exponentially with temperature according to the Arrhenius expression shown in Equation 1.4.

$$\text{Rate} = A \exp (Ea / RT)$$

Equation 1.4. Rate of film growth.

where Ea is the apparent activation energy, R is the gas constant, and T is the temperature.

The rate is limited by chemical kinetics; uniform film thickness can be achieved by minimising temperature variations. In the intermediate temperature regime growth rate is almost independent of temperature as mass transport to the surface controls the rate. This temperature independence is quite desirable in cold walled systems where it is difficult to obtain completely uniform substrate heating. At high temperatures growth rates may decrease due to an increase in the rate of reactant desorption. Alternative reaction pathways may also become available. Gas phase reactions become increasingly important with increasing temperature and partial pressure of reactants. High reactant concentrations may lead to gas phase nucleation. This leads to a decline in film quality and yield.

1.3.3.4 Precursors

A wide variety of precursors may be used in CVD and ideally they must be volatile, decompose cleanly and be inexpensive. Precursor delivery occurs either from a single source or multiple sources. Single-source precursors are compounds where bonds between the elements of the target compound are already present within the precursor. For example, for the formation of a film of TiO_2 then the single-source precursor must contain Ti–O bonds as illustrated in Figure 1.9.

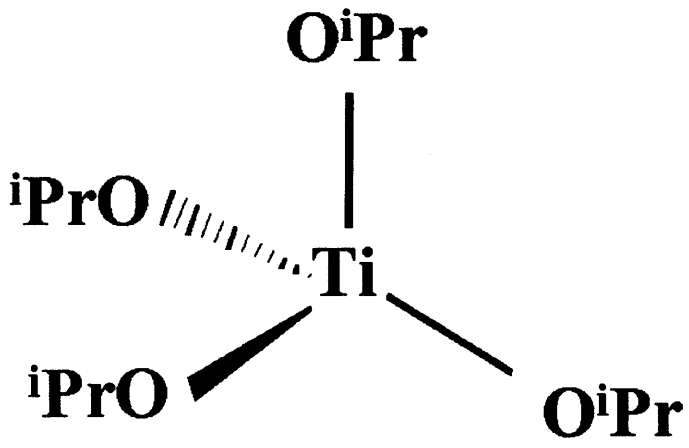

Figure 1.9. Structure of titanium iso-propoxide

Single source precursors are useful in that their decomposition and reaction properties can be tuned by changing the ligands. These precursors may suffer from contamination as they have bonds to species that are undesirable in the resultant film, for example carbon. Also they may be used in lower temperature depositions. Often the limiting step in such cases is the temperature at which the compound decomposes. Single-source precursors tend to be less toxic, but are generally not commercially available and expensive. Multisource precursors are when two or more different compounds are reacted together in the reaction chamber, e.g. Equation 1.5.

$$WF_{6\,(g)} + 3/2\ O_{2\,(g)} \rightarrow WO_{3\,(s)} + 3F_{2\,(g)}$$

Equation 1.5. An example of a dual source CVD reaction.

The advantages of this methodology are that these compounds tend to be cheap, thermally stable in transport and volatile. Disadvantages are that film contamination

can be an issue, higher substrate temperatures are often required and many of the compounds used are either toxic or have toxic by products.[4]

1.3.4 Types of CVD

Sometimes traditional heating of the substrate is undesirable (if for example the substrate has a low melting point or the film you are trying to make may decompose). In these cases other methods of getting the additional energy into the system for reaction to occur must be sought.

1.3.4.1 Photo Assisted CVD

Photo assisted CVD (PACVD) may help grow a film in two ways.[4] Firstly in a photolytic manner, when a laser beam is shone across or just above the surface, the laser light excites the gaseous precursor species meaning less heating of the substrate is needed to initiate reaction.

The second way lasers can be used is in a pyrolytic sense. A laser is focused on one spot on the surface of a substrate and this point heats up and a film can be selectively deposited. By using optical technology intricate and precise patterns on the substrate can be produced. By varying the power of the laser the surface may also be selectively etched. This technology has applications in the microelectronics industry.

1.3.4.2 Plasma Enhanced CVD

Plasma Enhanced CVD (PECVD) [4] works in a similar way to photolytic PACVD in that precursor species are activated before they reach the surface of the substrate. Species are activated by travelling through a plasma, created using a radio

frequency electric field. This field interacts with gaseous electrons and accelerates them; this causes the electrons to collide with precursor species and potentially ionise them. The field also interacts with ions but because of the larger mass of these has negligible effect.

1.3.4.3 Aerosol Assisted CVD

AACVD uses an aerosol vaporisation technique.[5] The precursor is dissolved into a solvent and an aerosol mist is generated using a piezo-electric device. These ultrasonic waves pass through the precursor solution generating a wave pattern on the surface of the liquid. When the height of the wave is sufficient; the wave crests become unstable and form droplets that are ejected from the surface, thus generating an aerosol mist. The mist is transported to the reaction chamber using a positive nitrogen pressure. In the reaction chamber, which is usually heated in excess of 200 °C, the solvent evaporates to leave the precursor as a vapour from whence a CVD reaction occurs.

1.3.5 Applications of CVD

CVD has applications in five main areas:

1) microelectronics
2) optoelectronics
3) protective and decorative coatings
4) optical coatings
5) Glazing

CVD is used extensively in the microelectronics industry to deposit semiconductors, metals and insulators. The optoelectronic materials market is an area

of growth and increasing importance. Materials such as cubic boron nitride are deposited via CVD onto tools to increase their working lifetimes; there is also considerable interest in fibre reinforced composites and coatings for the aerospace industry. Optical coatings is probably a smaller area but nevertheless an area of important technological developments. CVD in the glazing industry has been used to produce films of titanium dioxide for self-cleaning uses or other materials such as tin dioxide for solar control applications.

1.4 Gas Sensing

Gas sensors are a type of chemical sensor, which may be defined as a simple to use, robust device that is capable of reliable quantitative or qualitative recognition of atomic, molecular or ionic species. Gas sensing can be achieved in a variety of manners, for example electrochemical devices, solid state semi-conducting metal oxide devices, metal phthalocyanine devices, electrolytic fuel cells and infrared spectroscopy.[6]

1.4.1 Metal Oxide Semiconductor Gas Sensors

The current widely held view of gas sensors [7] states that the conductivity of semi-conducting oxides in air is determined by the trapping of electrons in surface states associated with surface absorbed oxygen. If interstitials or oxygen vacancies are immobile in the lattice, then the behaviour is described in terms of electron distribution between bulk and surface states. The surface conductivity is sensitive to small amounts of reactive gas as catalytic surface processes result in a change in the surface coverage of the oxygen surface trap states. If oxygen defects are mobile within the lattice then the conductivity is determined by the equilibrium between bulk lattice defects and

oxygen in the gas phase, and sensitivity to trace reactive gases is lost. A further case for gas sensing can arise where there is a time dependence on the equilibration of lattice and surface states. Conductivity time dependence can also be observed as a result of lattice defect migration, which alters the potential and thus the charge carrier distribution near the surface. Due to a microstructural effect, part of the conductivity is gas sensitive due to modification in surface reactions whilst the conductivity contributed by the bulk far enough away from the surface is not gas sensitive.[8] If the films are especially thin (100's of nm) then dense films such as those produced by CVD methodology may produce high quality gas sensors. Typically solid-state gas sensors are made of semiconductor materials. The band structure of these materials creates electronic lattice defects; these defects may be mobile and migrate to the surface of the material creating and increased number of trap states and thus catalytic sites. Reactions at these sites result in a change of the fractional surface coverage of this acceptor state and thus a change a change in conductivity. For example, in a p-type semiconductor where holes are majority charge carriers and electrons the minority the resistance will increase in the presence of a reducing gas (CO, alcohols, alkanes, etc.). The classification n and p is used to describe gas sensitive semiconductor materials because it is believed that this reflects the charge type of the majority carrier in the two cases. The most widely used semiconductor in solid-state gas sensors is tin oxide, which gives a large response to a number of reducing gasses.[6] Materials are often doped into the tin oxide, or a thin layer applied to the surface in order to improve selectivity and response.[6]

In this chapter the fundamentals of band theory, semiconductor behaviour, chemical vapour deposition and metal oxide semiconductor gas sensing have been discussed. In the next chapter the experimental and analytical methodology is outlined.

Chapter 2 - Experimental

2.1 Atmospheric Pressure Chemical Vapour Deposition

The apparatus and procedure described here was used for the production of all films described in chapters three and four. Nitrogen (99.99%) was obtained by BOC and used as supplied. Coatings were obtained on SiO_2 coated float glass. Atmospheric pressure chemical vapour deposition (APCVD) experiments were conducted on 150 mm x 45 mm x 3 mm pieces of glass using a flat bed cold walled APCVD reactor (Figures 2.1 and 2.3). A graphite block containing a Whatman cartridge heater was used to heat the glass substrate. The temperature of the substrate was monitored by a Pt-Rh thermocouple. Independent thermocouple measurements indicated that temperature gradients of up to 50 °C were observable at 600 °C across the surface of the glass. The rig was designed so that three independent gas lines could be used.

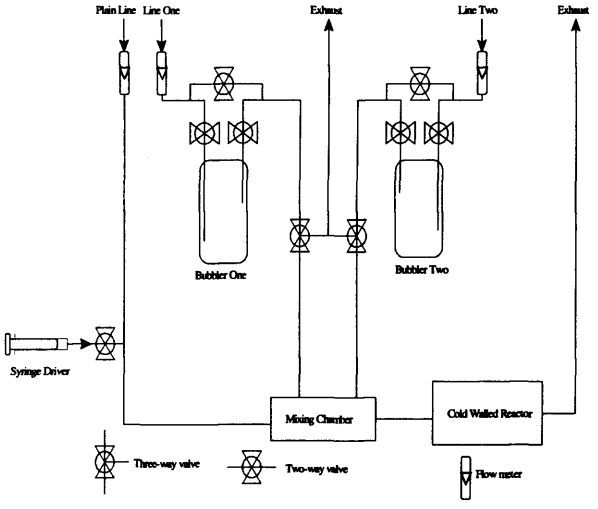

Figure 2.1. Schematic diagram of an APCVD rig.

All gas handling lines, regulators and flow valves were made of stainless steel and were ¼" internal diameter except for the inlet to the mixing chamber and the exhaust line from the apparatus that were ½" in diameter. In these experiments three gas lines were used. Gases came directly from a cylinder and were preheated by passing along 2 m lengths of stainless steel tubing, which was curled and inserted inside a tube furnace. The temperatures of all the gas inlet lines were monitored by Pt-Rh thermocouples and Eurotherm heat controllers. Precursors were placed into separate stainless steel bubblers. The bubblers were heated to appropriate temperatures by a heating jacket and introduced into the gas streams by passing hot nitrogen gas through the liquids. The two components of the system were mixed by the use of two concentric pipes of ¼" and ½" diameter respectively, the inner pipe being 3 cm shorter than the outer pipe. The concentric pipes were attached directly to the reaction chamber of the coater. The reaction chamber (Figure 2.2) was designed to ensure an even, reactor wide laminar flow.

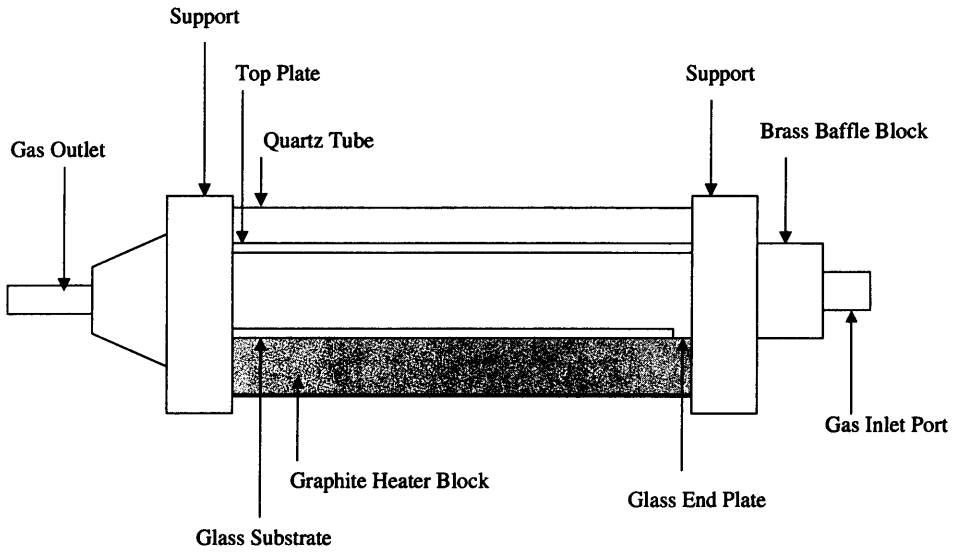

Figure 2.2. Schematic diagram of an APCVD reaction chamber.

Gas flows were adjusted using suitable regulators and flow controllers. The exhaust from the reactor was vented directly into the extraction system of a fume cupboard.

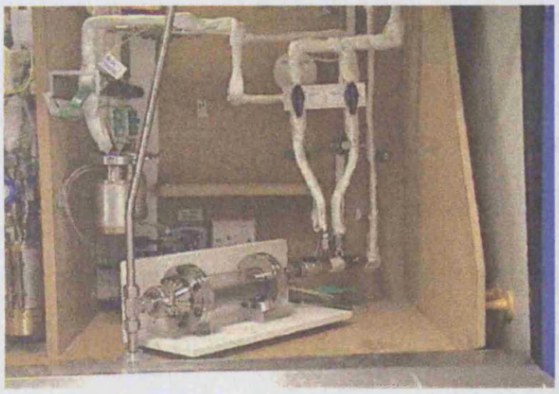

Figure 2.3. Photo of an APCVD rig.

Precursors were loaded into the bubblers in a Safron Scientific Equipment Ltd glove box type 2p.

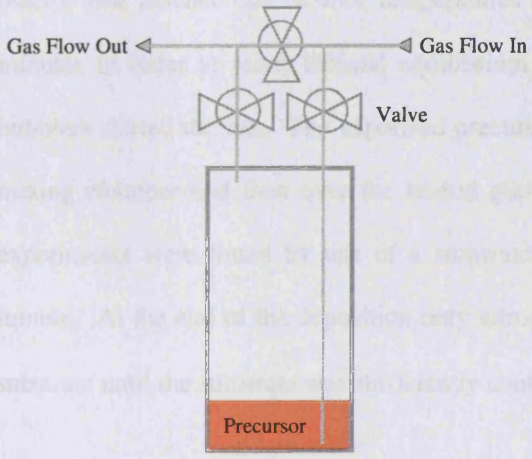

Figure 2.4. Schematic diagram of a bubbler.

When nitrogen gas is passed through the bubbler the chemicals are entrained in the gas flow and transported to the reaction chamber and substrate (Figure 2.4). Bubblers may be heated to melt precursors that are solid at room temperature. Gases may be added by mixing with the plain flow line or by the addition of another gas line to the reactor. Liquid precursors may also be injected directly into the gas flow using a syringe driver.

Prior to use the glass substrates were cleaned by washing with petroleum ether (60-80 °C) and isopropanol and then dried in air. Once placed into the reactor all of the equipment was baked out with nitrogen at 150 °C. The graphite-heating block was turned on and allowed to heat to its set temperature at a rate of 10 °C min^{-1}. Faster heating could lead to the glass substrate cracking. The bubbler heating collars were also turned on and allowed to heat up to the desired temperature. This temperature was estimated based on data given in the handbook of Chemistry and Physics; [9] where such data was unavailable it was based on the boiling point of the precursor less 20-30 °C and improved during the course of the experiments. When the lines, bubblers and reactor had reached the desired temperatures the system was left for a further ten minutes in order to reach thermal equilibrium. Admitting hot nitrogen gas into the bubblers started the run. The vaporised precursors were then allowed to flow into the mixing chamber and then over the heated glass substrate in the reactor. Deposition experiments were timed by use of a stopwatch and were conducted typically for 1 minute. At the end of the deposition only nitrogen was allowed to flow over the glass substrate until the substrate was sufficiently cool to handle (~60 °C).

2.2 Aerosol Assisted Chemical Vapour Deposition

Aerosol assisted chemical vapour deposition (AACVD) was used in the experiments described in chapter six. The precursor was dissolved in solvent and an aerosol was generated at room temperature by use of a PIFCO air humidifier. Nitrogen was passed through the aerosol mist, thus forcing the aerosol particles encapsulated with precursor into the heated reaction chamber. The exhaust from the reaction chamber was vented directly into a fume cupboard. Deposition experiments were carried out by heating the flatbed cold-wall reactor to the desired temperature before diverting the nitrogen flow through the generated aerosol mist and into the reactor. Deposition experiments were timed by stopwatch for one hour. At the end of the deposition the nitrogen flow through the aerosol was diverted and only nitrogen passed over the substrate. A schematic diagram of the deposition set up is shown in Figure 2.5 and a photograph in Figure 2.6.

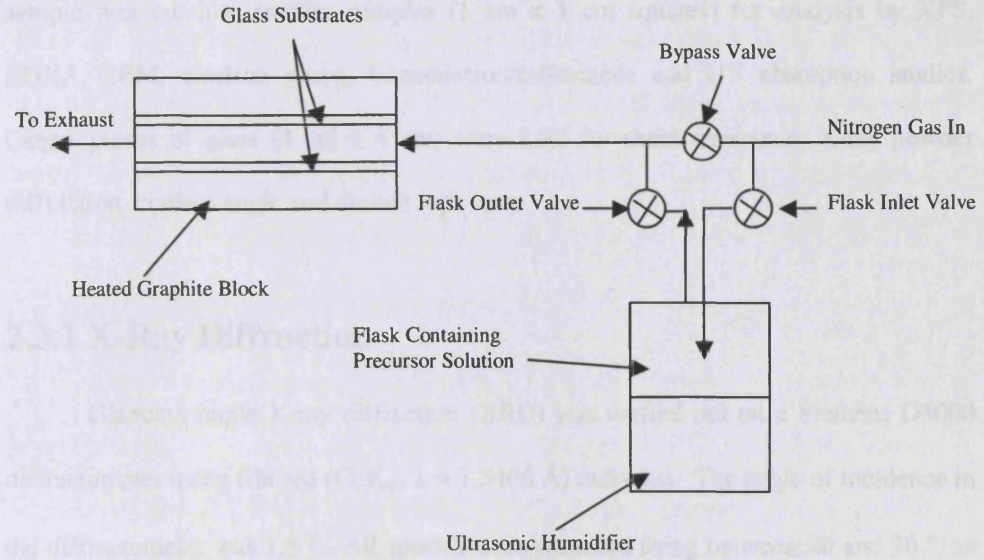

Figure 2.5. Schematic diagram of the AACVD setup.

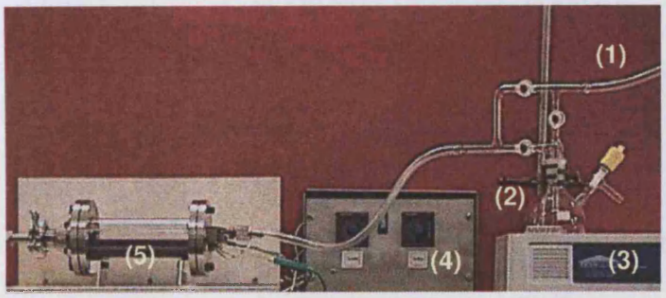

(1) Nitrogen line
(2) Flask containing precursor
(3) Ultrasonic humidifier
(4) Heat controller
(5) Cold wall, flat bed reactor

Figure 2.6. Photograph of the AACVD set up.

2.3 Analysis

Cool, coated samples were handled and stored in air. The large coated glass sample was cut into smaller samples (1 cm x 1 cm squares) for analysis by XPS, EDXA, SEM, electron probe, transmission/reflectance and UV absorption studies. Larger pieces of glass (4 cm x 4 cm) were used for sheet resistance, X-ray powder diffraction, contact angle and Scotch tape tests.

2.3.1 X-Ray Diffraction

Glancing angle X-ray diffraction (XRD) was carried out on a Siemens D5000 diffractometer using filtered ($CuK_{\alpha 1}$ $\lambda = 1.5406$ Å) radiation. The angle of incidence in the diffractometer was 1.5 °. All spectra were recorded using between 20 and 70 °, as this covered all of the major peaks for the known phases of the compounds under investigation.

2.3.2 Raman Spectroscopy

Raman spectra were obtained using a Renishaw Raman system 1000 using a helium neon laser of wavelength 632.8 nm. The Raman system was calibrated against the emission spectrum of neon.

2.3.3 Energy Dispersive X-ray Analysis

EDXA was used to obtain atomic ratios on a JEOL 35-CF instrument typically using an accelerating voltage of 20 KV and a working distance of 39 mm. All elements were standardised relative to cobalt. All data was quantified using Oxford Link ISIS

software. As the films made were very thin, breakthrough to the underlying glass was observed. This posed several problems as some of the constituents of the glass had lines in the EDXA spectrum that overlapped with those of the target film. An additional problem in the analysis of the silicon containing films is that compared to the film, glass contains an enormous amount of silicon. This meant that EDXA could not be used to analyse atomic ratios of these films with any accuracy.

2.3.4 Scanning Electron Microscopy

SEM was carried out on a Hitachi S570 filament scanning electron microscope. Working distances between 10 and 39 mm were used. Accelerating voltages were between 10 KV and 30 KV depending on the sample. Magnification ranged from x 1000 to x 40,000.

2.3.5 X-ray Photoelectron Spectroscopy

XPS has two analytical purposes. It can be used to calculate the elemental composition of a sample. This technique can also be used to gain information on the oxidation states and local environment of atoms. However, determining elemental ratios using this method can be difficult as lighter atoms are more easily sputtered than heavier atoms. This can potentially lead to misrepresentative results.

XPS spectra were recorded using a VG ESCALAB 220I XL instrument using a focused (300 μm spot) monochromatic Al-K_α radiation at a pass energy of 20 eV. Scans were acquired with steps of 50 meV. A flood gun was used to control charging and the binding energies were referenced to an adventitious C 1s peak at 284.6 eV. Depth profiling measurements were obtained by using argon beam sputtering.

2.3.6 Transmittance / Reflectance Spectroscopy

This was carried out to determine the optical properties of the films, such as heat mirror capabilities. Spectra were recorded between 300 and 1150 nm by a Zeiss miniature spectrometer. Measurements were standardised relative to a rhodium mirror (reflectance) and air (transmission).

2.3.7 Adhesion Tests

The standard Scotch tape test was carried out. Samples also underwent scratch tests with tissue paper, a brass and steel scalpel.

2.3.8 Ultra Violet / Visible Spectroscopy

UV/Vis spectra were obtained using a Helios double beam instrument between 200 - 1100 nm. The results from these were used to calculate band gaps using the direct and indirect methods.[10]

2.4 Gas Sensing

For gas response, metal oxide films were deposited by APCVD onto commercially produced sensor substrates. For comparison sensors were also prepared by screen-printing. The raw metal oxide materials were obtained as powders from Aldrich. These powders were then mixed with a commercial organic vehicle (ESL400) in a weight : weight ratio of 1:1 then triple roll milled to ensure a homogenous

dispersion of the powder in the vehicle. The ink was screen-printed using a DEK 1202 onto a 3 x 3 mm sensor chip. The printed sensor chips were subsequently fired for 30 minutes in air at 600 °C. Typically, screen-printing produced a film with a thickness of 10 μm ±2 μm. The sensor chips consist of a gold track printed on the top of an alumina tile and a platinum heater track printed on the reverse side of the tile. Gold electrodes were formed using laser trimming. This produced an interdigitized section with gap and finger widths of 50 μm (Figure 2.7.).

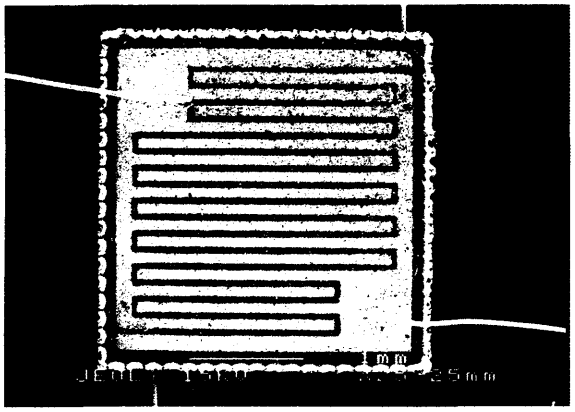

Figure 2.7. An SEM micrograph of a blank gas sensor substrate.

Contacts to the devices were formed by spot welding 50 μm diameter platinum wire to pads of the track material in the corner of the sensor chip. The sensor heater was kept at constant resistance and hence constant temperature by incorporating it into a Wheatstone bridge. Electrical experiments were formed on a locally constructed test rig.[11] Test gasses were diluted from cylinders of synthetic air (79% nitrogen, 21% oxygen) containing ethanol (100 ppm). The devices were investigated over a variety of operating temperatures between 400 and 600 °C.

Chapter 3 - Main Group Metal Phosphides

Metal phosphides are postulated to have interesting optical properties and also find use in the microelectronics industry.[12] No in depth investigation has been undertaken to examine these materials as thin films, other than gallium and indium phosphides, which are not investigated for this reason. In this chapter the production of some main group metal phosphides using atmospheric pressure chemical vapour deposition is examined.

3.1 Introduction

Preparation of bulk phosphides can be completed in many ways: heating a metal with phosphorus, [12-14] the reaction of metal oxides in the presence of phosphorus and iodine and heating a metal in a stream of phosphine [12] are the older better-known routes. The reaction of a metal with Ca_3P_2 [16,17] or electrolysis [12] is more difficult to do in terms of cost and time. The reduction of a phosphate with carbon and the reaction of metal with a phosphide to alter the stiochiometry [12] are ways of producing new phosphides. The use of solid-state metathesis reactions is a relatively recent development [18-23] as is the use of sonochemical reactions.[24]

Phosphides can be classified into four main groups.[12] Metal rich phosphides (where M/P >1) these tend to be hard, brittle and refractory materials, usually with a metallic lustre. They display high thermal and electronic conductivity, good thermal stability and general chemical inertness.

Monophosphides (M/P = 1) have a variety of structures and properties, which are influenced by both the metal atom size and other electronic effects. They may be insulators, semiconductors or metallic conductors.

Phosphorus rich phosphides (M/P < 1) tend to have much lower melting points and thermal stabilities compared with other phosphide types. Often they are semiconductors rather than metallic conductors and may feature catenation of phosphorus atoms, which can extend in a 3d network through out the material.

The last group is called pseudophosphides and includes non-metal phosphides such as boron phosphide. Again there are a variety of structures and properties that are known for these materials.

The study of phosphides began in the late 1700's [13] and a wealth of work has been done since this time. Phosphides of almost all elements are known. Often elements have more than one known stiochiometry of phosphide and the properties of these differ accordingly. Only antimony, bismuth, lead and mercury are considered not to form phosphides because these compounds are considered thermodynamically unstable,[12] although several papers have been published claiming that these compounds have been made.[77,78]

Phosphides appear in a large and diverse number of structures; to name but a few, pyrites such as PtP_2, skullerites (NiP_3, CoP_3) and zinc blendes (GaP, InP) are all known.[13,14,25-29]

Formation of metal phosphide films has received little attention, especially by the use of Chemical Vapour Deposition (CVD). Transition metal phosphides have a variety of properties that could potentially find commercial applications. They are metallic conductors, hard, refractory materials and in some cases resistant to

oxidation.[30,31] Despite this they have found only limited use as catalysts[32] and as diffusion barrier layers in semiconductor devices,[33] where as the corresponding metal nitrides have many technological applications.[34,35] Of the main group phosphides indium phosphide and gallium phosphide are the best known.[12] Both are III-V type semiconductors and are of great importance in the microelectronics industry, being used in the production of microchips, diode lasers and the like. A variety of synthetic techniques have been developed to produce these materials.[36]

Considerable work has also been done on boron phosphide, which is used as a hard, scratch resistant coating,[37-42] and along with many other phosphides a spectral modifier.[43] Aluminium phosphide is known as a rat poison and fumigant.[44-46]

3.1.1 Tin Phosphides

These phosphides, as bulk materials, have been known for some time.[47] An investigation into the thermodynamic properties of the tin phosphide system was published in 1974.[48,49] Crystal structures of bulk materials were published between 1957 and 1972 [50-54] and later refined.[55-56] Recently tin phosphides have received attention as potentially interesting nanomaterials.[57] It is anticipated that such nanomaterials may have interesting mechanical, optical and electrical properties due to quantum confinement effects.[58] They are also known to be catalysts of alkylation reactions.[59]

3.1.2 Germanium Phosphide

To our knowledge no work has been published on the formation of thin films of germanium phosphides by any technique. Bulk germanium phosphide (GeP) has been prepared and known for some time.[60] The thermodynamic properties of the germanium

phosphide system have also been investigated.[61] Crystal structures of the only known stoichiometric bulk materials GeP and GeP_3 have also been published.[62-66] Germanium phosphide (GeP) is a semiconductor with a band gap of 0.95 eV.[67] Quantum dots of this material may have been prepared.[68]

3.1.3 Copper Phosphide

The formation of copper phosphide films has received scant attention. Crystal structures of the various copper phosphides (Cu_3P, Cu_2P_7 and CuP_2) have been elucidated and refined.[69-71] It has been suggested that CuP_2 has semi conducting properties,[72] whilst Cu_3P has been formed previously, by accident, under CVD conditions [73] and has been used as an additive to improve the wear properties of some high-speed steels.[74]

3.1.4 Silicon Phosphide

Silicon based alloys have been widely studied and used in microelectronic optical devices.[75] Silicon phosphide is not well known [13,14] although several theoretical studies have been carried out concerning this material.[76]

3.1.5 Antimony Phosphide

There have only been a small number of papers regarding the production of antimony phosphide,[77,78] indeed, along with bismuth and lead phosphides it is considered to be unknown.[12-14]

3.1.6 Boron Phosphide

Boron phosphide has been studied since the late 1800's.[79,80] Investigation has taken place into the production of thin films at elevated temperature (>1000°C) [81-84] and also using molecular beam methods.[85] Boron phosphide has similar properties to boron nitride, which is an extremely hard, refractory material [86] used as coatings for cutting tools [87] and wear resistant coatings [88] in other areas such as aerospace technology. Boron phosphide may have an advantage over hexagonal boron nitride in that unlike hexagonal boron nitride it does not delaminate easily. However, cubic boron nitride does not suffer from this problem and so production routes to boron phosphide would have to be more efficient in order to surpass cubic boron nitride use.

3.2 Experimental Details

Metal halides are often used as CVD precursors because they are generally very volatile and highly reactive.[89] This is certainly true of tin, germanium and silicon tetrachloride, antimony pentachloride and boron tribromide and to a lesser extent tin tetrabromide. Indeed tin tetrachloride is used in the commercial coating of glass.[90] Phosphine gas has been widely used in the production of gallium, indium and boron phosphides. But PH_3 is unsuitable for large-scale processes as it is highly flammable, explosive and very toxic. Substituted phosphines such as cyclohexylphosphines or phenyl phosphines are much less dangerous and easier to handle, as they are liquids or solids rather than a gas.

The metal halides were reacted with a wide variety of substituted phosphines. The phosphines used were monocyclohexylphosphine, biscyclohexylphosphine,

triscyclohexylphosphine, monophenylphosphine and monotertiarybutylphosphine. It was found that bis and tris phenylphosphines were unsuitable as CVD precursors as they did not provide a high enough vapour pressure to be utilised with the apparatus available.

3.3 Results and Discussion

3.3.1 Tin Phosphide and Germanium Phosphide

3.3.1.1 Tin Phosphide and Germanium Phosphide Results

Atmospheric Pressure Chemical Vapour Deposition (APCVD) of tin phosphide and germanium phosphide films were achieved on glass substrates from the dual source CVD reaction of MCl_4 or MBr_4 (where M = Sn or Ge) and a substituted phosphine ($PCyc^{hex}H_2$, $PCyc^{hex}{}_2H$, $PCyc^{hex}{}_3$ or $PhPH_2$). The process was studied at different substrate temperatures and flow rates of precursor (Table 3.1 and 3.2.).

Table 3.1. Table of reaction conditions and micro-analytical results for the tin phosphide system.

Substrate Temperature / °C	Nitrogen Flow through SnX_4 bubbler l/min (SnX_4) [Bubbler temperature / °C]	Nitrogen Flow through R_xPH_{3-x} bubbler l/min (R_xPH_{3-x}) [Bubbler temperature / °C]	Nitrogen Flow of make up gas l/min.	EDAX and Electron Probe analysis
500	0.5 ($SnCl_4$) [35]	0.5 ($CyhexPH_2$) [120]	1.0	Sn
500	0.5 ($SnCl_4$) [35]	0.5 ($CyhexPH_2$) [120]	1.4	$SnP_{0.40}$
500	0.5 ($SnCl_4$) [35]	0.5 ($CyhexPH_2$) [120]	1.8	$SnP_{0.66}$
500	0.2 ($SnCl_4$) [35]	0.8 ($CyhexPH_2$) [120]	1.0	$SnP_{0.40}$
500	0.3 ($SnCl_4$) [35]	0.3 ($CyhexPH_2$) [120]	1.0	$SnP_{1.00}$
500	0.8 ($SnCl_4$) [35]	0.2 ($CyhexPH_2$) [120]	1.0	Sn
550	0.3 ($SnCl_4$) [35]	0.3 ($CyhexPH_2$) [120]	1.0	$SnP_{1.00}$
600	0.3 ($SnCl_4$) [35]	0.3 ($CyhexPH_2$) [120]	1.0	$SnP_{1.00}$
500	0.3 ($SnCl_4$) [35]	0.3 ($PhPH_2$) [145]	1.0	$SnP_{0.66}$
500	0.3 ($SnCl_4$) [35]	0.5 ($PhPH_2$) [145]	1.0	$SnP_{1.33}$
600	0.3 ($SnCl_4$) [35]	0.5 ($PhPH_2$) [145]	1.0	$SnP_{1.00}$
600	0.3 ($SnCl_4$) [35]	0.7 ($Cyhex_2PH$) [250]	0.7	$SnP_{0.66}$
600	0.3 ($SnCl_4$) [35]	1.8 ($Cyhex_3PH$) [250]	0.2	$SnP_{1.00}$
600	0.5 ($SnBr_4$) [200]	0.3 ($CyhexPH_2$) [120]	0.8	$SnP_{1.00}$
600	0.4 ($SnBr_4$) [200]	0.4 ($CyhexPH_2$) [120]	0.8	$SnP_{1.33}$

Table 3.2. Table of reaction conditions and micro-analytical results for the germanium phosphide system.

Substrate Temperature / °C	Nitrogen Flow through GeX_4 bubbler l/min (GeX_4) [Bubbler temperature / °C]	Nitrogen Flow through R_xPH_{3-x} bubbler l/min (R_xPH_{3-x}) [Bubbler temperature / °C]	Nitrogen Flow of make up gas l/min.	EDAX and Electron Probe analysis
600	0.3 ($GeCl_4$) [40]	0.3 ($CyhexPH_2$) [120]	1.0	Various Oxides
600	0.3 ($GeCl_4$) [40]	0.3 ($CyhexPH_2$) [120]	0.8	Ge_2P
600	0.3 ($GeCl_4$) [40]	0.3 ($CyhexPH_2$) [120]	0.3	$GeP_{1.10}$
600	0.3 ($GeCl_4$) [40]	0.3 ($CyhexPH_2$) [120]	1.0	$GeP_{1.00}$
600	0.3 ($GeBr_4$) [140]	0.3 ($CyhexPH_2$) [120]	1.0	Ge_2P
600	0.3 ($GeBr_4$) [140]	0.3 ($CyhexPH_2$) [120]	0.6	Ge_2P_3
600	0.3 ($GeBr_4$) [140]	0.3 ($CyhexPH_2$) [120]	0.3	$GeP_{1.00}$
600	0.3 ($GeBr_4$) [140]	0.3 ($CyhexPH_2$) [120]	0.6	Ge_2P_3
500	0.3 ($GeBr_4$) [140]	0.3 ($CyhexPH_2$) [120]	0.6	Various Oxides
550	0.3 ($GeBr_4$) [140]	0.3 ($CyhexPH_2$) [120]	0.6	Various Oxides
600	0.3 ($GeBr_4$) [140]	0.5 ($CyhexPH_2$) [120]	0.6	$GeP_{1.20}$
600	0.3 ($GeBr_4$) [140]	0.7 ($CyhexPH_2$) [120]	0.6	$GeP_{1.20}$
600	0.5 ($GeBr_4$) [140]	0.3 ($CyhexPH_2$) [120]	0.6	$GeP_{1.10}$
600	0.7 ($GeBr_4$) [140]	0.3 ($CyhexPH_2$) [120]	0.6	$Ge_{1.10}P$

No tin phosphide film could be grown at substrate temperatures below 400 °C; uniform films were obtained at 500 °C and above. The films grown from the dual source CVD reaction of $SnCl_4$ or $SnBr_4$ and a substituted phosphine ($PCyc^{hex}H_2$, $Cyc^{hex}{}_2H$, $PCyc^{hex}{}_3$ or $PhPH_2$) were opaque in colour, although those grown at higher

temperatures had a blue tint. The films appeared unreflective. Germanium phosphide films could be grown at substrate temperatures of 550 °C or more; uniform films could were grown at 600 °C. All of the films prepared at higher temperatures exhibited some birefringence due to thickness effects. All of the films passed the Scotch tape test. They could not be marked with a wet towel but could be marked with a brass stylus or steel scalpel. The tin phosphide films prepared at higher precursor flow rates showed some "pin-holing" due to gas phase nucleation; this was not seen in the case of the germanium phosphide films. None of the films showed any optical change after storage in air for a year.

Raman microscopy was used to investigate all of the tin phosphide and germanium phosphide films. In all cases no Raman scattering due to the films was observed. It is thought that tin and germanium phosphides are poor Raman scatterers, indeed a sample of Sn_4P_3 purchased form Aldrich gave no discernable Raman spectra. In the samples prepared using $PCyc^{hex}H_2$ and $PhPH_2$ Raman detected no free carbon. This was not the case with films prepared using $PCyc^{hex}{}_2H$ and $PCyc^{hex}{}_3$ where free carbon was present in the films. No Raman scattering was observed from the film due to the presence of tin or germanium oxides (Figures 3.1 and 3.2). In previous work it has been shown that even trace amounts of tin oxides (SnO_2 or Sn_3O_4) give strong Raman patterns.[91-93]

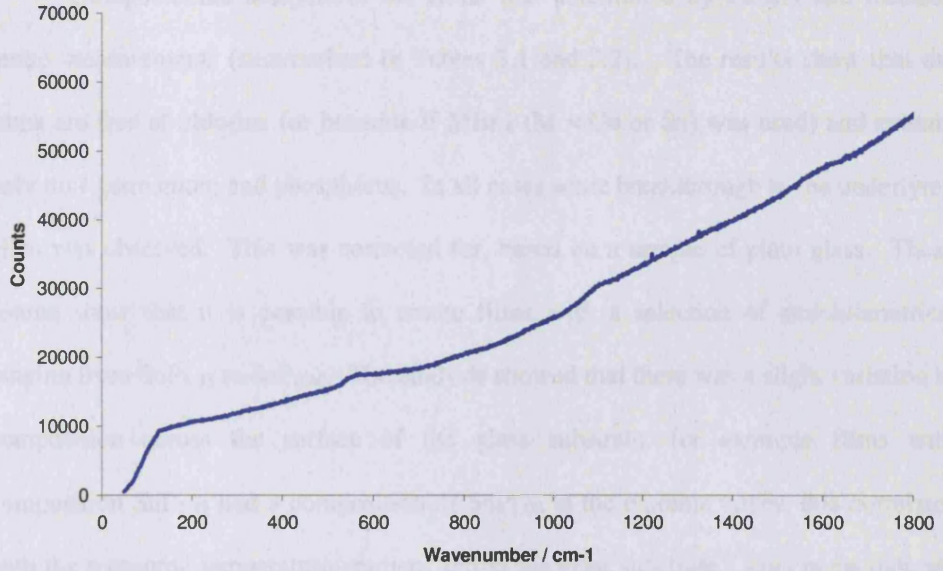

Figure 3.1. Raman pattern of a $SnP_{1.00}$ sample. The broad features of this spectrum are due to the amorphous glass substrate.

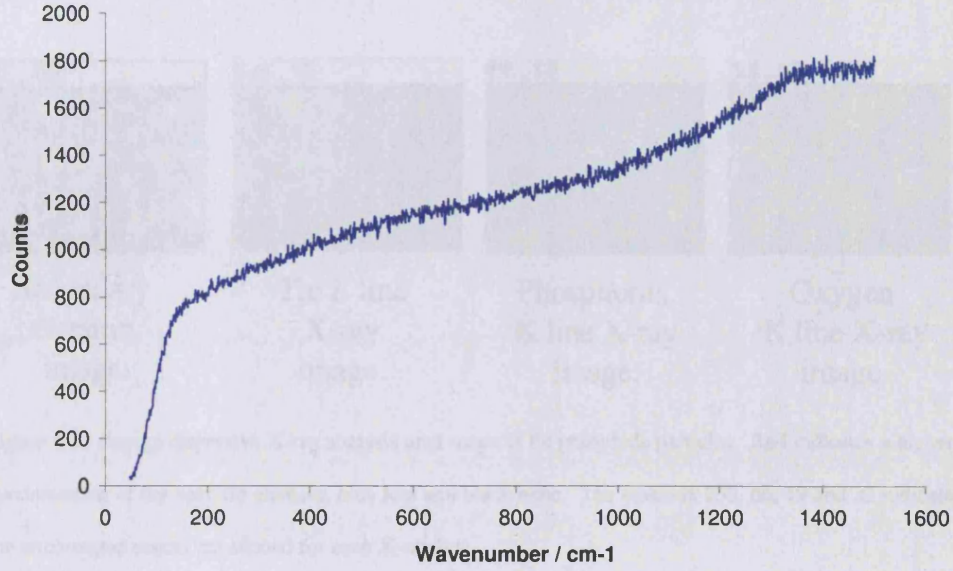

Figure 3.2. Raman pattern of a $GeP_{1.00}$ sample. The broad features of this spectrum are due to the amorphous glass substrate.

Compositional analysis of the films was determined by EDXA and electron probe measurements (summarised in Tables 3.1 and 3.2). The results show that the films are free of chlorine (or bromine if MBr_4 (M = Ge or Sn) was used) and contain only tin / germanium and phosphorus. In all cases some breakthrough to the underlying glass was observed. This was corrected for, based on a sample of plain glass. These results show that it is possible to create films with a selection of stoichiometries, ranging from $SnP_{1.33}$ to $SnP_{0.40}$. The analysis showed that there was a slight variation in composition across the surface of the glass substrate, for example films with composition $SnP_{1.33}$ had a composition of $SnP_{1.00}$ at the extreme edges, this correlates with the measured temperature gradient across the glass substrate. Area maps indicate that particles containing tin and phosphorus are made (Figure 3.3.), and that no oxygen is present in these particles.

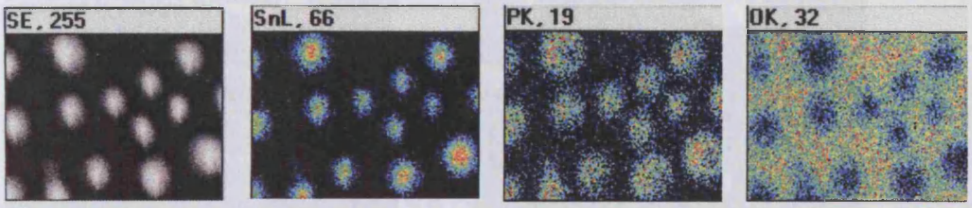

Figure 3.3. Energy dispersive X-ray analysis area maps of tin phosphide particles. Red indicates a higher concentration of the specific element, blue less and black none. The numbers 255, 66, 19 and 32 indicate the uncorrected counts per second for each X-ray line.

A wide variety of germanium phosphide film stoichiometries were also possible; these ranged from Ge_3P to GeP_2 (including non-stoichiometric phases such as $Ge_{1.1}P$).

These films were free of phosphate or oxide materials. Similarly the germanium phosphide films had a stoichiometry variation across the surface. For example a film with a composition of Ge_2P_3 had a composition of $GeP_{1.00}$ at the extreme edge of the substrate.

SEM analysis of the phosphide films (Figure 3.4) showed that the deposition reaction proceeded via an island growth mechanism. The majority of tin phosphide samples consisted of microspheres of tin phosphide covering the majority of the surface. This was not observed in the case of the germanium phosphide films, where a more conventional platelet type of island growth occurs.

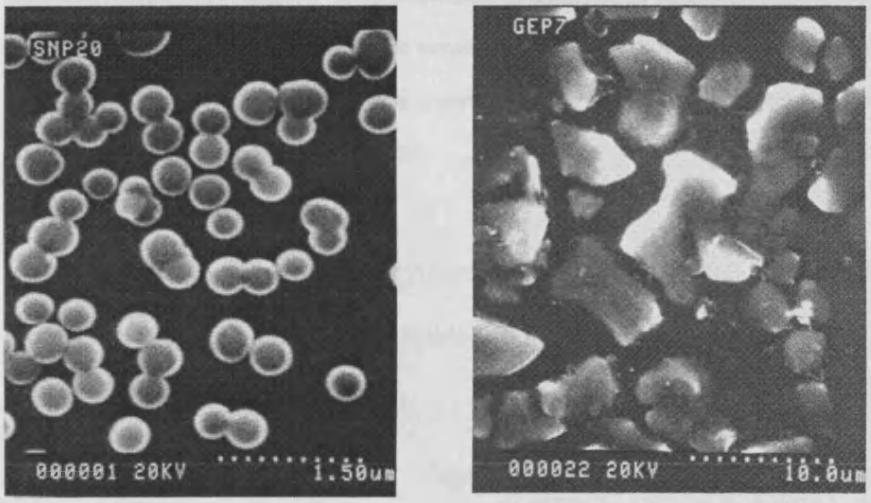

Figure 3.4. Typical SEM photos for samples of tin phosphide (left) and germanium phosphide (right)

Use of different phosphine precursors had an effect on film morphology in the tin phosphide system. Using more substituted phosphine precursors decreased the size of the microspheres on the substrate. This is probably due to a decrease in the rate of surface reaction. The use of bis and tris substituted cyclohexylphosphines leads to smaller particle size and less surface coverage (Figure 3.5.). The use of

monophenylphosphine whilst decreasing particle size ensures good surface coverage comparable to that observed with monocyclohexylphosphine (Figure 3.5.).

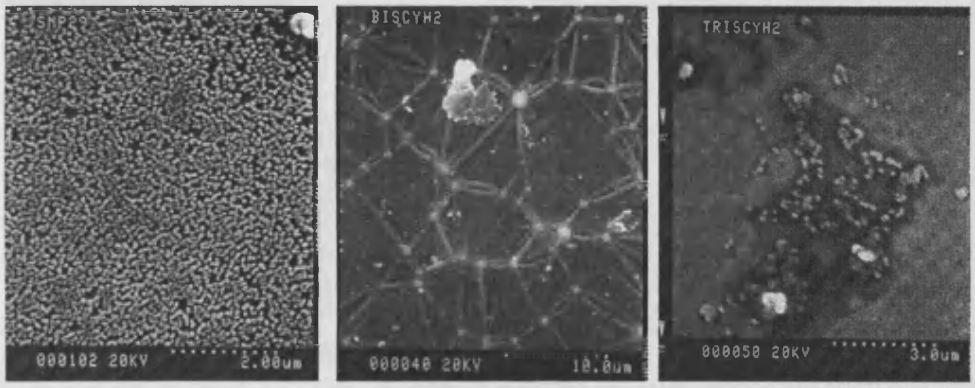

Figure 3.5. SEM pictures of tin phosphide samples prepared with different phosphorus precursors: left; tin tetrachloride and monophenylphosphine, centre; tin tetrachloride and biscyclohexylphosphine, right; tin tetrachloride and triscyclohexylphosphine.

Reaction with biscyclohexylphosphine produced films with highly exotic morphologies (Figure 3.5.). It is possible that these are forming according to a vapour, liquid, solid routine (Figure 3.6).[94]

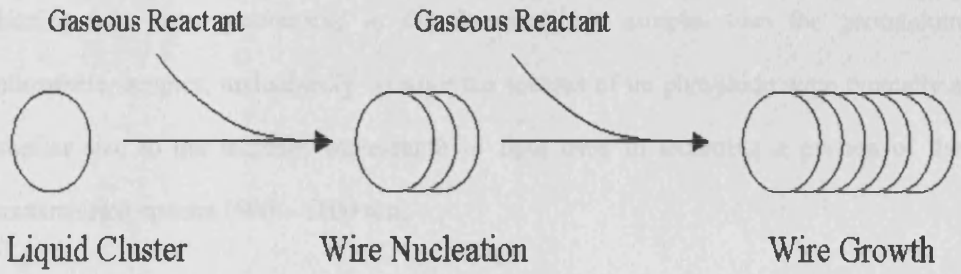

Figure 3.6. Illustration of the vapour-liquid-solid growth mechanism.

The use of more highly substituted phosphines with germanium precursors did not yield any films. Use of monophenylphosphine led to production of very thin films

of germanium phosphide ($GeP_{1.00}$). These are barely distinguishable from the glass surface except by film defects (Figure 3.7.).

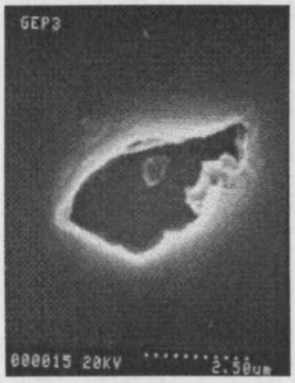

Figure 3.7. SEM picture of a thin film of germanium phosphide.

The optical properties of the germanium and tin phosphide films were studied by reflectance / transmission measurements (Figure 3.8.) and UV absorption between 400 nm and 1100 nm. All samples showed a shift in the absorption edge relative to the plain glass substrate. The films showed minimal reflectivity (2%, Figure 3.8), less so than the substrate (10%). The transmission spectra were indicative of hazing; this is due to scattering by particles in the film of a similar size to the wavelength of the light. Hazing was more pronounced in the tin phosphide samples than the germanium phosphide samples, undoubtedly because the spheres of tin phosphide were typically a similar size to the incident wavelength of light used in recording a portion of the transmission spectra (800 – 1100 nm).

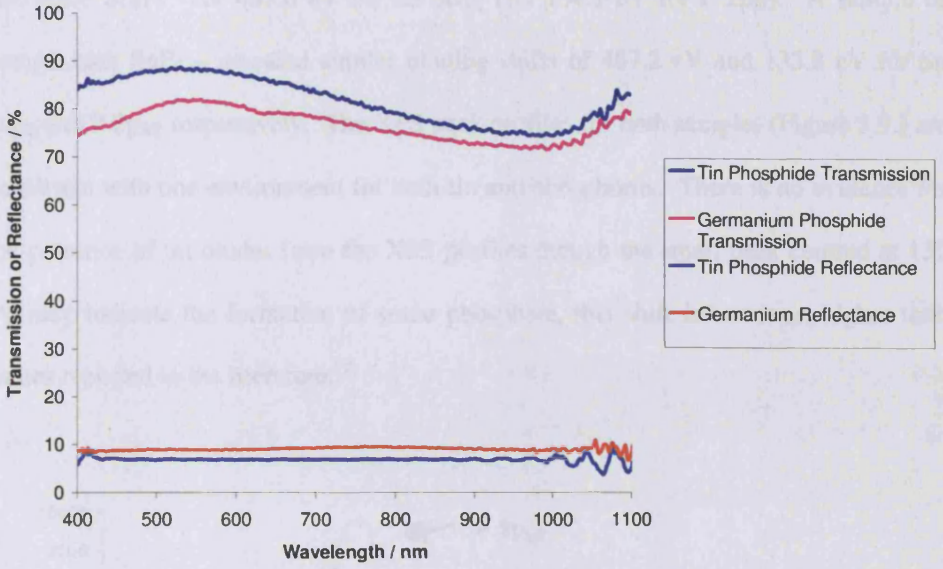

Figure 3.8. Illustration to show typical transmission and reflectance data for samples of tin phosphide and germanium phosphide.

By plotting $\alpha hf^{-1/2}$ against hf in eV (Tauc methodology) and extrapolating the flat part of the curve to the x-axis the value of the indirect band gap can be calculated.[10] For the measured SnP samples this corresponded to 2.2 eV. For other samples an accurate measurement could not be made as the glass substrate causes the signal to appear very noisy if the film is very thin. In addition to this the opaque nature of the thicker tin phosphide films led to a poor transmission profile which also contributed to a noisy plot. The germanium phosphide samples had band gaps of 1.1 eV, similar to literature values for the bulk material (0.95 eV).[67]

XPS measurements on a sample of $SnP_{1.00}$ composition, revealed binding energy shifts of 487.2 eV and 133.6 eV for Sn $3d_{5/2}$ and P $2p_{3/2}$ respectively. These are in reasonable agreement with previous values published in the literature concerning

nanoscale Sn_4P_3 [57] of 487.6 eV for Sn $3d_{5/2}$ and 134.1 eV for P $2p_{3/2}$. A sample of composition $SnP_{0.40}$ revealed similar binding shifts of 487.2 eV and 133.8 eV for Sn $3d_{5/2}$ and P $2p_{3/2}$ respectively. The XPS peak profiles for both samples (Figure 3.9.) are consistent with one environment for both tin and phosphorus. There is no evidence for the presence of tin oxides from the XPS profiles though the small peak centred at 139 eV may indicate the formation of some phosphate, this shift is however, higher than values reported in the literature.[95]

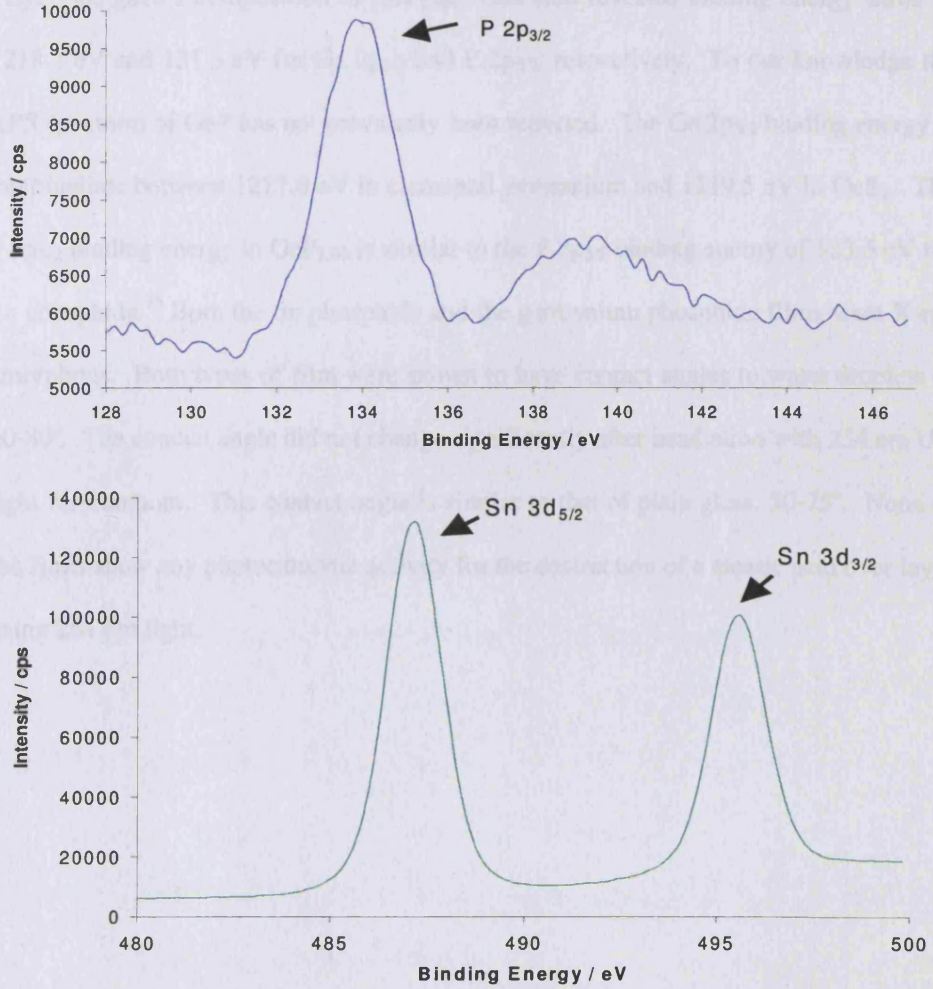

Figure 3.9. The XPS spectra for a sample of tin phosphide.

The XPS peak profiles for the GeP films observed after sputtering (Figure 3.10) are consistent with one environment for both germanium and phosphorus, although at the surface the shifts are slightly higher indicating perhaps, the presence of germanium phosphate. This is confirmed by observing a peak in the oxygen O_{1s} region that is not due to surface oxygen. After the first sputtering there is no evidence for the presence of germanium oxides or phosphate from the XPS profiles – the bulk of the film corresponds to GeP. XPS measurements on a sample of the film prepared by the dual source atmospheric pressure chemical vapour deposition reaction of $GeCl_4$ and $PCyc^{hex}H_2$ gave a composition of $GeP_{1.00}$. This film revealed binding energy shifts of 1218.2 eV and 131.5 eV for Ge $2p_{3/2}$ and P $2p_{3/2}$, respectively. To our knowledge the XPS spectrum of GeP has not previously been reported. The Ge $2p_{3/2}$ binding energy is intermediate between 1217.0 eV in elemental germanium and 1219.5 eV in GeS_2. The P $2p_{3/2}$ binding energy in $GeP_{1.00}$ is similar to the P $2p_{3/2}$ binding energy of 133.5 eV for tin phosphide.[95] Both the tin phosphide and the germanium phosphide films were X-ray amorphous. Both types of film were shown to have contact angles to water droplets of 60-80°. The contact angle did not change significantly after irradiation with 254 nm UV light for one hour. This contact angle is similar to that of plain glass, 50-75°. None of the films show any photocatalytic activity for the destruction of a stearic acid over layer using 254 nm light.

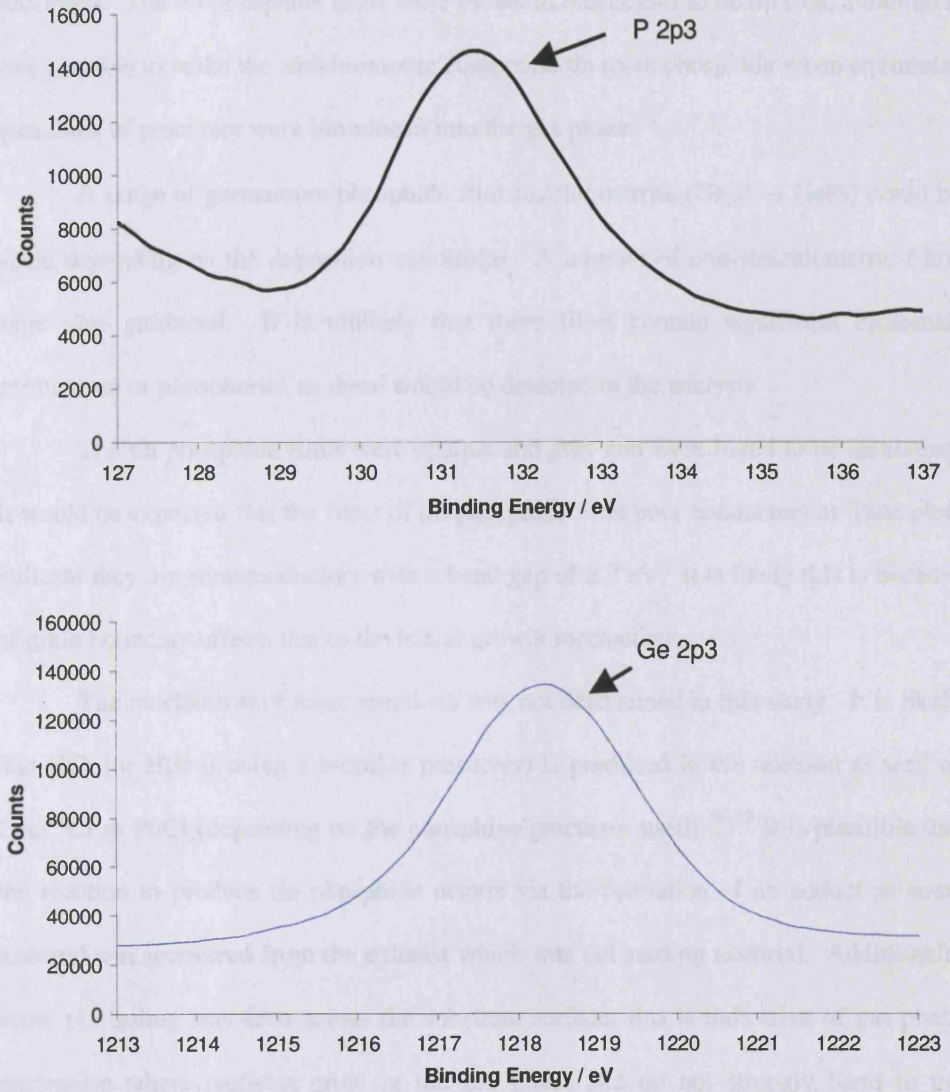

Figure 3.10. The post sputtering XPS spectra for a sample of germanium phosphide.

3.3.1.2 Discussion

Reaction of MCl_4 or MBr_4 (M = Sn or Ge) and a substituted phosphine ($PCyc^{hex}H_2$, $PCyc^{hex}{}_2H$, $PCyc^{hex}{}_3$ or $PhPH_2$) under atmospheric pressure chemical vapour deposition affords opaque films of tin or germanium phosphide on glass

substrates. The tin phosphide films were shown in most cases to be tin rich, although it was possible to make the stoichiometric compound tin monophosphide when equimolar quantities of precursor were introduced into the gas phase.

A range of germanium phosphide film stoichiometries ($Ge_3P \rightarrow GeP_2$) could be made depending on the deposition conditions. A number of non-stoichiometric films were also produced. It is unlikely that these films contain significant elemental germanium or phosphorus, as these would be detected in the analysis.

The tin phosphide films were opaque and grey and were found to be insulating. It would be expected that the films of tin phosphide were poor conductors as Tauc plots indicate they are semiconductors with a band gap of 2.2 eV. It is likely this is because of grain boundary effects due to the island growth mechanism.

The mechanism of these reactions was not determined in this study. It is likely that HCl (or HBr if using a bromide precursor) is produced in the reaction as well as $Cyc^{hex}Cl$ or PhCl (depending on the phosphine precursor used). [96,97] It is plausible that the reaction to produce tin phosphide occurs via the formation of an adduct as some material was recovered from the exhaust which was not starting material. Additionally some pin holing was seen across the substrate surface; this is indicative of gas phase nucleation where particles grow in the gas phase and do not strongly bond to the substrate surface and may be blown off or fall off during handling. Previous work also suggests that similar deposition processes occur via adducts.[98] No significant solid material was observed in the exhaust line of the experimental set up suggesting that this is not the case with the germanium phosphide system; the film formation onset temperature is higher in this system; this may be because gas phase adduct formation does not take place, and additional energy is required to form adducts at the surface, where as in the tin phosphide system adducts may merely decompose on the surface of

the substrate to form a film. These films show no Raman spectra. They shift the absorption edge of, and undergo less transmission and reflection than SiO_2 coated glass due to scattering haze. Analysis of the UV/Vis data using the Tauc method indicates a band gap of 2.2 eV for SnP and 1.1 eV for GeP. EDAX and electron probe results suggest that the composition over the surface of the glass is similar. SEM shows that whilst various morphologies are possible, one, that of spheres of tin phosphide predominates in samples of tin phosphide films. In the germanium phosphide samples a platelet type of island growth is observed.

There is no variation of film stoichiometry with different precursors where films are deposited. It was noted that discrete phases (such as $SnP_{1.33}$, $SnP_{1.00}$, $SnP_{0.66}$ and $SnP_{0.40}$ or Ge_2P, $GeP_{1.00}$, Ge_2P_3.) were seen and no intermediate phases were observed. With tin phosphide samples higher nitrogen flow rates had the effect of lowering the phosphorus content of the resultant films. Variation of the phosphorus or tin precursor flow rate appeared to not have a significant effect. This indicates that phosphorus precursor dilution is a limiting factor in the rate of reaction. Using di- and tri-substituted phosphines required higher substrate temperatures (600 °C) for films to form; this is most likely because there are a larger number of bonds to break and therefore more energy is required. Where films did form at lower substrate temperatures (500 °C) with the di- and tri- substituted phosphines they were lower in phosphorus content than those formed at higher substrate temperatures suggesting incomplete and partial reactions.

Germanium content in the films increased with the flow rate of the germanium precursor. A similar trend was not observed with the variation of flow rate of the phosphorus precursor. It appears to be the case that the concentration of germanium

precursor in the reactor is the limiting reagent. Where the flow of nitrogen gas is higher less phosphorus incorporation into the final film was observed.

The precursor halides and phosphines were chosen for this study as they are volatile and give sufficient carryover for APCVD. The phosphines are commercially available and do not have the toxicity and extreme pyrophoric characteristics of PH_3.

3.3.2 Copper Phosphide

3.3.2.1 Copper Phosphide Results

The reaction between copper metal and $PCyc^{hex}H_2$ afforded films of copper phosphide (Cu_3P). The process was studied at different temperatures and with different co-reactant "activating" metal halides (none, $SnCl_4$, $SbCl_5$, $TiCl_4$ and $SiCl_4$.) (Table 3.3).

The metal halides were not incorporated directly into the Cu_3P films. However, they did affect the film morphology and colour. Films were found to form uniformly at substrate temperatures of 500 °C from the reaction of copper sheets and $PCyc^{hex}H_2$. However, films could be produced at substrate temperatures as low as 300 °C. The films produced from the reaction of copper substrates and $PCyc^{hex}H_2$ were light grey in colour, and appeared unreflective. The use of a metal halide co-reactant ($SnCl_4$, $SbCl_5$, $TiCl_4$ or $SiCl_4$), led to darker grey films. All of the films passed the Scotch tape test and could not be marked by abrasion with a wet towel. They could however, be marked with a brass stylus or steel scalpel.

Table 3.3. Table of reaction conditions and micro-analytical results for the copper phosphide system.

Substrate Temperature / °C	Nitrogen Flow through MCl_x bubbler l/min (MCl_x) [Bubbler temperature / °C]	Nitrogen Flow through phosphine bubbler l/min / [Bubbler temperature / °C]	Make up nitrogen flow / substrate type	EDAX, EPMA and XRD analysis
500	0.3 ($SnCl_4$) [35]	0.3 [120]	1.0 / Copper	Amorphous Cu_3P.
600	0.3 ($SnCl_4$) [35]	0.3 [120]	1.0 / Copper	Crystalline Cu_3P
500	0.3 ($SiCl_4$) [35]	0.3 [120]	1.0 / Copper	Crystalline Cu_3P
600	0.3 ($SiCl_4$) [35]	0.3 [120]	1.0 / Copper	Crystalline Cu_3P
500	0.3 ($SbCl_5$) [110]	0.3 [120]	1.0 / Copper	Amorphous Cu_3P
600	0.3 ($SbCl_5$) [110]	0.3 [120]	1.0 / Copper	Amorphous Cu_3P
500	0.3 ($TiCl_4$) [35]	0.3 [120]	1.0 / Copper	Amorphous Cu_3P
600	0.3 ($TiCl_4$) [35]	0.3 [120]	1.0 / Copper	Crystalline Cu_3P
500	None	0.3 [120]	1.0 / Copper	Amorphous Cu_3P
600	None	0.3 [120]	1.0 / Copper	Amorphous Cu_3P

Raman microscopy was used to investigate the films. Raman scattering was not observed in any instance. It is believed that copper phosphides are poor Raman scatterers. No evidence of graphitic carbon or metal oxides was observed in any of the spectra.

Compositional analysis of the films was conducted by EDAX and EPMA studies. The results indicate that the films are free of halide and metal from the co-

reactant. These results show that only one phase of copper phosphide (Cu_3P) was produced. This phase was invariant across the surface of the substrate.

SEM analysis of the films revealed that film growth occurred via an island growth mechanism. The morphology of the sample could be varied by using a different co-reactant or by changing the temperature of the experiment. It was found that an increase in substrate temperature led to the production of thicker films and more consistent morphological ordering. Variation of the co-reactant decided the overall morphology (Figure 3.11.).

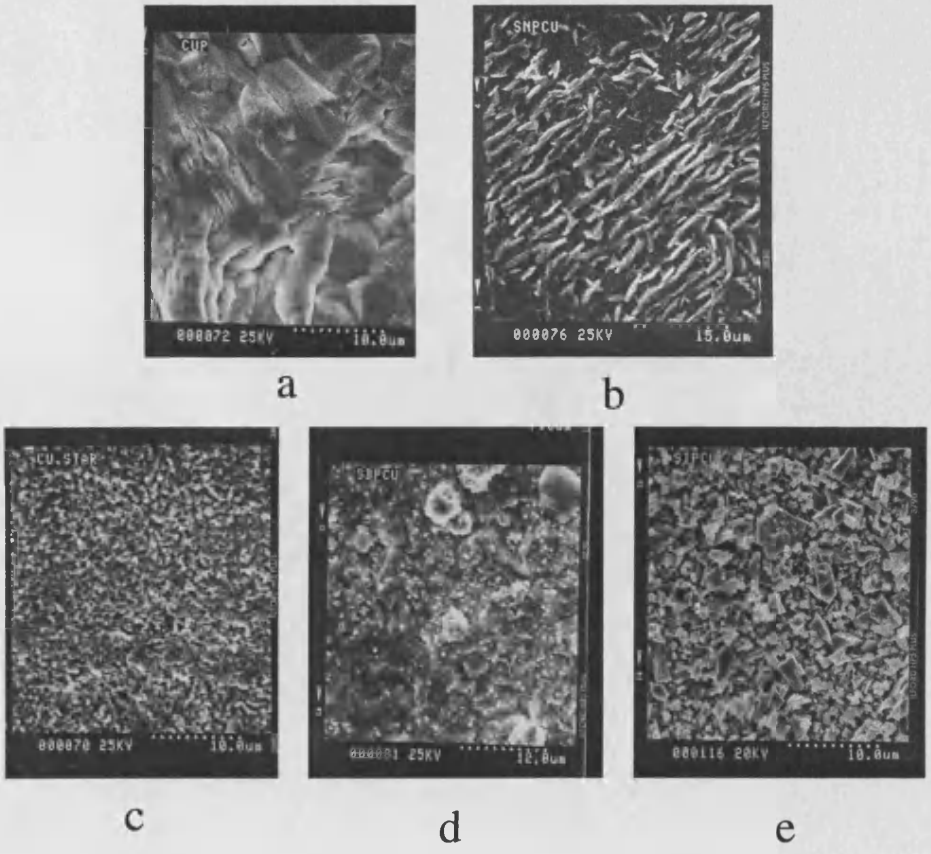

Figure 3.11. SEM secondary electron images of thin film samples produced from the reaction of a copper substrate and PCychexH2 (a) and $SnCl_4$ (b) $TiCl_4$ (c) $SbCl_5$ (d) and $SiCl_4$ (e).

XPS measurements on a sample of Cu_3P composition, revealed binding energy shifts of 933.2 eV and 129.2 eV for Cu $2p_{3/2}$ and P $2p_{3/2}$ respectively. These are in agreement with previous values for transition metal phosphides (Figure 3.12.).[95] The copper phosphide films were in the main X-ray amorphous. Samples produced at 600 °C were crystalline by X-ray diffraction investigation and identified as Cu_3P (Figure 3.13.). [99] Indexing indicated a hexagonal lattice with parameters a = 6.972(1) Å and c = 7.148(1) Å similar to those seen in the literature.[99]

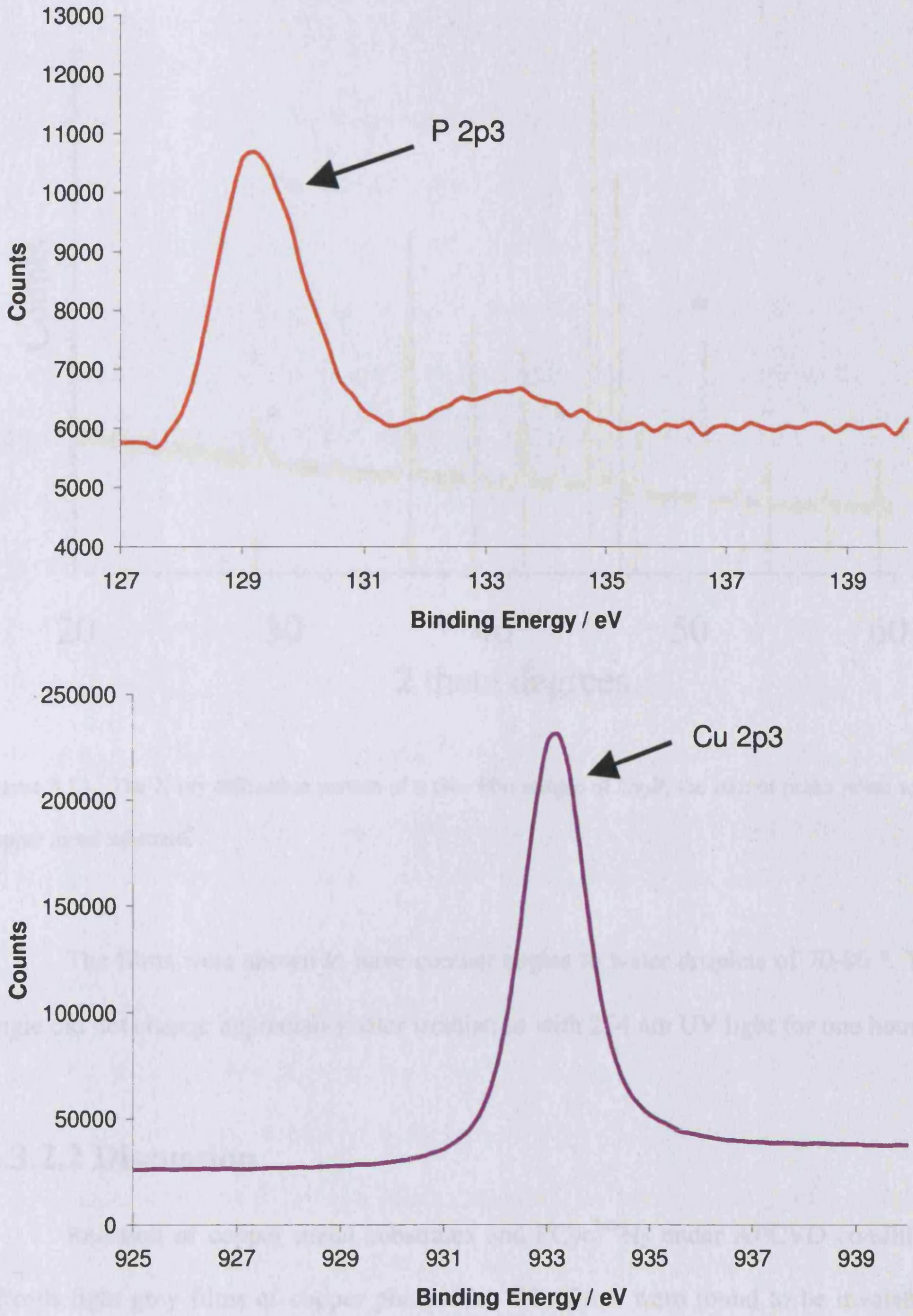

Figure 3.12. XPS spectra for a sample of copper phosphide.

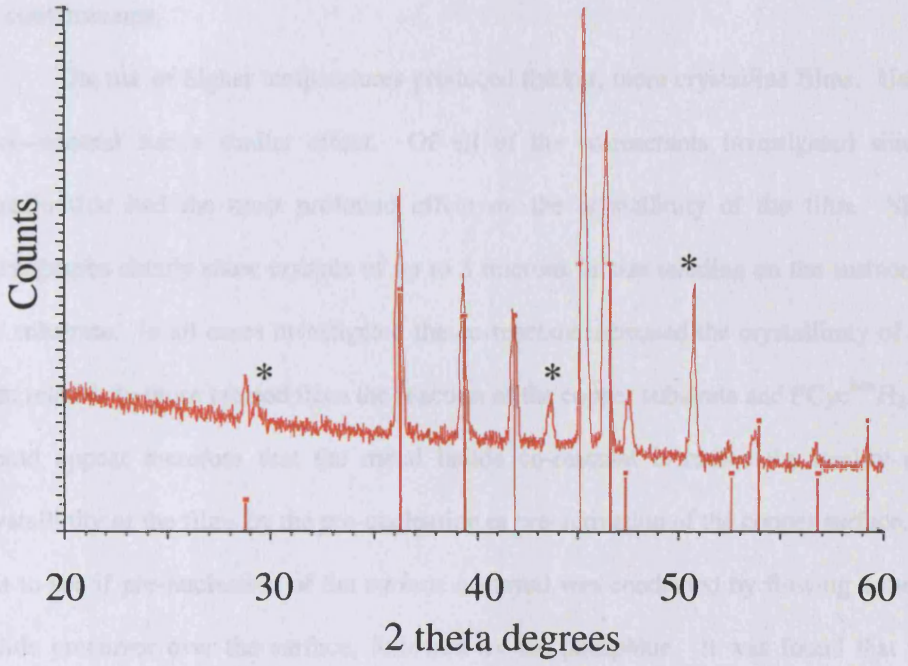

Figure 3.13. The X-ray diffraction pattern of a thin film sample of Cu_3P, the starred peaks relate to the copper metal substrate.

The films were shown to have contact angles to water droplets of 70-80 °. This angle did not change appreciably after irradiation with 254 nm UV light for one hour.

3.3.2.2 Discussion

Reaction of copper metal substrates and $PCyc^{hex}H_2$ under APCVD conditions affords light grey films of copper phosphide. The films were found to be insulating, which is surprising as metal rich phosphides tend to be metallic in character. If a sensitising co-reactant metal halide is used in the reaction the resultant films appear

darker in tone. In all cases the films are shown to be monophasic Cu_3P by EDAX with no contaminants.

The use of higher temperatures produced thicker, more crystalline films. Using a co-reactant had a similar effect. Of all of the co-reactants investigated silicon tetrachloride had the most profound effect on the crystallinity of the film. SEM micrographs clearly show crystals of up to 3 microns in size residing on the surface of the substrate. In all cases investigated the co-reactant increased the crystallinity of the film relative to those created from the reaction of the copper substrate and $PCyc^{hex}H_2$. It would appear therefore that the metal halide co-reactant increases the quality and crystallinity of the films by the pre-nucleation or pre-activation of the copper surface. A test to see if pre-nucleation of the surface occurred was conducted by flowing a metal halide precursor over the surface, followed by the phosphine. It was found that the films were no different from those runs using only the phosphine. Therefore the effect of the metal halide is probably a gas phase effect. It is likely that the metal halide reacts with the $PCyc^{hex}H_2$ in the gas phase to produce activated species, and that the by products of this reaction contain the metal from the metal halide. This is suggested by the failure of EDAX to detect any metal other than copper in the films.

These films display no Raman spectra, indicating the absence of graphitic carbon and some metal oxides from the films. SEM analysis (Figure 3.12) indicates that various morphologies are obtainable depending on the co-reactant and conditions used. There is no variation of film stoichiometry with different conditions or co-reactant. One distinct phase (Cu_3P) was observed. EDAX and EPMA studies indicated that the composition over the substrate is uniform and that no metal from co-reactant precursors was found in the films.

Similar reactions were carried out with iron and aluminium substrates. In these cases films of iron oxide (Fe_2O_3) and aluminium oxide (Al_2O_3) respectively were produced. The reaction between a copper metal substrate and $PCyc^{hex}H_2$ is hence somewhat unique under the conditions evaluated.

The mechanism of this reaction was not investigated but it is likely that the co-reactants activate the gas phase species towards surface reaction.

3.3.3 Silicon Phosphide

3.3.3.1 Silicon Phosphide Results and Discussion

A number of films were made on tin oxide coated glass substrates under dual source atmospheric pressure chemical vapour deposition (APCVD) conditions from the reaction of $SiCl_4$ or $SiBr_4$ and a substituted phosphine ($PCyc^{hex}H_2$). The process was studied at different substrate temperatures and flow rates of precursor (Table 3.4.). No film could be grown at substrate temperatures below 600 °C; above 600 °C uniform films were obtained. The films appeared an almost metallic grey colour but were quite dull and as such unreflective. The films prepared at higher precursor flow rates showed some pinhole defects due to gas phase nucleation or possibly adduct formation as non-starting material debris was recovered from the reactor exhaust. Those films prepared at higher temperatures exhibited some birefringence due to thickness effects. None of the films could be marked with a wet towel or brass stylus but could be marked with a steel scalpel. All of the films passed the Scotch tape test. The films showed no optical change after storage in air for six months. Raman was used to investigate all of the films. No Raman scattering due to the films was observed. No free carbon was detected by Raman in the samples prepared using monocyclohexyl phosphine.

Table 3.4. Table showing reaction conditions and micro-analytical results for the silicon phosphide system.

Substrate Temperature / °C	Nitrogen Flow through SiX_4 bubbler l/min (SiX_4) [Bubbler temperature / °C]	Nitrogen Flow through R_xPH_{3-x} bubbler l/min (R_xPH_{3-x}) [Bubbler temperature / °C]	Nitrogen Flow of make up gas l/min.	EDAX and Electron Probe analysis
600	0.5 ($SiCl_4$) [35]	0.5 ($CyhexPH_2$) [120]	1.0	No Film
600	0.5 ($SiCl_4$) [35]	0.7 ($CyhexPH_2$) [120]	1.0	No Film
600	0.7 ($SiCl_4$) [35]	0.5 ($CyhexPH_2$) [120]	1.0	No Film
600	0.3 ($SiCl_4$) [35]	0.7 ($CyhexPH_2$) [120]	1.0	Si and P present
600	0.7 ($SiCl_4$) [35]	0.3 ($CyhexPH_2$) [120]	1.0	No Film
600	0.5 ($SiBr_4$) [200]	0.5 ($CyhexPH_2$) [120]	1.0	No Film
600	0.5 ($SiBr_4$) [200]	0.7 ($CyhexPH_2$) [120]	1.0	No Film
600	0.7 ($SiBr_4$) [200]	0.5 ($CyhexPH_2$) [120]	1.0	No Film
600	0.3 ($SiBr_4$) [200]	0.7 ($CyhexPH_2$) [120]	1.0	No Film
600	0.7 ($SiBr_4$) [200]	0.3 ($CyhexPH_2$) [120]	1.0	Si and P present
600	0.3 ($SiBr_4$) [200]	0.7 ($CyhexPH_2$) [120]	1.2	Si and P present
600	0.3 ($SiBr_4$) [200]	0.7 ($CyhexPH_2$) [120]	1.4	Si and P present
600	0.3 ($SiBr_4$) [200]	0.7 ($CyhexPH_2$) [120]	1.6	Si and P present
600	0.3 ($SiBr_4$) [200]	0.7 ($CyhexPH_2$) [120]	1.8	Si and P present
550	0.3 ($SiBr_4$) [200]	0.7 ($CyhexPH_2$) [120]	2.0	Si and P present

Compositional analysis of the films was determined by EDXA and electron probe measurements (summarised in Table 3.4.). The results of both experiments show that the films are free of chlorine and contain silicon and phosphorus. In the case of EDXA breakthrough to the underlying glass was confirmed as potassium was observed in the spectra. It was difficult to correct for this based on a sample of plain glass that mainly consists of silicon and oxygen and as such no conclusions are drawn about the possible stoichiometry of the films based on EDXA.

SEM analysis of the films (figure 3.14.) showed mostly discrete particles on the surface, indicative of an island growth mechanism.

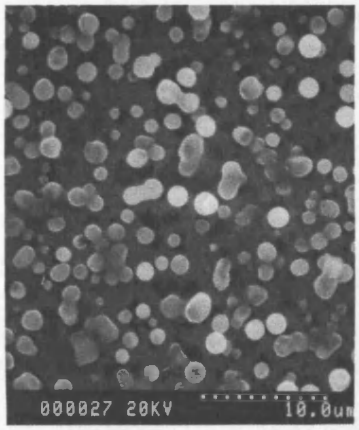

Figure 3.14. SEM photograph of a silicon phosphide thin film.

The optical properties of the films were studied by UV absorption between 400 nm and 1100 nm and reflectance / transmission measurements. All samples showed a shift in the absorption edge relative to the plain glass substrate. The films showed minimal reflectivity (3%), less so than the substrate (10%). The transmission spectra were indicative of hazing; this is due to scattering by particles in the film of a similar

size to the wavelength of the light. No Tauc plot to indicate an indirect band gap was possible as the film was opaque.

XPS measurements on a sample (Figure 3.15.), revealed binding energy shifts of 105.8 eV and 134.2 eV for Si 2p and P $2p_{3/2}$ respectively confirming the presence of silicon and phosphorus in the films. The phosphorus shift is quite high compared to literature values for other phosphides, [95] but comparable to that seen with tin phosphide (133.5 eV). The silicon shift is similar to that of tetramethyl silicon (105.9 eV).[10]

Analysis by X-ray diffraction indicated the formation of a crystalline phase in the film (Figure 3.16.); attempts to index this pattern to anything containing silicon and phosphorus have proved to be unsuccessful. There are a large number of densely packed peaks of similar intensity in the XRD pattern; this may be indicative of a multiphase film.

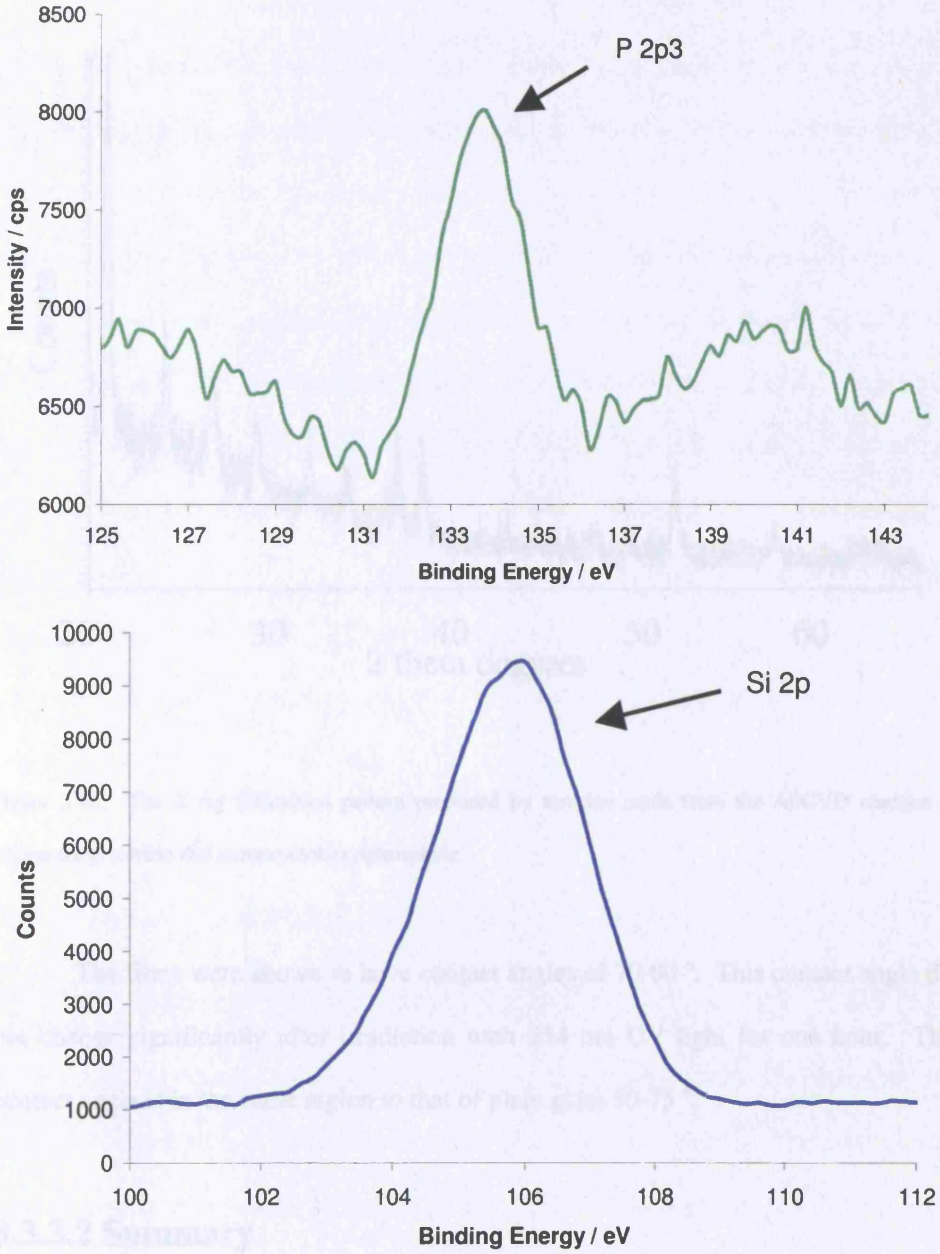

Figure 3.15. XPS peaks for a sample produced from the reaction of silicon tetrabromide and monocyclohexylphosphine.

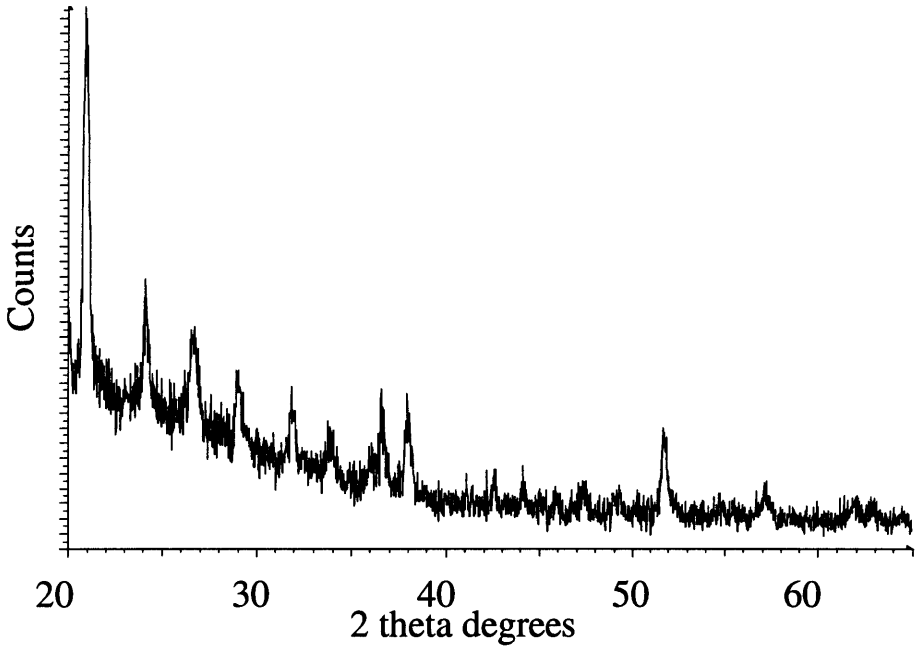

Figure 3.16. The X-ray diffraction pattern produced by samples made from the APCVD reaction of silicon tetrabromide and monocyclohexylphosphine.

The films were shown to have contact angles of 70-80 °. This contact angle did not change significantly after irradiation with 254 nm UV light for one hour. This contact angle is in the same region to that of plain glass 50-75 °.

3.3.3.2 Summary

Reaction of silicon tetrabromide and monocyclohexylphosphine under atmospheric pressure chemical vapour deposition affords opaque films on tin dioxide coated glass substrates. The films were found to be insulating.

These films show no Raman spectra. They shift the absorption edge of, and undergo less transmission and reflection than SnO_2 coated glass. EDAX and electron probe results suggest that the films contain silicon and phosphorus. There is a large amount of oxygen present in the analysis and it is unclear if this originates from the deposited film or the substrate. SEM indicates that a single morphology dominates.

In some cases an absence of phosphorus was seen from EDXA or XPS. These films are likely to contain silicon dioxide. This is because silicon is extremely oxophillic: should any oxygen enter the system then it would be expected that silicon oxides would be produced preferentially to any other possible product. XPS analysis is inconclusive because a large amount of oxygen is present at the surface and upon etching. Film deposition did not occur on other substrates, only on tin dioxide coated glass. Silicon wafers, aluminium, copper and iron sheets were all tried but no film was observed that was silicon phosphide.

3.3.4 Antimony Phosphide

3.3.4.1 Antimony Phosphide Results

APCVD reaction of antimony pentachloride and monocyclohexylphosphine led to the production of thin films of antimony metal on glass substrates. The process was studied at different substrate temperatures and carrier gas flow conditions (table 3.5.).

Table 3.5. Table of reaction conditions and micro-analytical results for the antimony phosphide system.

Substrate Temperature / °C	Nitrogen Flow through $SbCl_5$ bubbler l/min ($SbCl_5$) [Bubbler temperature / °C]	Nitrogen Flow through R_xPH_{3-x} bubbler l/min (R_xPH_{3-x}) [Bubbler temperature / °C]	Nitrogen Flow of make up gas l/min.	EDAX and Electron Probe analysis
300	0.5 ($SbCl_5$) [120]	0.5 ($CyhexPH_2$) [120]	1.0	Sb Metal
350	0.5 ($SbCl_5$) [120]	0.5 ($CyhexPH_2$) [120]	1.0	Sb Metal
400	0.5 ($SbCl_5$) [120]	0.5 ($CyhexPH_2$) [120]	1.0	Sb Metal
450	0.5 ($SbCl_5$) [120]	0.5 ($CyhexPH_2$) [120]	1.0	Sb Metal
500	0.5 ($SbCl_5$) [120]	0.5 ($CyhexPH_2$) [120]	1.0	Sb Metal
550	0.5 ($SbCl_5$) [120]	0.5 ($CyhexPH_2$) [120]	1.0	Sb Metal
600	0.5 ($SbCl_5$) [120]	0.5 ($CyhexPH_2$) [120]	1.0	Sb Metal, 1% P
600	0.5 ($SbCl_5$) [120]	0.3 ($CyhexPH_2$) [120]	1.0	Sb Metal, 1% P
600	0.3 ($SbCl_5$) [120]	0.5 ($CyhexPH_2$) [120]	1.0	Sb Metal, 1% P
600	0.5 ($SbCl_5$) [120]	0.3 ($^tbutPH_2$) [70]	1.0	No Film
600	0.3 ($SbCl_5$) [120]	0.5 ($^tbutPH_2$) [70]	1.0	No Film

Films were deposited at temperatures as low as 300°C and up to 600°C, the maximum possible with the experimental set up. All of the films appeared uniform. All of the films had a dull, dark metallic grey in appearance; as such they were unreflective. They all failed the Scotch tape test, could be marked by a brass stylus and could be wiped from the substrate using a dry cloth. No optical change was apparent in the films over the course of three months.

SEM analysis of the films highlighted that films grew via island growth mechanism and that cubic crystals of antimony metal were produced on the substrate (Figure 3.17.).

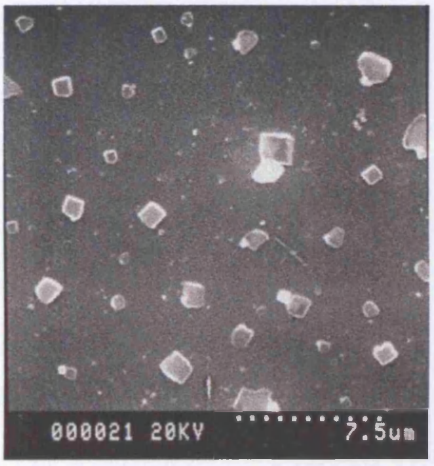

Figure 3.17. An SEM picture of an antimony (phosphide?) sample.

Compositional analysis of the films was determined by EDXA. In all cases some breakthrough to the underlying glass substrate was observed; this was corrected for based on a sample of plain glass. The results indicate that the films consist almost entirely of antimony. In some cases small amounts of phosphorus (~1%) were observed. EDXA of a small area of the substrate devoid of antimony metal crystallites indicated a film composition of SbP.

The optical properties of the films were investigated using transmission / reflectance measurements and UV absorption between 1100 nm and 400 nm. All samples showed a shift in absorption edge relative to plain glass due to absorption by the deposited film. The films showed minimal reflectivity (2%) and transmission (5-10%) between 1100 nm and 400 nm. The films were examined under X-ray diffraction conditions and returned XRD patterns identical to those produced previously by

antimony metal (figure 3.18.).[99] Indexing indicated a trigonal hexagonal lattice with lattice parameters: a = 4.3224(8) Å and c = 11.312(2) Å, indicating a slightly larger unit cell than reported previously.[99]

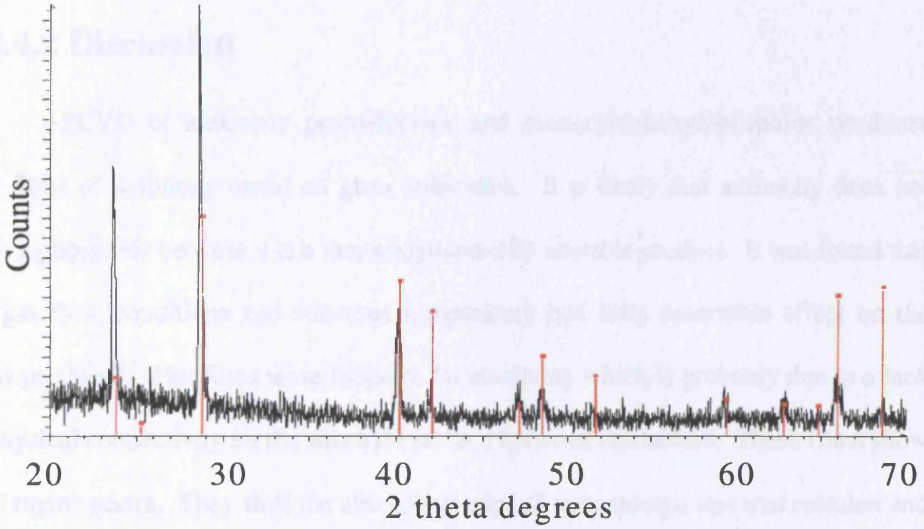

Figure 3.18. XRD pattern indicating the formation of antimony metal

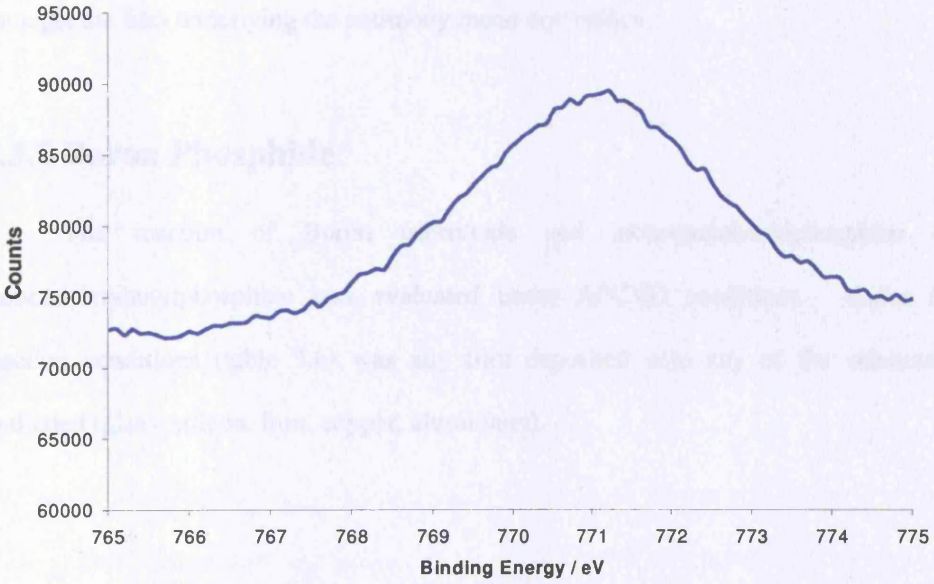

Figure 3.19. The XPS peak of antimony in an antimony (phosphide?) sample.

XPS measurements on a sample of antimony (phosphide?) (Figure 3.19.) revealed binding energies of 771.1 eV for Sb3p3. If any phosphorus was present it was beyond the detectable limit of 1% of this method of analysis.

3.3.4.2 Discussion

APCVD of antimony pentachloride and monocyclohexylphosphine produces thin films of antimony metal on glass substrates. It is likely that antimony does not form a phosphide because it is a thermodynamically unstable product. It was found that the gas flow conditions and substrate temperature had little detectable effect on the films produced. The films were found to be insulating which is probably due to a lack of physical connectivity on the substrate surface between crystallites. These films show no Raman spectra. They shift the absorption edge of and undergo less transmission and reflection of light than the glass substrates used in these deposition experiments. All of the films have similar morphologies. EDXA indicates the presence of phosphorus amongst the film underlying the antimony metal crystallites.

3.3.5 Boron Phosphide

The reaction of Boron tribromide and monocyclohexylphosphine or monotertiarybutylphosphine was evaluated under APCVD conditions. Under no reaction conditions (table 3.6) was any film deposited onto any of the substrates evaluated (glass, silicon, iron, copper, aluminium).

Table 3.6. Table of reaction conditions and micro-analytical results for the boron phosphide system.

Substrate Temperature / °C	Nitrogen Flow through BBr_3 bubbler l/min (BBr_3) [Bubbler temperature / °C]	Nitrogen Flow through R_xPH_{3-x} bubbler l/min (R_xPH_{3-x}) [Bubbler temperature / °C]	Nitrogen Flow of make up gas l/min.	EDAX and Electron Probe analysis
600	0.5 (BBr_3) [35]	0.5 ($CyhexPH_2$) [120]	1.0	No Film
600	0.5 (BBr_3) [35]	0.7 ($CyhexPH_2$) [120]	1.0	No Film
600	0.7 (BBr_3) [35]	0.5 ($CyhexPH_2$) [120]	1.0	No Film
600	0.3 (BBr_3) [35]	0.7 ($CyhexPH_2$) [120]	1.0	No Film
600	0.7 (BBr_3) [35]	0.3 ($CyhexPH_2$) [120]	1.0	No Film

It is anticipated that reaction temperature was too low. Previous examples quoted in the literature of the reaction of phosphine gas and boron tribromide were conducted in excess of 1000°C.[81-84] This temperature was impossible to achieve with the reactor system used here, which had a maximum substrate temperature of 650 °C.

3.4 Conclusions

Reaction of metal halides ($SnCl_4$, $SnBr_4$, $GeCl_4$, $GeBr_4$) and a substituted phosphine ($PCyc^{hex}H_2$, $PCyc^{hex}{}_2H$, $PCyc^{hex}{}_3$ or $PhPH_2$) under atmospheric pressure chemical vapour deposition affords opaque films of tin or translucent films germanium phosphide on glass substrates. The films show good surface coverage, adhesion and reasonable uniformity. Tin phosphide films with a range of stoichiometries ($SnP_{0.40}$ - $SnP_{1.33}$) could be obtained depending on the experimental conditions used; these were all opaque in appearance and electrical insulators. A Tauc plot indicates that tin

monophosphide films are semi-conducting with a band gap of 2.2 eV. Germanium phosphide films with a range of stoichiometries (Ge_3P – GeP_2) could be obtained. These were all translucent in appearance and poor electrical conductors. A Tauc plot indicated that germanium monophosphide films are semi-conducting with an indirect band gap of 1.1eV.

Reaction of a copper metal substrate and monocyclohexylphosphine under APCVD conditions affords thin films of copper phosphide (Cu_3P). The use of a co-reactant produces thicker, more crystalline films. The films show excellent surface coverage, uniformity and good adhesion properties. Copper phosphide films (Cu_3P) could be obtained; these were grey in appearance and electrical insulators. Reaction of antimony pentachloride and monocyclohexylphosphine lead to the production of antimony metal films. EDXA evidence indicates a small level of phosphorus in regions of the substrate that are clear from metal crystallites; XPS is inconclusive. Boron tribromide was reacted with monocyclohexylphosphine under APCVD conditions; however, no product was observed.

In this chapter we have examined the reaction conditions for producing thin films of main group metal phosphides under atmospheric pressure chemical vapour deposition conditions. A variety of metal phosphides can be formed with a wide range of stoichiometries. Higher substrate temperatures led to the formation of monophosphides and phosphorous rich phosphides. Lower substrate temperatures tended to lead to the production of phosphorous deficient phosphides; the incomplete reaction of the phosphide precursor on the substrate surface may be responsible for these unusual stiochiometries.

Chapter 4 – Main Group Metal Oxides

4.1 Introduction

Facile routes to metal oxide thin films are of interest because of their applicability to the microelectronics and gas sensing industries. In this chapter the formation of metal oxide thin films under atmospheric pressure conditions is discussed. In the following chapter the gas sensing properties of these films are presented and evaluated.

4.1.1 Gallium Oxide

Gallium oxide (Ga_2O_3) is a wide band gap semiconductor material, [100,101] with a host of current and potential applications. It has received attention as a compound semiconductor surface passivator, [102] as a luminescent phosphor [103-105] as a potential deep ultraviolet transparent conducting oxide, [106] as a nanomaterial [107-109] and in acid / base catalysis.[110-112] Recently Ga_2O_3 prepared by PVD has received attention as a gas sensor.[113] It has been reported as a having a response to oxidising gases at elevated temperature (>900 °C) [114] and a response to reducing gases at lower temperatures (500 °C).[115]

Thin films of Ga_2O_3 have been prepared in a variety of ways. Physical vapour deposition methods such as magnetron sputtering and electron-beam evaporation have been utilised.[116,117] Low-pressure chemical vapour deposition of gallium fluoroalkoxides,[118] homoleptic gallium alkoxides,[119] and gallium tris-hexafluoroacetylacetonate has also been conducted.[120]

4.1.2 Tin Oxide

Tin oxide (SnO_2) is a well-known material with a wide variety of applications and uses. It has received attention as a chemical sensor [121] and has been prepared for this purpose by a variety of methods including; sputtering,[121] sol gel techniques [122] and thick film screen-printing.[123] Tin oxide finds particular use as a gas sensor because it is a wide band gap (3.6 eV) n-type semiconductor, whose conductivity is due to oxygen vacancies.[124]

Tin oxide has a found use as a catalyst support.[125] An investigation into the nano-scale properties has been undertaken.[126]

Thin films of tin dioxide haves been prepared in a variety of different ways. Physical methods such as PVD, [121] thermal evaporation [127] and spray pyrolysis [128] have all been conducted. Chemical vapour deposition methods are well known ranging from low-pressure examples [129] to metal organic CVD,[130] and atmospheric pressure CVD; which is used in the glazing industry to make low emmisivity coatings on glass.[131,132]

4.1.3 Antimony Oxide

Antimony oxide (Sb_2O_3) has received interest as a co-catalyst, [133] and as an additive in flame resistant polymers. [134] Additionally it has been used as the base for a new type of glass,[135] and has an application within ceramics.[136] Several investigations have been conducted into antimony oxide as a nanomaterial.[137-139] There is increasing interest in antimony oxide as a gas sensor.[140,141]

Antimony oxide thin films have received attention. An extensive investigation into the electrical, optical and structural properties of films produced by thermal vacuum evaporation has taken place.[142,143] Additionally investigations by sputtering [144] and spray pyrolysis have also been conducted. Metal organic CVD has been conducted using precursors such as antimony butoxide or tri-ethyl antimony [141] deposited at 600 °C. Aerosol assisted CVD has been conducted using antimony (V) chloride and water.[145,146] It was found in all cases that films of Sb_2O_3 were produced, though there was some contamination with Sb_6O_{13}.

4.1.4 Niobium Oxide

Niobium oxide has received much attention due to its wide ranging industrial applications particularly in the Optoelectronic industry.[147] Niobium oxide has been prepared by a variety of methods including: oxidation of metallic niobium, hydrolysis of niobium alkoxides, niobium (V) chloride or alkali metal niobiate.[148] Niobium oxide has a wide range of crystal structures with at least 12 having been identified.[99] Niobium oxide is an insulator but becomes an n-type semiconductor at non-stoichiometric levels of oxygen. Niobium oxide and niobium oxide derived materials have found functions within a variety of fields such as: battery technology,[149,150] electrochromism,[151] solar cells,[152,153] catalysis [154,155] and gas sensors.[156,157]

The production of thin films of niobium oxide has been studied extensively. Films have been produced using a variety of physical methods such as pulsed laser deposition,[157] magnetron sputtering, [158-160] and thermal oxidation, [161] chemical methods such as sol gel and notably a variety of chemical vapour deposition techniques.[162-168]

4.2 Results

Atmospheric pressure chemical vapour deposition reaction of a metal chloride (where the metal is gallium, tin, antimony or niobium) and methanol or ethyl acetate (as an oxygen source.) led to the creation of metal oxide thin films on a variety of substrates: glass, silicon, quartz, iron, aluminium and gas sensor. The process was studied across a range of different substrate temperatures and flow conditions.

Table 4.1. Table of reaction conditions and micro-analytical results for the gallium oxide system.

Substrate Temperature / °C	Nitrogen Flow through MX_4 bubbler l/min (MX_4) [Bubbler temperature / °C]	Nitrogen Flow through Oxygen precursor bubbler l/min (precursor) [Bubbler temperature / °C]	Nitrogen Flow of make up gas l/min.	EDAX and Electron Probe analysis
400	0.5 ($GaCl_3$) [150]	0.5 (CH_3OH) [50]	1.0	Ga_2O_3
450	0.5 ($GaCl_3$) [150]	0.5 (CH_3OH) [50]	1.4	Ga_2O_3
500	0.5 ($GaCl_3$) [150]	0.5 (CH_3OH) [50]	1.8	Ga_2O_3
550	0.5 ($GaCl_3$) [150]	0.5 (CH_3OH) [50]	1.0	Ga_2O_3
600	0.5 ($GaCl_3$) [150]	0.5 (CH_3OH) [50]	1.0	Ga_2O_3
600	0.3 ($GaCl_3$) [150]	0.5 (CH_3OH) [50]	1.0	Ga_2O_3
600	0.3 ($GaCl_3$) [150]	0.7 (CH_3OH) [50]	1.0	Ga_2O_3
600	0.5 ($GaCl_3$) [150]	0.3 (CH_3OH) [50]	1.0	Ga_2O_3
600	0.7 ($GaCl_3$) [150]	0.3 (CH_3OH) [50]	1.0	Ga_2O_3
600	0.5 ($GaCl_3$) [150]	0.5 (CH_3OH) [50]	1.0	Ga_2O_3
600	0.5 ($GaCl_3$) [150]	0.5 (CH_3OH) [50]	1.5	Ga_2O_3

Table 4.2. Table of reaction conditions and micro-analytical results for the tin oxide system.

Substrate Temperature / °C	Nitrogen Flow through MX_4 bubbler l/min (MX_4) [Bubbler temperature / °C]	Nitrogen Flow through Oxygen precursor bubbler l/min (precursor) [Bubbler temperature / °C]	Nitrogen Flow of make up gas l/min.	EDAX and Electron Probe analysis
400	0.5 ($SnCl_4$) [35]	0.5 ($C_2H_5OCOCH_3$) [45]	1.0	SnO_2
450	0.5 ($SnCl_4$) [35]	0.5 ($C_2H_5OCOCH_3$) [45]	1.0	SnO_2
500	0.5 ($SnCl_4$) [35]	0.5 ($C_2H_5OCOCH_3$) [45]	1.0	SnO_2
550	0.5 ($SnCl_4$) [35]	0.5 ($C_2H_5OCOCH_3$) [45]	1.0	SnO_2
600	0.5 ($SnCl_4$) [35]	0.5 ($C_2H_5OCOCH_3$) [45]	1.0	SnO_2
600	0.3 ($SnCl_4$) [35]	0.5 ($C_2H_5OCOCH_3$) [45]	1.0	SnO_2
600	0.7 ($SnCl_4$) [35]	0.5 ($C_2H_5OCOCH_3$) [45]	1.0	SnO_2
600	0.5 ($SnCl_4$) [35]	0.3 ($C_2H_5OCOCH_3$) [45]	1.0	SnO_2
600	0.5 ($SnCl_4$) [35]	0.7 ($C_2H_5OCOCH_3$) [45]	1.0	SnO_2
600	0.3 ($SnCl_4$) [35]	0.7 ($C_2H_5OCOCH_3$) [45]	1.0	SnO_2
600	0.7 ($SnCl_4$) [35]	0.3 ($C_2H_5OCOCH_3$) [45]	1.0	SnO_2
600	0.5 ($SnCl_4$) [35]	0.5 ($C_2H_5OCOCH_3$) [45]	1.5	SnO_2

Table 4.3. Table of reaction conditions and micro-analytical results for the antimony oxide system.

Substrate Temperature / °C	Nitrogen Flow through MX_4 bubbler l/min (MX_4) [Bubbler temperature / °C]	Nitrogen Flow through Oxygen precursor bubbler l/min (precursor) [Bubbler temperature / °C]	Nitrogen Flow of make up gas l/min.	EDAX and Electron Probe analysis
550	0.5 ($SbCl_5$) [120]	0.5 ($C_2H_5OCOCH_3$) [45]	1.0	Sb_2O_3
600	0.5 ($SbCl_5$) [120]	0.5 ($C_2H_5OCOCH_3$) [45]	1.0	Sb_2O_3
600	0.5 ($SbCl_5$) [120]	0.3 ($C_2H_5OCOCH_3$) [45]	1.0	No Film
600	0.5 ($SbCl_5$) [120]	0.7 ($C_2H_5OCOCH_3$) [45]	1.0	Sb_2O_3
600	0.7 ($SbCl_5$) [120]	0.5 ($C_2H_5OCOCH_3$) [45]	1.0	No Film
600	0.3 ($SbCl_5$) [120]	0.5 ($C_2H_5OCOCH_3$) [45]	1.0	Sb_2O_3
600	0.7 ($SbCl_5$) [120]	0.3 ($C_2H_5OCOCH_3$) [45]	1.0	No Film
600	0.3 ($SbCl_5$) [120]	0.7 ($C_2H_5OCOCH_3$) [45]	1.0	Sb_2O_3
600	0.5 ($SbCl_5$) [120]	0.5 ($C_2H_5OCOCH_3$) [45]	1.5	Sb_2O_3

Table 4.4. Table of reaction conditions and micro-analytical results for the niobium oxide system.

Substrate Temperature / °C	Nitrogen Flow through MX_4 bubbler l/min (MX_4) [Bubbler temperature / °C]	Nitrogen Flow through Oxygen precursor bubbler l/min (precursor) [Bubbler temperature / °C]	Nitrogen Flow of make up gas l/min.	EDAX and Electron Probe analysis
600	0.3 ($NbCl_5$) [220]	1.8 ($C_2H_5OCOCH_3$) [45]	2.0	Nb_2O_5
600	0.5 ($NbCl_5$) [220]	1.8 ($C_2H_5OCOCH_3$) [45]	2.0	No Film
600	0.7 (NbCl5) [220]	1.8 ($C_2H_5OCOCH_3$) [45]	2.0	No Film

Films would not grow at substrate temperatures lower than 400 °C for gallium oxide and tin oxide films or 550 °C for antimony oxide. Niobium oxide films would only grow at 600 °C. Uniform films were obtained at 550 °C and above in the tin and gallium oxide systems or at 600 °C for the niobium and antimony systems. In all cases films appeared transparent, unreflective, colourless and birefringence was observed. The films all passed the Scotch tape test and were resistant to marking by a wet towel or a brass stylus, but could be marked by a steel scalpel. None of the films showed any change in their appearance on storage in air for six months.

Compositional analysis was determined by EPMA and EDXA and indicated that the films had single compositions: Ga_2O_3, SnO_2, Sb_2O_3 and Nb_2O_5. With EDXA some breakthrough to the underlying glass substrate was seen. The EDXA results showed that the films were free from contaminants such as chlorine. In the case of thinner films

such as the niobium oxide some breakthrough to the underlying substrate was observed. This was corrected for based on a sample of the pure substrate. Further analysis revealed that the samples of niobium, tin and gallium oxides had a uniform composition and thickness across the surface of the substrate in this deposition set up; this is in contrast to what has been observed earlier with the phosphides in chapter 3. These results indicate it is possible to create single-phase metal oxide thin films by APCVD.

Scanning electron microscopy analysis of the films indicated that, in all cases, deposition occurred through an island growth mechanism. The morphology varied according to the material being made (Figure 4.1.). Gallium oxide films appear to have circular surface growths whereas tin, niobium and antimony oxides consisted of grains of material forming a coherent coating across the surface of the substrate. There was no change or even variation of film morphology with differing substrate. Direct measurements of film thickness using scanning electron microscopy were made with samples of gallium oxide and tin oxide. Gallium oxide samples had film thicknesses of between 500 nm at 400 °C and 900 nm at 600 °C. Tin oxide was similar giving thicknesses of 500 nm at 400 °C and 1200 nm at 600 °C. Surface coverage appeared insufficient to directly measure film thickness of the antimony or niobium oxide films. In all cases experiments were conducted for one minute; this leads to nominal growth rates of 500 $nm.min^{-1}$ at 400 °C for both tin and gallium oxides and growth rates of 900 $nm.min^{-1}$ and 1200 $nm.min^{-1}$ for gallium oxide and tin oxide respectively at 600 °C.

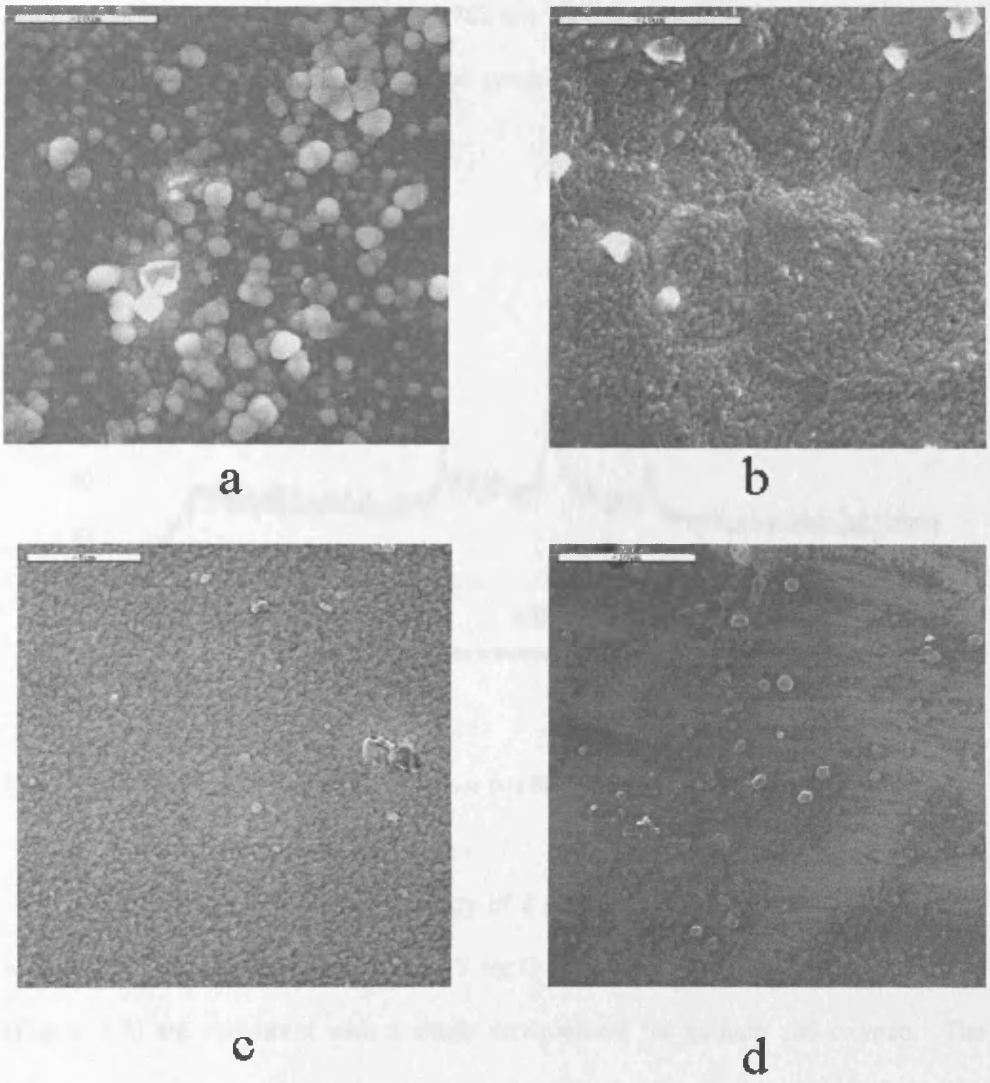

Figure 4.1. Typical SEM pictures for: a gallium oxide, b antimony oxide, c tin oxide, d niobium oxide. In all cases samples were produced by APCVD from the metal chloride and ethyl acetate with a reactor temperature of 600 °C. The scale bars represent 10 μm for a, b and d and 5 μm for c.

All of the films were investigated using Raman microscopy but only in the case of tin oxide (SnO_2) was a pattern due to the deposited film observed (Figure 4.2.). This Raman pattern is similar to that which has been previously published in the literature

with peaks appearing at 476, 638 and 782 cm^{-1}.[91-93] Raman microscopy did, however, indicate the absence of impurities such as graphitic carbon.

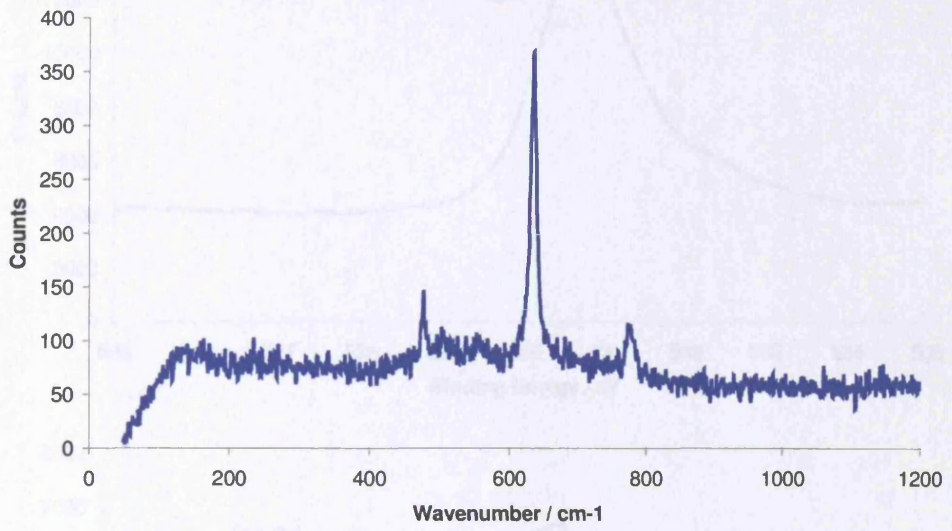

Figure 4.2. The Raman pattern given by a tin oxide thin film sample.

X-ray photoelectron spectroscopy of a Ga_2O_3 sample revealed binding energy shifts of 20.3 eV for Ga 3d and 530.6 eV for O 1s respectively. The XPS peak profiles (Figure 4.3) are consistent with a single environment for gallium and oxygen. The binding energy shifts are in agreement with previous literature values of 20.3 eV for Ga 3d and 530.5 eV for O 1s.[95]

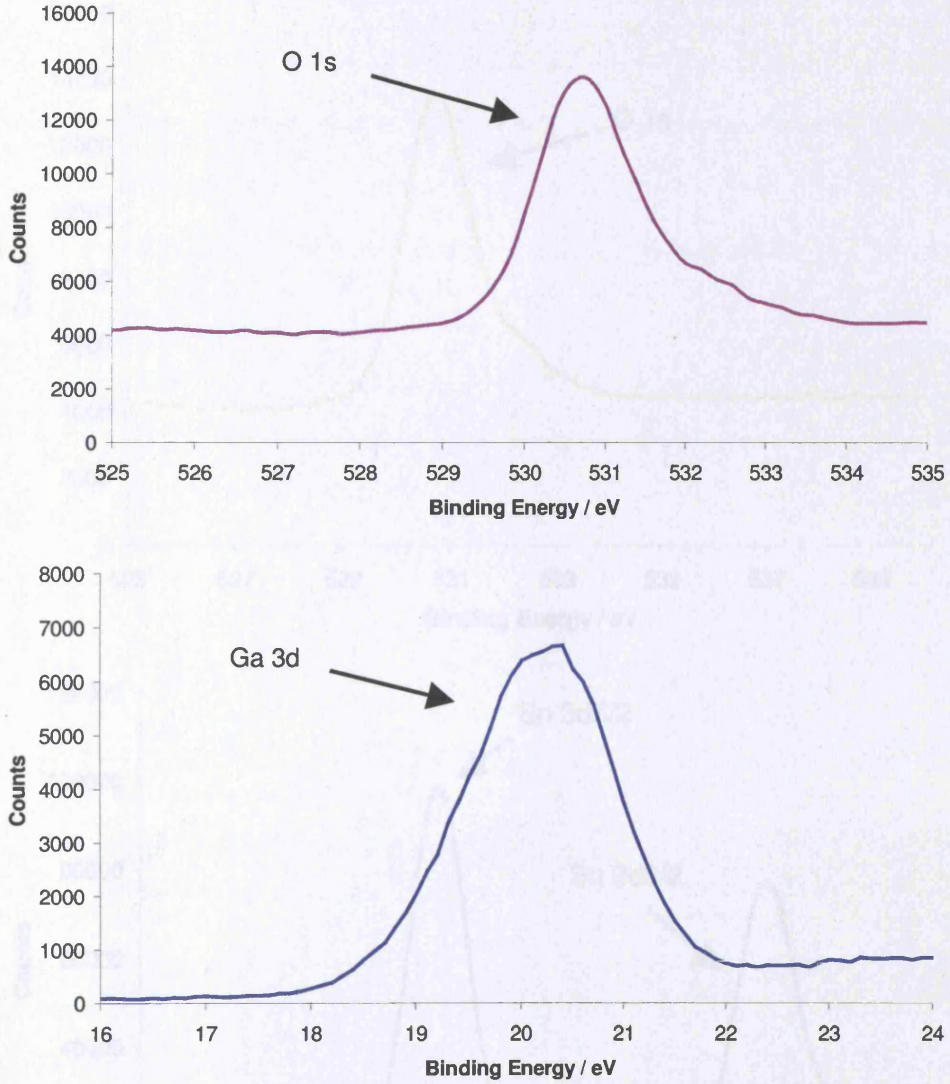

Figure 4.3. XPS peaks produced from a sample of gallium oxide.

X-ray photoelectron spectroscopy of a sample of SnO_2 revealed binding energy shifts of 530.6 eV for O 1s and 487.2 eV for Sn 3d5/2. The XPS peak profiles (Figure 4.4.) are consistent with a single environment for tin and oxygen. The binding energy shifts are in agreement with previous literature values of 487.3 eV for Sn 3d5/2 and 530.5 eV for O 1s.[95]

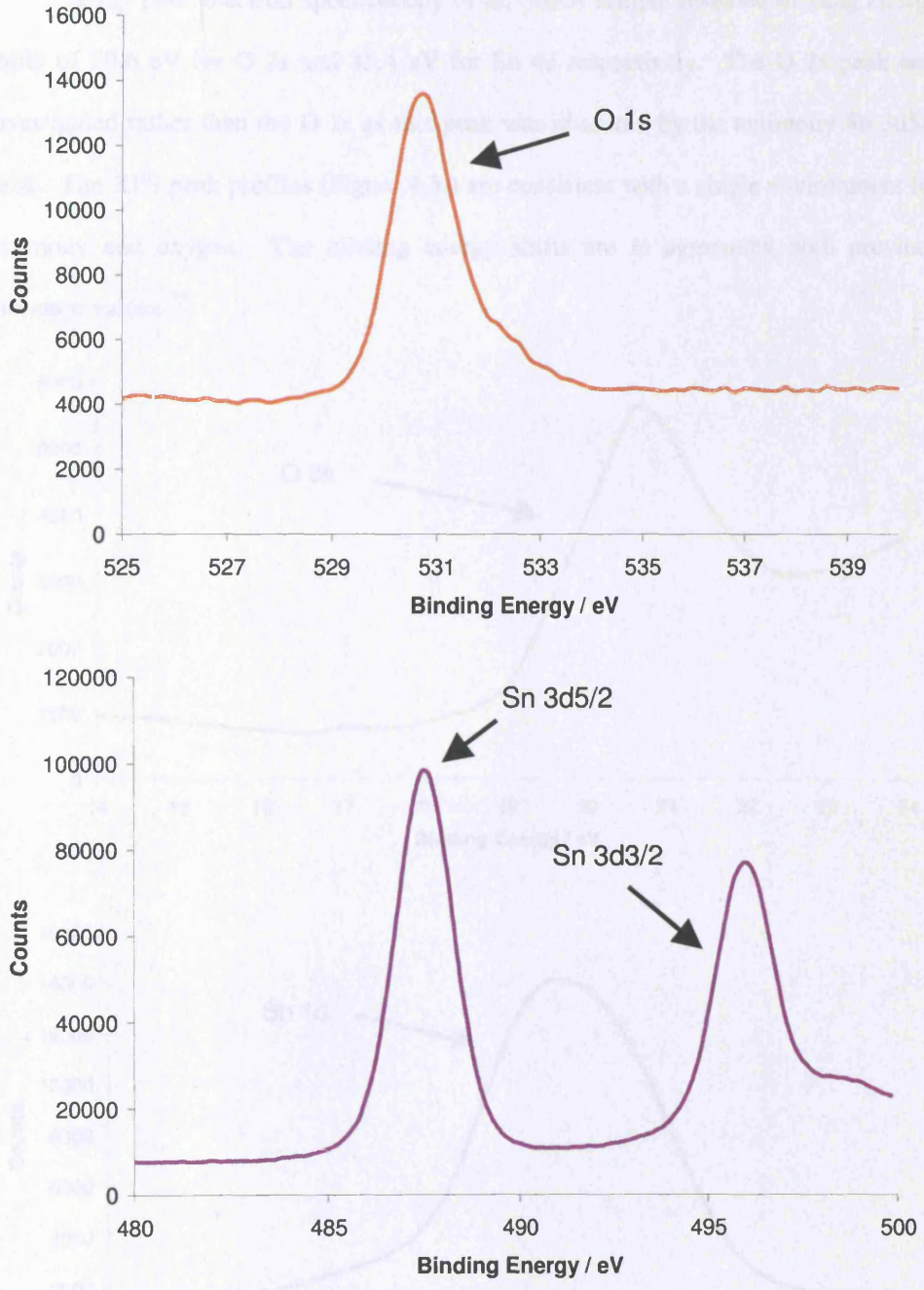

Figure 4.4. XPS peaks produced from a sample of tin oxide.

X-ray photoelectron spectroscopy of an Sb_2O_3 sample revealed binding energy shifts of 20.6 eV for O 2s and 35.4 eV for Sb 4d respectively. The O 2s peak was investigated rather than the O 1s as this peak was obscured by the antimony Sb 3d5/2 peak. The XPS peak profiles (Figure 4.5.) are consistent with a single environment for antimony and oxygen. The binding energy shifts are in agreement with previous literature values.[95]

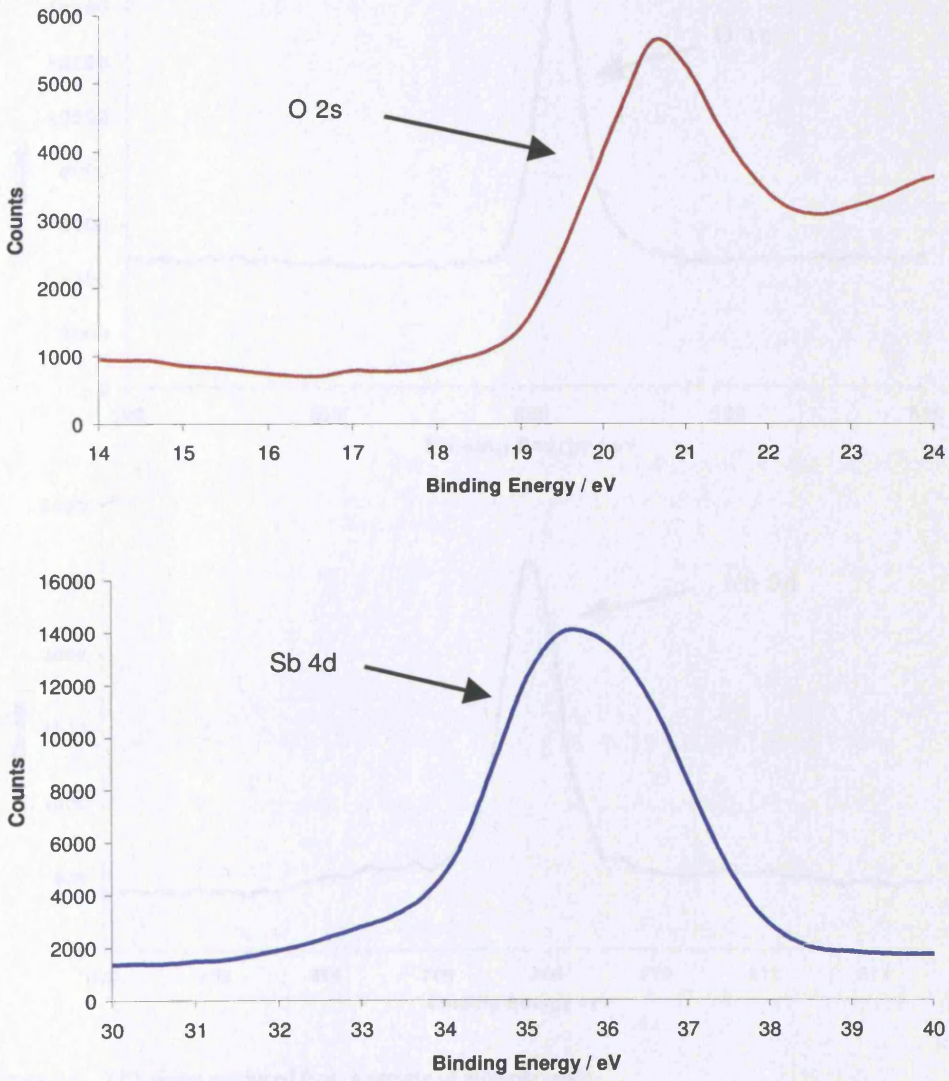

Figure 4.5. XPS peaks produced from a sample of antimony oxide.

X-ray photoelectron spectroscopy of a sample of Nb_2O_5 revealed binding energy shifts of 530.6 eV for O 1s and 207.0 eV for Nb 3d respectively. The XPS peak profiles (Figure 4.6.) are consistent with a single environment for niobium and oxygen. The binding energy shifts are in agreement with previous literature values of 207.2 eV for Nb 3d and 530.5 eV for O 1s.[95]

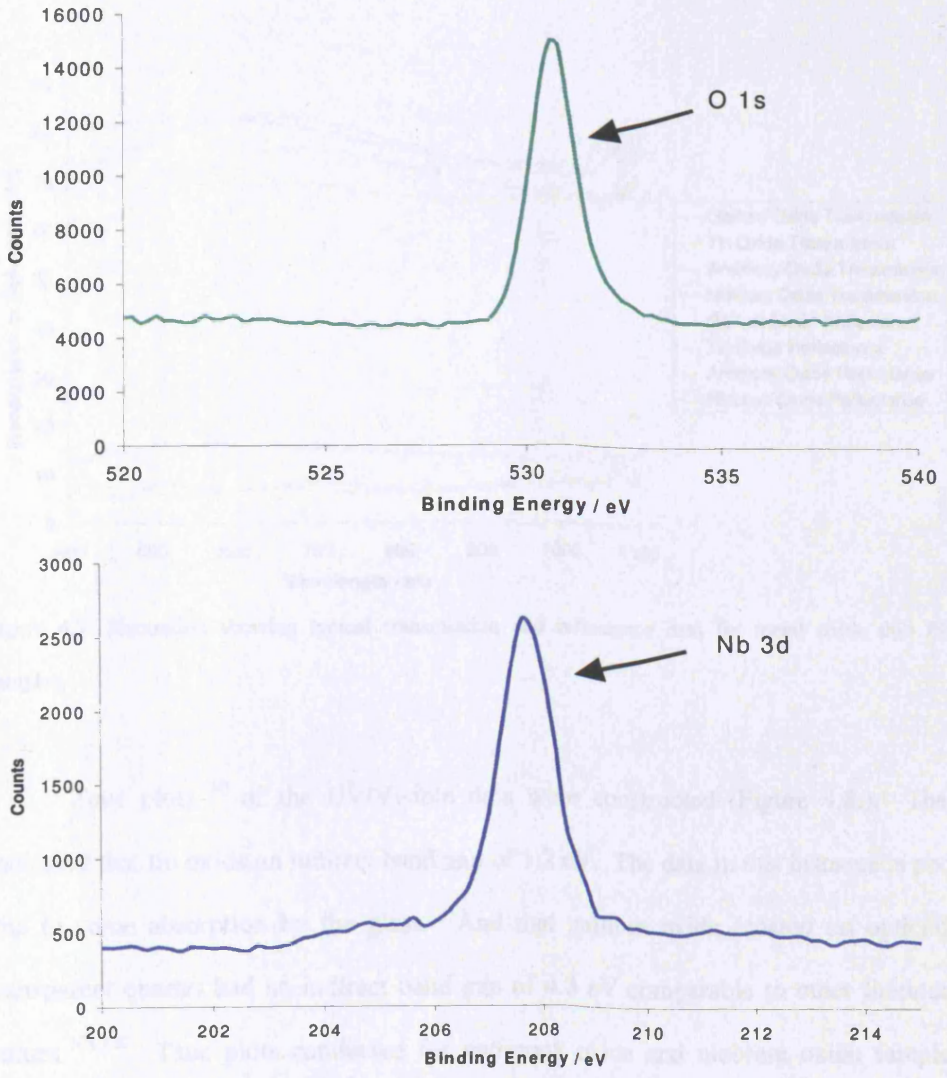

Figure 4.6. XPS peaks produced from a sample of niobium oxide.

The optical properties of the films were investigated using reflectance, transmission and UV/Visible measurements between 400 – 1100 nm. All samples showed a slight shift in the adsorption edge towards the visible relative to a plain glass substrate. The films displayed minimal reflectivity (5-15 %) and high transmission (60-80 %) (Figure 4.7.).

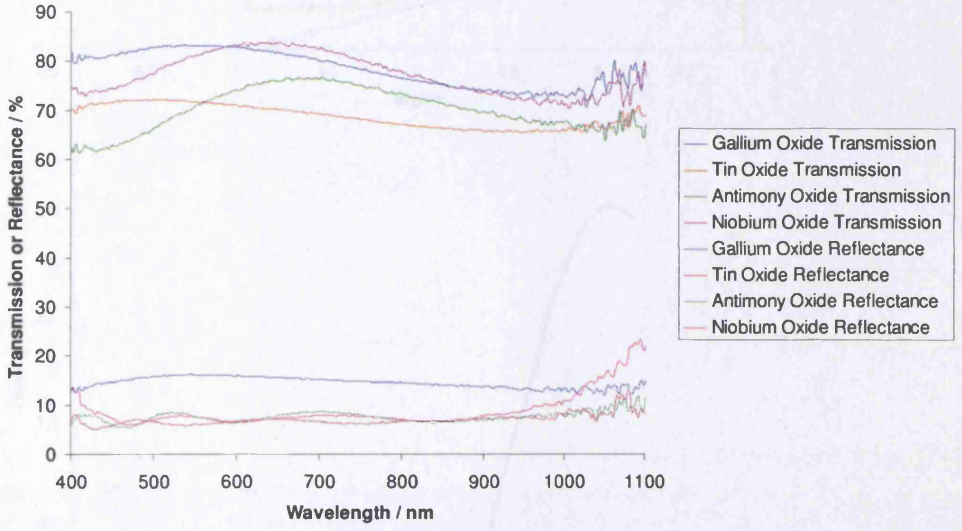

Figure 4.7. Illustration showing typical transmission and reflectance data for metal oxide thin film samples.

Tauc plots [10] of the UV/Visible data were constructed (Figure 4.8.). They indicated that tin oxide an indirect band gap of 1.2 eV. The data in this instance is poor due to some absorption by the glass. And that gallium oxide (coated on optically transparent quartz) had an indirect band gap of 4.3 eV comparable to other literature values.[101,102] Tauc plots conducted for antimony oxide and niobium oxide samples failed to elucidate information on the band structure of these materials.

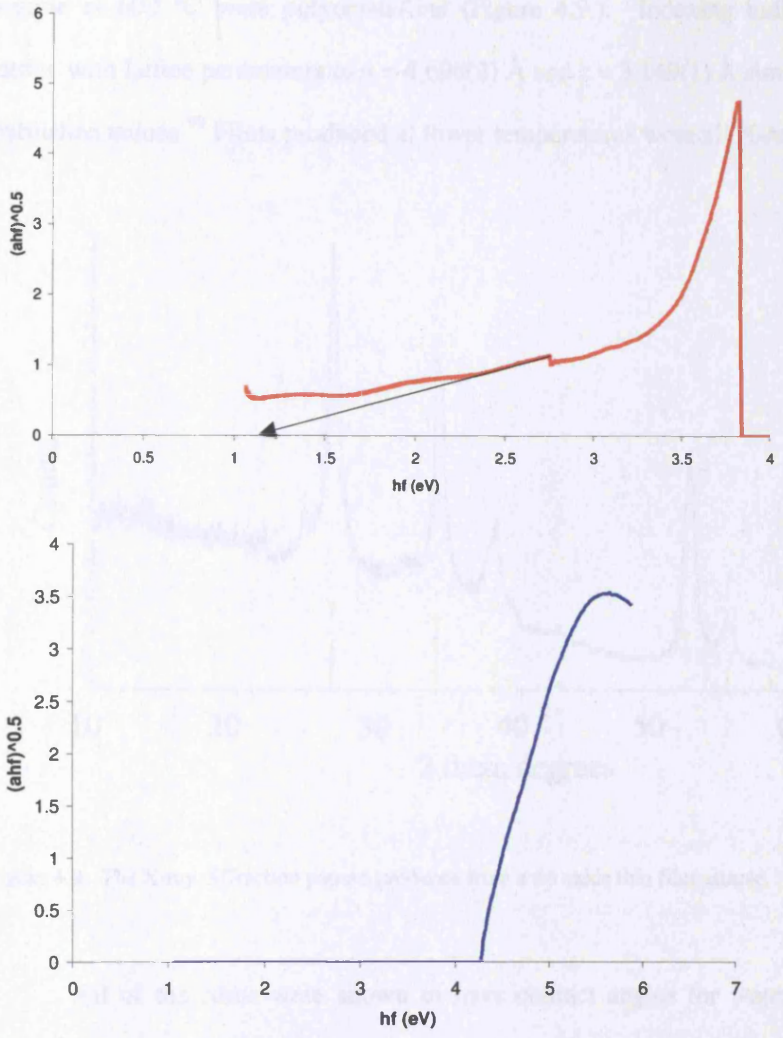

Figure 4.8. Tauc plots for tin oxide on glass (red) and gallium oxide on quartz (blue).

Previous work on the growth of gallium oxide thin films under low-pressure chemical vapour deposition conditions at 600°C indicates that these are X-ray amorphous. Similarly the gallium oxide thin films produced by atmospheric pressure chemical vapour deposition in this work were X-ray amorphous, as are the thin films of niobium oxide and antimony oxide. Tin oxide films produced under the APCVD

regime at 600 °C were polycrystalline (Figure 4.9.). Indexing indicated tetragonal lattice with lattice parameters of a = 4.698(2) Å and c = 3.149(1) Å similar to previously published values.[99] Films produced at lower temperatures were all X-ray amorphous.

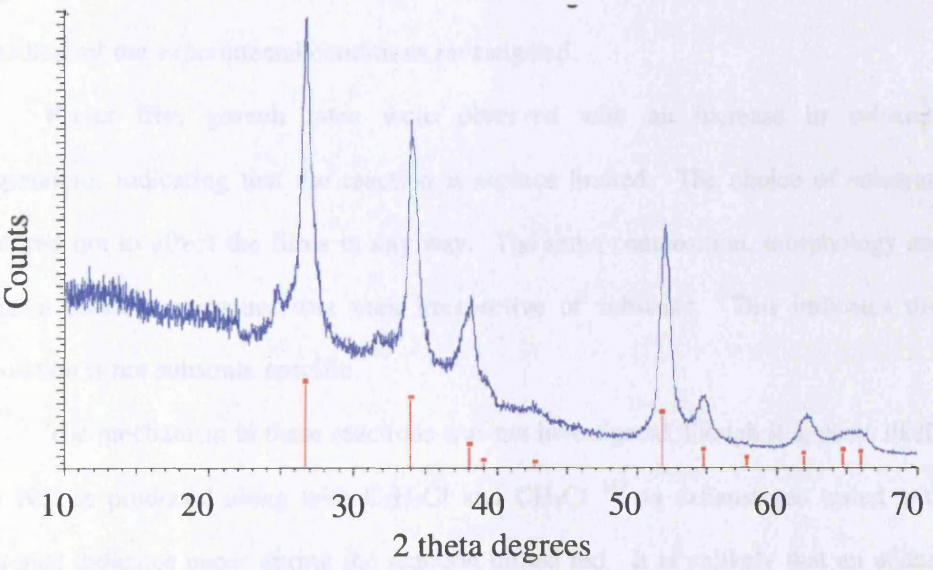

Figure 4.9. The X-ray diffraction pattern produced from a tin oxide thin film sample.

All of the films were shown to have contact angles for water droplets in the region of 65 - 85°. This is similar to that of plain glass 60-75°.

4.3 Discussion

Reaction of metal chloride and methanol or ethyl acetate under atmospheric pressure chemical vapour deposition conditions affords thin films of metal oxides on a range of substrates. The metal oxide films were found to be of a uniform phase regardless of the experimental conditions investigated.

Faster film growth rates were observed with an increase in substrate temperature, indicating that the reaction is surface limited. The choice of substrate appeared not to affect the films in any way. The same composition, morphology and reaction onset temperature was seen irrespective of substrate. This indicates that deposition is not substrate specific.

The mechanism in these reactions was not investigated, though it appears likely that HCl is produced along with C_2H_5Cl and CH_3Cl [169] as exhaust gas tested with universal indicator paper during the reaction turned red. It is unlikely that an adduct reaction occurs as no material other than product was recovered from the reactor. No evidence of pin holing was observed as has been observed where an adduct mechanism is likely to be taking place.[170]

Reaction of metal (M = Sb, Nb, Sn or Ga) chlorides with methanol or ethyl acetate under APCVD conditions affords clear films of metal oxides on a variety of substrates. The films show good surface coverage, adhesion and uniformity. Oxide films of a single phase were obtained. These were colourless in appearance and were electrical insulators at room temperature, with the exception of gallium oxide, which had low electrical conductivity at room temperature.

Previous work done on gallium oxide films produced by CVD [118-120] indicates some similar results to those obtained here. Films deposited from the CVD of $Ga(hfac)_3$

at temperatures between 450 and 500 °C were X-ray amorphous and had a uniform, smooth morphology as determined by scanning electron microscopy though were black in appearance; this was not observed here and may have been caused by carbon contamination within the film. Similarly deposition from homoleptic gallium alkoxide complexes led to the production of thin films of gallium oxide which were also X-ray amorphous and had a fine-grained surface structure as determined by SEM. XPS analysis conducted on these samples gave binding energies of 21.1 eV for Ga 3d and 531.8 eV for O 1s. This is in reasonable agreement with binding energies elucidated here of 20.3 eV for Ga 3d and 531.8 eV for O 1s. Gallium oxide films deposited from the APCVD reaction of gallium chloride and methanol or ethyl acetate were also X-ray amorphous. The main difference between the films seems to be one of morphology. The surface of the APCVD films investigated here is relatively uneven and rough. There is evidence of gas phase nucleation in that the surface consists mainly of interlinking spheres. However, there is an absence of "pin holing" normally associated with gas phase nucleation and seen in chapter 3 with tin phosphide. Additionally no solid material was recovered from the reactor exhaust as is usually the case where gas phase nucleation is observed. It is perhaps the case that nucleation can occur in the gas phase but due to precursor species concentration or gas phase residence time being low means that particle growth is surface limited.

The tin oxide films produced here share similar properties and characteristics with tin oxide produced by APCVD in other work. The same fine-grained columnar growth found here is also seen elsewhere.[130-132] APCVD produced films are highly adherent to the substrate surface; this may prove to be an advantage over thick film technologies used in the production of sensor materials.

Previous work on the production of antimony oxide thin films by CVD and thermal evaporation show some similarities with the antimony oxide films produced here. Films of antimony oxide produced by thermal evaporation of Sb_2O_3 powder were made up of small grains of antimony oxide; these were typically in the range of 50 – 150 nm across in size. The films were shown to be crystalline by XRD. Likewise niobium oxide films grown from the CVD of niobium alkoxides produced crystalline films. In this instance however, a strictly island growth mechanism is seen with particles typically around 2 microns in diameter. Multiple phases were observed in these reaction systems. Some Sb_6O_{13} was observed amongst the Sb_2O_3 on the substrate. These were found to increase if oxygen was added to the reactant gas flow. This is in contrast to what is observed here. No mixed phases were observed, only Sb_2O_3 was found, although it is difficult to be exact about this as the oxygen 1s and antimony 3d5/2 peaks overlap and the signals from the oxygen 2s and antimony 4d are close together and affected by preferential sputtering, which destabilises the baseline reading and distorts chemical shift peak shapes.[95] The Sb_2O_3 films were X-ray amorphous and an island growth mechanism prevailed.

The niobium oxide films produced here have properties and characteristics in sharp contrast to those produced using the same reaction and methodology in work done previously.[171] At 600 °C in previous work a high surface coverage and columnar style island growth is observed; in this work however, surface coverage is much more sparse and there is no columnar character to the surface particle growth. This could be because the experiments in the previous work were conducted for a greater length of time, typically 3 minutes rather than the one-minute employed with the current work. The

films produced here were not found to be crystalline by XRD, in stark contrast to the previous work, nor was a Raman spectrum observed.

4.4 Conclusion

Metal oxide films were formed on a variety of substrates from the APCVD reaction of metal chlorides and ethyl acetate or methanol between temperatures of 400 and 600 °C. The films display good surface coverage, adhesion and uniformity. Films of single-phase gallium oxide (Ga_2O_3), tin oxide (SnO_2), antimony oxide (Sb_2O_3) and niobium oxide (Nb_2O_5) were formed. These films were colourless in appearance.
In this chapter we have examined the production of some metal oxide thin films. In the next chapter we evaluate these metal oxide thin films as gas sensors.

Chapter 5 – Gas Sensing

5.1 Introduction

The production of thin films by CVD affords inexpensive, adhesive, reproducible films with low impurity levels, [172] and may therefore provide an advantageous method of producing gas sensors. APCVD in particular is of interest because of fast growth rates and high surface coverage.[173, 174] CVD methods are directly compatible with Si – micro fabrication technology. It is important to evaluate whether the generally dense films produced by CVD are compatible with solid-state oxide gas-sensors. Typically solid-state oxide gas-sensors are made by screen-printing and tend to be very porous.

The current widely held view of gas sensors [7] states that the conductivity of semi-conducting oxides in air is determined by the trapping of electrons in surface states associated with surface absorbed oxygen. If interstitials or oxygen vacancies are immobile in the lattice, then the behaviour is described in terms of electron distribution between bulk and surface states. The surface conductivity is sensitive to small amounts of reactive gas as catalytic surface processes result in a change in the surface coverage of the oxygen surface trap states. If oxygen defects are mobile within the lattice then the conductivity is determined by the equilibrium between bulk lattice defects and oxygen in the gas phase, and sensitivity to trace reactive gases is lost. A further case for gas sensing can arise where there is a time dependence on the equilibration of lattice and surface states. Conductivity time dependence can also be observed as a result of lattice defect migration, which alters the potential and thus the charge carrier distribution near the surface. Due to a micro-structural effect part of the conductivity is gas sensitive due to modification in surface reactions whilst the conductivity contributed

by the bulk is not gas sensitive.[8] If the films are especially thin (100's of nm) then dense films such as those produced by CVD methodology may produce high quality gas sensors. Semiconductor gas sensors are either n-type or p-type; this affects the type of gas response they provide. In an n-type semi-conducting oxide, such as tin oxide, oxygen adsorption decreases the charge carrier density at the surface; this is balanced by the charge carried on the ionised donors. A p-type semi-conducting oxide in contrast has an increased charge carrier density at the surface due to adsorption; this increase in charge is balanced by holes in the valence band.

5.1.1 Gallium Oxide

Gallium oxide has received an extensive amount of attention as a solid-state gas sensor prepared by physical vapour deposition methods such as magnetron sputtering and electron beam evaporation.[116, 117] It has been reported to have a response to reducing gases at lower temperatures (~500 °C) [114] and a response to oxidizing gases at elevated temperatures (> 900 °C).[115]

5.1.2 Antimony Oxide

Pure antimony oxide has received scant attention for its gas sensing properties, though antimony oxide gas sensors have been produced via MOCVD using antimony (III) alkoxides where preliminary results suggest a rapid response to methane gas and a full recovery on the removal of the gas.[175] More usually a few weight percent of antimony oxide is doped into tin oxide to aid selectivity towards hydrocarbons.[176]

5.1.3 Niobium Oxide

Niobium oxide sensors have been produced using pulsed laser deposition [157] and screen-printing.[156] The response of these niobium oxide sensors has been evaluated using a variety of gases such as methanol, carbon monoxide and ammonia. In all cases a quick response was observed although information regarding sensitivity is not readily available.

5.1.4 Tin Oxide

Tin oxide is the main commercially available metal oxide semiconductor gas-sensor. It has been used widely for a number of years and is routinely doped to improve selectivity and sensitivity.[176] Doping also occurs in an attempt to lessen the effect of "sensor drift", whereby the zero exposure reading of the sensor changes. This is a particular problem for tin oxide sensors in the presence of humidity or variable humidity atmospheres. Tin oxide sensors have been shown to have sensitivities in the range of 20-50 towards a variety of hydrocarbon compounds at an operating temperature of 400 °C.[177] In this chapter a wide range of metal oxides were deposited onto gas sensing substrates by CVD. The films were evaluated as gas sensors and comparisons made with traditional screen-printed materials.

5.2 Results

The production and characterisation of metal oxide thin films on gas sensor substrates was discussed in the previous chapter. Here we shall concentrate on the gas

sensing properties of the deposited films. Gas response has been measured as the ratio between R (the resistance when exposed to ethanol) and R_0 (the resistance at the point immediately preceding the introduction of ethanol). The resistance was measured between the two electrodes of an interdigitized gold electrode structure on an alumina tile. Samples of Ga_2O_3, Sb_2O_5, SnO_2 and Nb_2O_5 were prepared by CVD and screen-printing for comparative purposes. All samples were tested across a range of operation temperatures, from 400 °C to 600 °C, for their response to ethanol gas at concentrations ranging from 1 ppm to 100 ppm. Additionally the sensors produced by CVD were evaluated for their response in dry air and humid air (50 % humidity).

5.2.1 Gallium Oxide

The Ga_2O_3 films showed a p type response to ethanol at a variety of temperatures. In all cases gas response increased with ethanol concentration, a representative example is shown in Figure 5.1. The gas response was rapid and a near plateau was reached within minutes of exposure to ethanol.

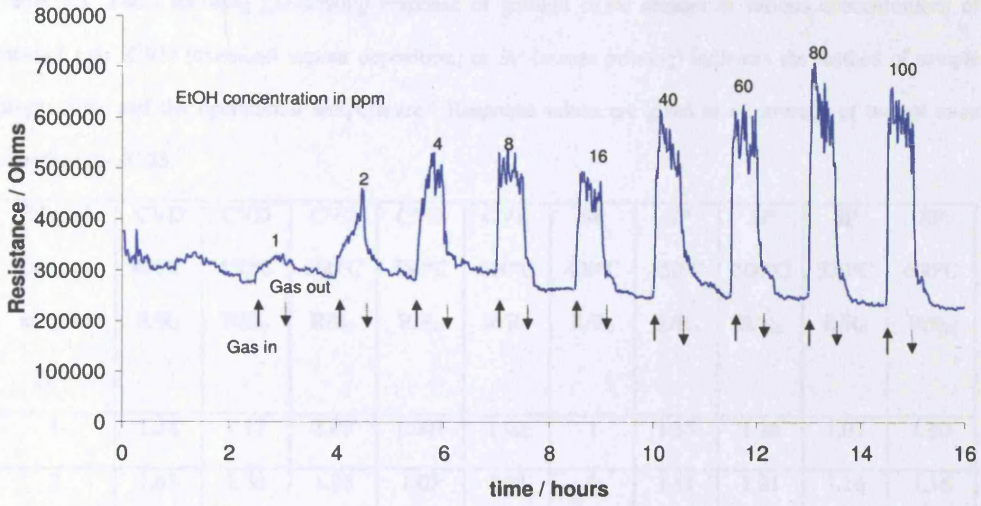

Figure 5.1. The gas response of a CVD prepared gallium oxide sensor to varying concentrations of ethanol at an operational temperature of 400 °C.

When the ethanol flow was stopped the response also dropped rapidly to near the baseline level and then tailed off more slowly to the baseline. Throughout the duration of the experiment the baseline remained stable showing only a slight downward drift. Some signal noise is evident. Above 60 ppm of ethanol gas the response level remained fairly constant and did not vary to any great extent. Evaluation of response to a gas concentration of 100 ppm of ethanol indicated that the greatest response of R/R_0 at 2.84 occurred at 400 °C (Table 5.1.). As expected a maximum is reached and then tails off to a plateau. It is believed this is an instrumental effect rather than experimental as it is seen in all cases and in previous work conducted on the same equipment.[11]

Table 5.1. Table showing gas-sensing response of gallium oxide sensors to various concentrations of ethanol gas. CVD (chemical vapour deposition) or SP (screen printing) indicates the method of sample preparation, and the operational temperature. Response values are given as an average of two or more experiments ±0.25.

Ethanol concentr-ation in ppm	CVD 400°C R/R_0	CVD 450°C R/R_0	CVD 500°C R/R_0	CVD 550°C R/R_0	CVD 600°C R/R_0	SP 400°C R/R_0	SP 450°C R/R_0	SP 500°C R/R_0	SP 550°C R/R_0	SP 600°C R/R_0
1	1.38	1.17	1.03	1.001	1.02	1	1.35	1.26	1.07	1.00
2	1.65	1.36	1.05	1.02	1.04	1	1.41	1.31	1.16	1.16
4	1.68	1.51	1.12	1.09	1.07	1	1.58	1.40	1.28	1.23
8	1.65	1.67	1.09	1.14	1.14	1	1.53	1.64	1.44	1.28
16	1.86	1.95	1.11	1.17	1.19	1	1.80	1.72	1.55	1.46
40	2.06	2.45	1.16	1.24	1.29	1	2.00	1.83	1.56	1.51
60	3.01	2.76	1.32	1.35	1.49	1	2.00	1.94	1.67	1.62
80	3.28	2.52	1.36	1.49	1.74	1	2.00	2.04	1.78	1.72
100	2.84	2.78	1.37	1.47	1.77	1	2.07	2.12	1.84	1.72

Conversely the gallium oxide sensor prepared by screen-printing had a maximum p type response of R/R0 = 2.12 at 500 °C. This sensor gave no response to ethanol at 400 °C but follows a similar trend to the CVD produced sensors in that gas response decreases at higher operating temperatures once the optimum operating temperature has been surpassed. The response of the screen printed sensor (Figure 5.2.) shares many similar features to the response of the CVD produced sensor: the response was rapid and a near plateau was reached minutes after the initial exposure, once the ethanol flow is stopped the response falls rapidly to near base line level and then tails off more slowly; there is also evidence of noise. A notable difference is that there is an

upward shift in the baseline resistance as the experiment proceeded and that there is a p-type rather than n-type response, this is most likely due to a significant difference in charge carrier concentration.[6]

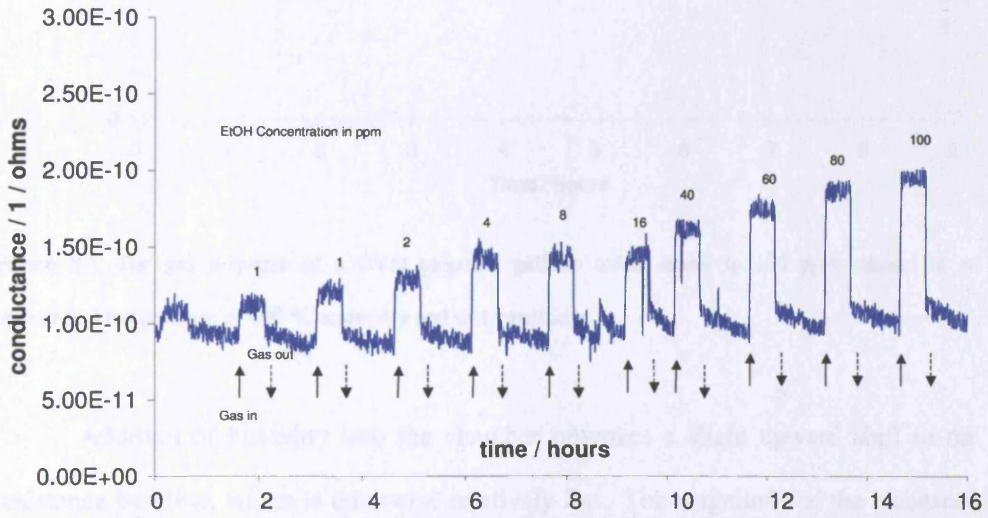

Figure 5.2. The gas response of a screen print prepared gallium oxide sensor to varying concentrations of ethanol at an operational temperature of 450 °C.

The gas response of the CVD produced gallium oxide sensor in the presence of 50% humidity was also evaluated (Figure 5.3.).

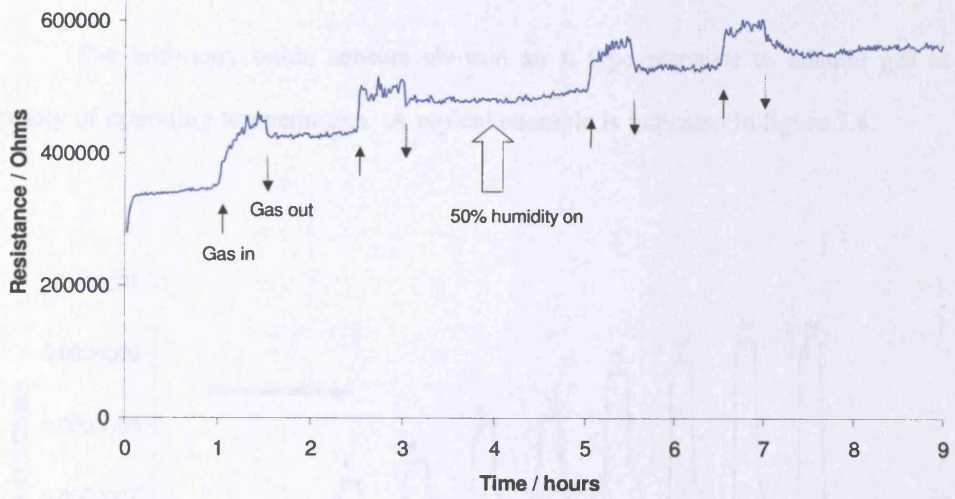

Figure 5.3. The gas response of a CVD prepared gallium oxide sensor to 100 ppm ethanol at an operational temperature of 400 °C under dry and wet conditions.

Addition of humidity into the chamber provokes a slight upward shift in the resistance baseline, which is otherwise relatively flat. The magnitude of the resistance response is similar in dry and humid air.

5.2.2 Antimony Oxide

The antimony oxide sensors showed an n type response to ethanol gas at a variety of operating temperatures. A typical example is indicated in figure 5.4.

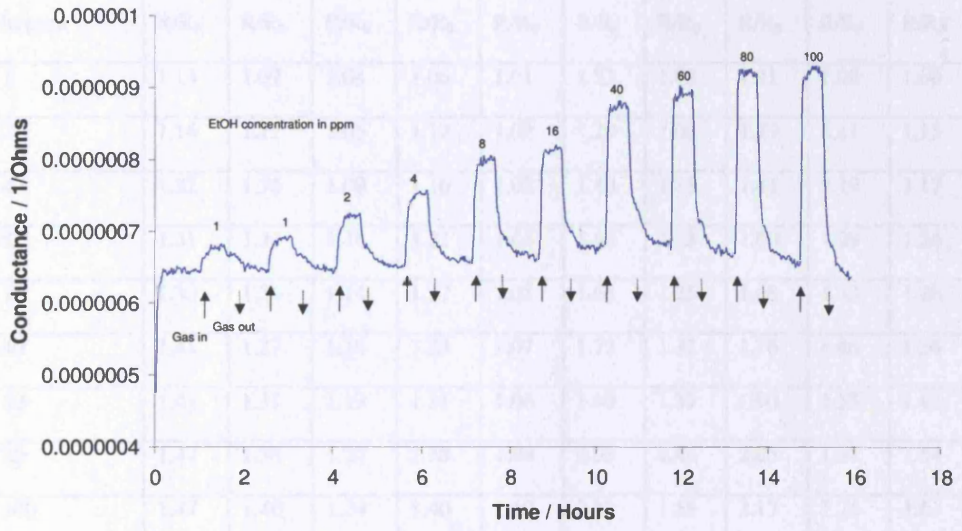

Figure 5.4. The gas response of a CVD prepared antimony oxide sensor to varying concentrations of ethanol at an operational temperature of 400 °C.

In all cases response increased with ethanol concentration. The response is initially fast but tails off as a near plateau is reached. Similarly to the gallium oxide sensors once ethanol flow is stopped the response rapidly falls to near baseline levels then tails off more slowly. There is minimal baseline drift throughout the course of the experiment. The greatest response (R/R_0) was 1.47 to 100 ppm ethanol gas at an operating temperature of 400 °C. Table indicates the responses of both CVD and screen-printed sensors at a variety of temperatures and ethanol concentrations.

Table 5.2. Table showing gas-sensing response of antimony oxide sensors to various concentrations of ethanol gas. CVD (chemical vapour deposition) or SP (screen printing) indicates the method of sample preparation, and the operational temperature. Response values are given as an average of two or more experiments ±0.25.

Ethanol concentration in ppm	CVD 400°C R/R_0	CVD 450°C R/R_0	CVD 500°C R/R_0	CVD 550°C R/R_0	CVD 600°C R/R_0	SP 400°C R/R_0	SP 450°C R/R_0	SP 500°C R/R_0	SP 550°C R/R_0	SP 600°C R/R_0
1	1.13	1.07	1.04	1.06	1.01	1.23	1.03	1.21	1.08	1.08
2	1.14	1.12	1.05	1.12	1.02	1.29	1.06	1.29	1.11	1.13
4	1.22	1.16	1.09	1.16	1.02	1.40	1.18	1.41	1.19	1.17
8	1.31	1.21	1.14	1.21	1.06	1.58	1.23	1.60	1.29	1.24
16	1.30	1.36	1.14	1.37	1.05	1.68	1.25	1.68	1.33	1.28
40	1.41	1.27	1.16	1.28	1.07	1.72	1.32	1.76	1.46	1.36
60	1.41	1.31	1.19	1.31	1.06	1.90	1.39	1.90	1.53	1.47
80	1.47	1.38	1.20	1.38	1.08	2.03	1.48	2.05	1.68	1.54
100	1.47	1.40	1.24	1.40	1.10	2.12	1.55	2.17	1.76	1.61

Antimony oxide sensors produced by screen-printing elucidated a maximum gas response of $R/R_0 = 2.17$ to 100 ppm of ethanol at an operational temperature of 500 °C. The gas response is similar with a rapid initial response and a quick return to near baseline levels on the ceasing of ethanol gas flow. There is also no apparent baseline drift during the experiment. The main difference in the response is that after the rapid initial response a plateau is not reached, giving rise to a response peak akin to a shark fin. A representative example is shown in figure 5.5.

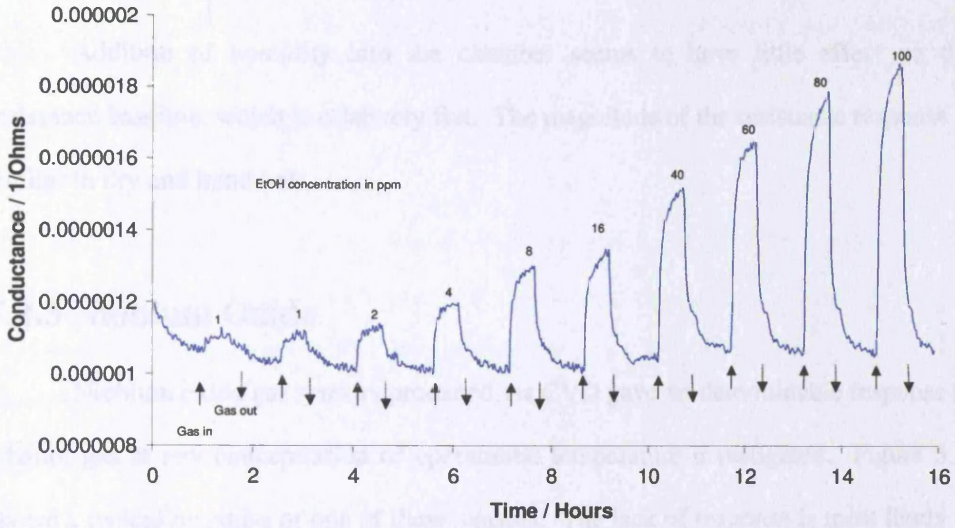

Figure 5.5. The gas response of a screen print prepared antimony oxide sensor to varying concentrations of ethanol at an operational temperature of 500 °C.

The gas response of the CVD produced antimony oxide sensor in the presence of 50% humidity was also evaluated (Figure 5.6.).

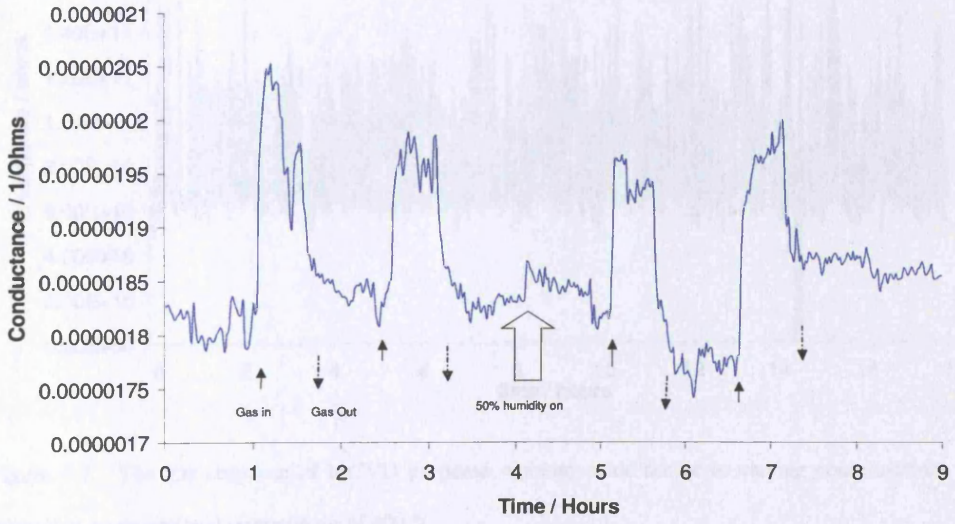

Figure 5.6. The gas response of a CVD prepared antimony oxide sensor to 100 ppm ethanol at an operational temperature of 400 °C under dry and wet conditions.

Addition of humidity into the chamber seems to have little effect on the resistance baseline, which is relatively flat. The magnitude of the resistance response is similar in dry and humid air.

5.2.3 Niobium Oxide

Niobium oxide gas sensors produced via CVD gave no determinable response to ethanol gas at any concentration or operational temperature investigated. Figure 5.7. shows a typical response of one of these sensors. The lack of response is most likely to be due to there being insufficient surface coverage of the film between the electrodes to give a change in resistance on exposure to the gas, hence that baseline resistance is very high as it is a measure of the resistance of the alumina tile.

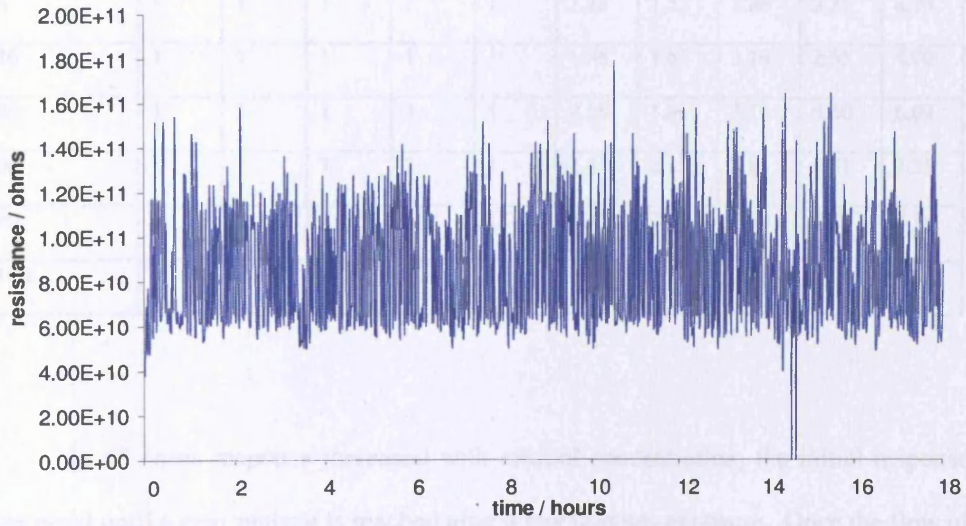

Figure 5.7. The gas response of a CVD prepared niobium oxide sensor to varying concentrations of ethanol at an operational temperature of 400 °C.

Sensors produced by screen-printing however, give an n type response to ethanol gas, the maximum of which was 10.13 to 100 ppm ethanol gas at an operational temperature of 600 °C. Other results are summarised in table 5.3.

Table 5.3. Table showing gas-sensing response of niobium oxide sensors to various concentrations of ethanol gas. CVD (chemical vapour deposition) or SP (screen printing) indicates the method of sample preparation, and the operational temperature. Response values are given as an average of two or more experiments ±0.25.

Ethanol concentration in ppm	CVD 400°C R/R_0	CVD 450°C R/R_0	CVD 500°C R/R_0	CVD 550°C R/R_0	CVD 600°C R/R_0	SP 400°C R/R_0	SP 450°C R/R_0	SP 500°C R/R_0	SP 550°C R/R_0	SP 600°C R/R_0
1	1	1	1	1	1	1.36	1.15	1.21	1.08	1.28
2	1	1	1	1	1	1.45	1.18	1.53	1.31	1.63
4	1	1	1	1	1	1.61	1.31	2.11	1.52	2.69
8	1	1	1	1	1	1.78	1.52	2.86	2.27	4.16
16	1	1	1	1	1	1.96	1.67	3.16	2.55	4.70
40	1	1	1	1	1	2.18	1.86	3.13	3.60	6.09
60	1	1	1	1	1	2.41	2.15	3.84	4.51	7.35
80	1	1	1	1	1	2.70	2.47	4.69	5.55	8.76
100	1	1	1	1	1	3.01	2.75	5.52	6.54	10.13

In all cases response increased with ethanol concentration, the initial response was rapid until a near plateau is reached after a few minutes exposure. Once the flow of ethanol gas is stopped response decreases to near baseline levels rapidly and then decreases more slowly. The response of the screen-printed niobium oxide sensors is free from noise. A typical response is shown in figure 5.8.

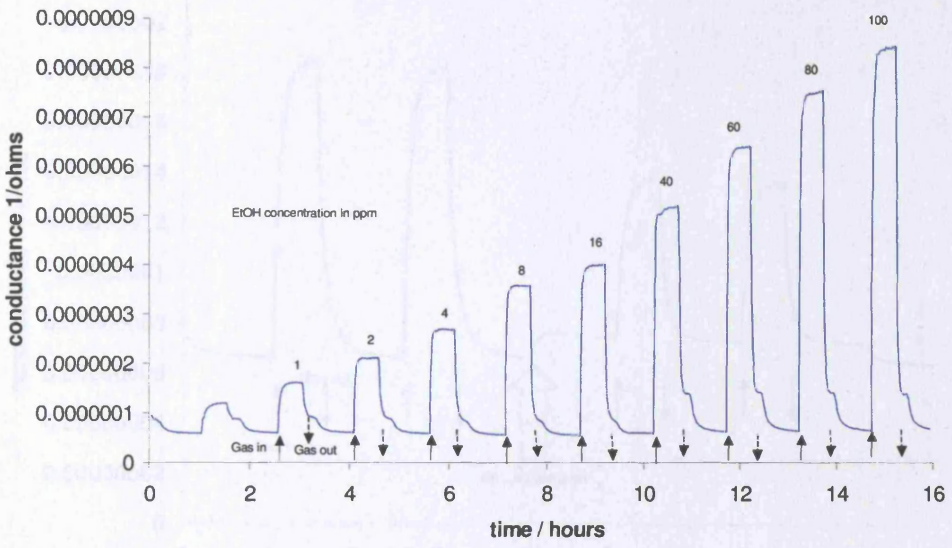

Figure 5.8. The gas response of a screen print prepared niobium oxide sensor to varying concentrations of ethanol at an operational temperature of 450 °C.

The response of niobium oxide sensors produced by screen-printing in humid conditions was also evaluated (figure 5.9.). A similar response to 100-ppm ethanol is seen in dry air; on the introduction of 50 % humidity the response decreases to approximately half the value in dry air (figure 5.9.).

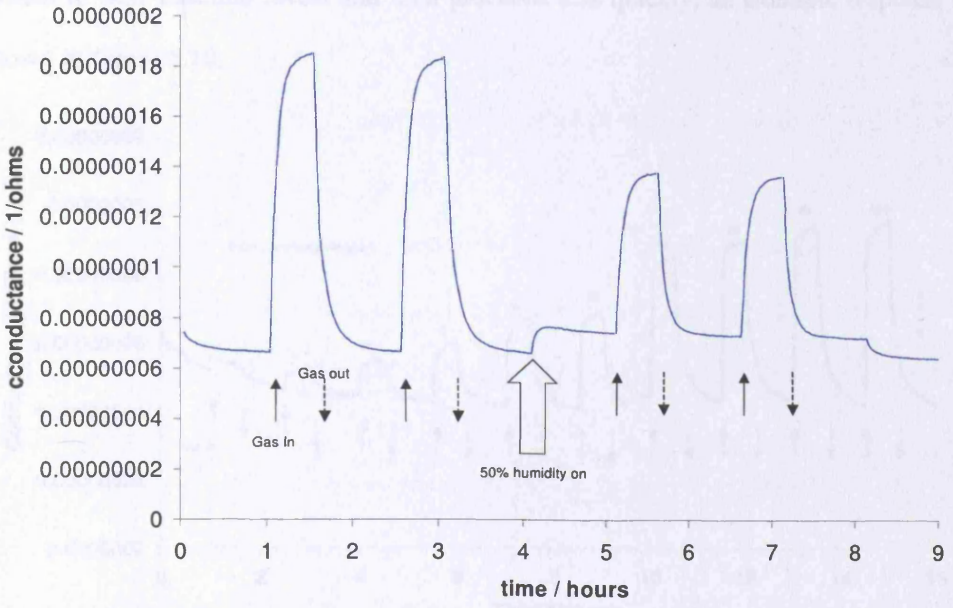

Figure 5.9. The gas response of a niobium oxide sensor prepared by screen printing to 100 ppm ethanol at an operational temperature of 450 °C under dry and wet conditions.

The response retains all of the same features in humid conditions as in dry conditions. The only discernable difference, other than magnitude of response, is that there is a slight increase in baseline resistance.

5.2.4 Tin Oxide

CVD produced tin oxide gas sensors give an n type response to ethanol gas. This response was found to be at a maximum of 1.86 when exposed to 100 ppm of ethanol gas at an operational temperature of 600 °C. The response was similar to other sensors produced by CVD investigated here; the initial response is quick until a near plateau is reached. The response falls away quickly once the flow of ethanol gas has

ceased to near baseline levels and then proceeds less quickly; an example response is shown in figure 5.10.

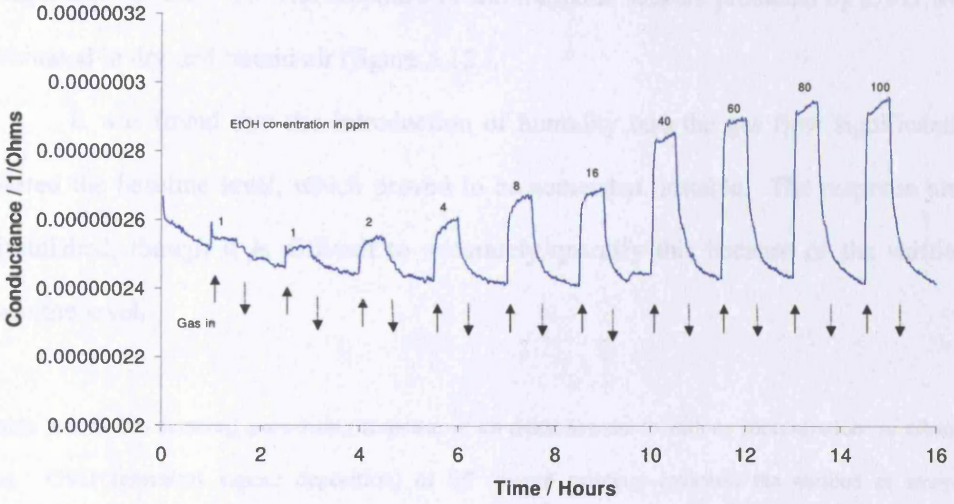

Figure 5.10. The gas response of a CVD prepared tin oxide sensor to varying concentrations of ethanol at an operational temperature of 600 °C.

A similar response is observed for tin oxide gas sensors produced by screen-printing (figure 5.11.).

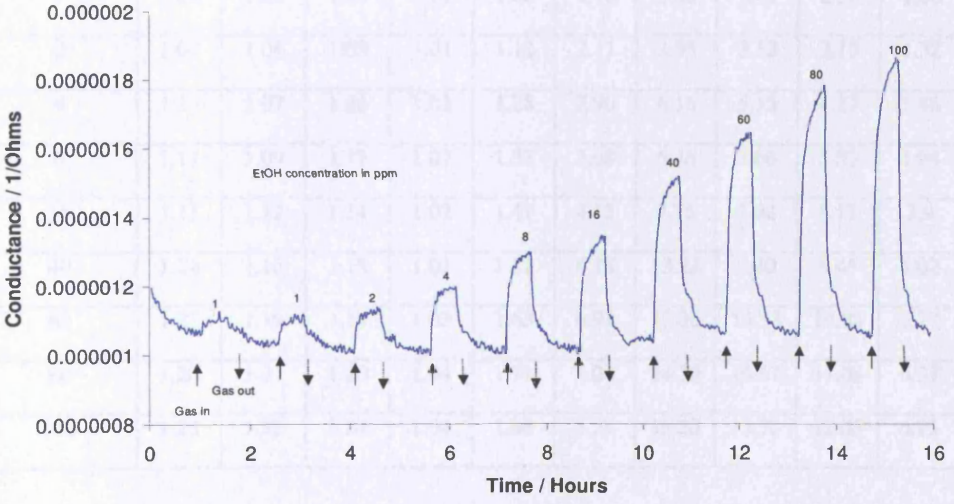

Figure 5.11. The gas response of a screen print prepared tin oxide sensor to varying concentrations of ethanol at an operational temperature of 500 °C.

In this case though the responses are much larger (table 5.4.).

A maximum response of 15.7 is observed to 100 ppm ethanol at an operational temperature of 500 °C. The response of the tin oxide sensors produced by CVD was evaluated in dry and humid air (figure 5.12.).

It was found that the introduction of humidity into the gas flow significantly altered the baseline level, which proved to be somewhat unstable. The response also diminished; though it is difficult to accurately quantify this because of the shifting baseline level.

Table 5.4. Table showing gas-sensing response of tin oxide sensors to various concentrations of ethanol gas. CVD (chemical vapour deposition) or SP (screen printing) indicates the method of sample preparation, and the operational temperature. Response values are given as an average of two or more experiments ±0.25.

Ethanol concentration in ppm	CVD 400°C R/R_0	CVD 450°C R/R_0	CVD 500°C R/R_0	CVD 550°C R/R_0	CVD 600°C R/R_0	SP 400°C R/R_0	SP 450°C R/R_0	SP 500°C R/R_0	SP 550°C R/R_0	SP 600°C R/R_0
1	1.04	1.02	1.03	1.01	1.08	1.78	3.06	2.81	2.36	1.00
2	1.09	1.04	1.03	1.01	1.12	2.11	3.95	3.52	3.15	1.32
4	1.13	1.07	1.06	1.02	1.28	2.90	6.16	5.15	4.27	1.43
8	1.17	1.09	1.12	1.02	1.32	3.68	6.46	7.66	5.53	1.94
16	1.17	1.12	1.14	1.02	1.47	4.13	7.76	7.02	8.17	3.9
40	1.24	1.16	1.18	1.02	1.52	6.18	13.23	6.40	8.45	5.02
60	1.27	1.19	1.19	1.03	1.63	6.91	13.36	13.33	10.03	5.77
80	1.28	1.21	1.20	1.04	1.71	8.04	14.30	16.67	11.08	6.37
100	1.28	1.22	1.24	1.04	1.86	8.28	15.20	15.70	12.05	6.93

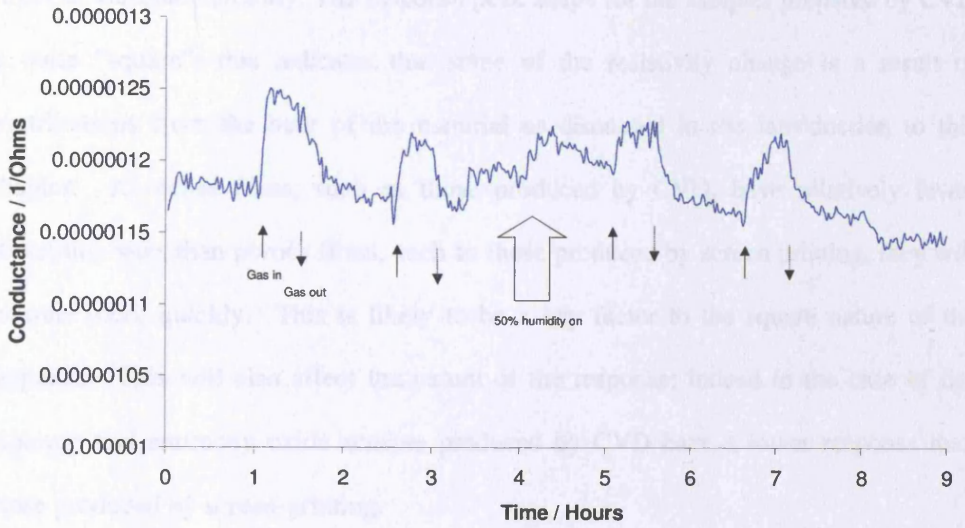

Figure 5.12. The gas response of a CVD prepared tin oxide sensor to 100 ppm ethanol at an operational temperature of 600 °C under dry and wet conditions.

5.3 Discussion

For the gallium and antimony oxide sensors made here the change in resistance is due to changes in oxygen trap sites in response to the catalytic oxidation of ethanol. This is not due to absorption, as we would expect to see a marked change in gas response on the introduction of humidity into the chamber. It is therefore likely that for these materials surface absorbed water is not associated with the same surface state as the surface absorbed ethanol. However, there is a marked change on the gas sensing response on the introduction of humidity into the chamber for the niobium and tin oxide sensors; indeed this is a current problem in sensor technology that makes SnO_2 (the most widely used) devices unsuitable for a range of applications.[178,179] For these materials surface states are non-specific towards absorbed species. Much work has been conducted to improve the surface selectivity of SnO_2 devices [176] to lessen the

effect of variable humidity. The response peak shape for the samples prepared by CVD is quite "square"; this indicates that some of the resistivity change is a result of contributions from the bulk of the material as discussed in the introduction to this chapter. As dense films, such as those produced by CVD, have relatively fewer absorption sites than porous films, such as those produced by screen printing, they will saturate more quickly. This is likely to be a key factor to the square nature of the response. This will also affect the extent of the response; indeed in the case of tin, niobium and antimony oxide sensors produced by CVD have a lower response than those produced by screen-printing.

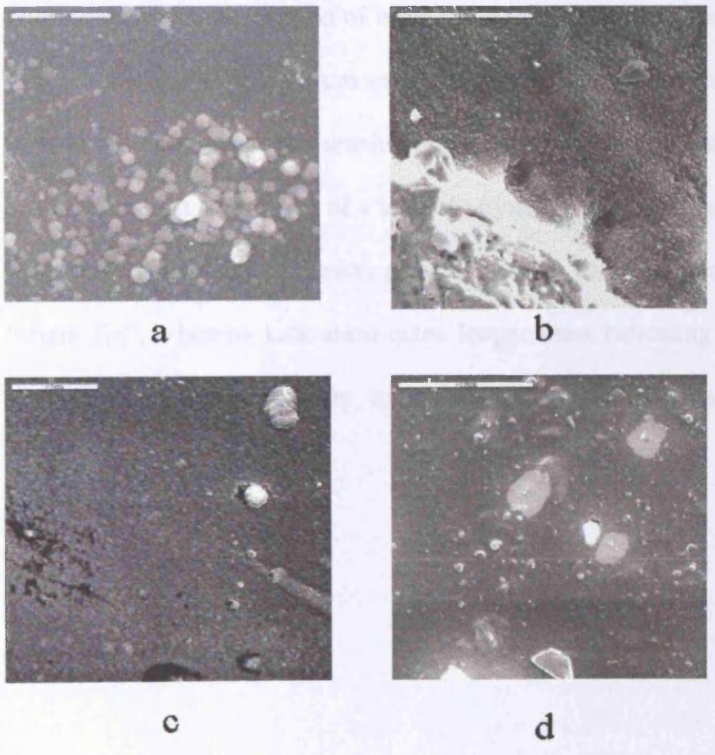

Figure 5.13. Typical SEM pictures for: a gallium oxide, b antimony oxide, c tin oxide, d niobium oxide. In all cases samples were produced by CVD with a reactor temperature of 600 °C. Scale bars indicate 10 μm for a, b and d; but 5 μm for c.

Sensors that give rise to a lower response are also subject to noise, which limits their usefulness in devices. Gallium oxide sensors produced by the two methodologies have similar responses; this is most likely because of the morphology of CVD produced gallium oxide films (figure 5.13.). The morphology of the gallium oxide film is one of spherical particles on the surface, which leads to a higher surface area relative to the flat morphologies of other CVD produced oxide sensors. Indeed the films produced of antimony oxide and tin oxides are relatively flat compared to the film of gallium oxide. In all cases island growth regime is observed. Poor physical connectivity between islands is observed in the case of niobium oxide, this is in contrast to previous work conducted on the production of niobium oxide via CVD methods.[171] In this work it was found that crystalline niobium oxide films could be grown with dense columnar island growth structures. No gas sensing response could be observed from the niobium oxide gas sensors, this is because of a lack of physical connectivity of niobium oxide between the sensor electrodes. Screen printed samples had a response shape more akin to a "shark fin", whereby saturation takes longer, thus indicating the increased number of absorption sites due to the more porous nature of sensors prepared using this methodology (Figure 5.14.).

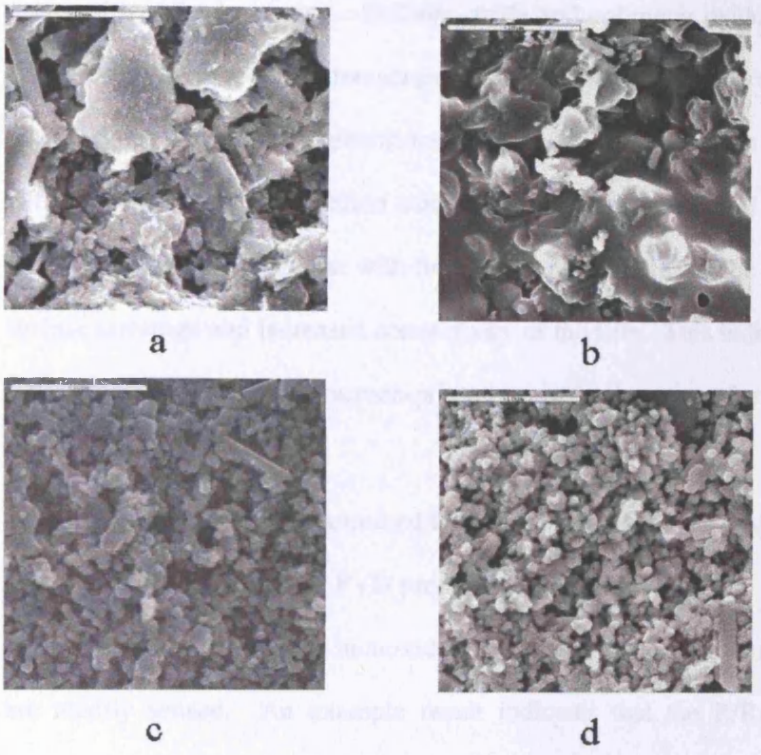

Figure 5.14. Typical SEM pictures for: a gallium oxide, b antimony oxide, c tin oxide, d niobium oxide. In all cases samples were produced by screen-printing the raw materials onto a gas sensor substrate. In all cases the scale bar indicates a distance of 10 μm.

In general it is felt that screen-printing is a more suitable method in the production of solid-state gas sensors. This is because the films are especially porous with a large number of sites for interaction between surface and gas phase species, resultantly the ratio of surface conductivity to bulk conductivity is high; not only does this increase the magnitude of response (for example between the two types of tin oxide sensor evaluated here), but leads to a much less noisy response. Other advantages of screen-printing include high surface coverage and high physical connectivity ensuring a good connection between sensor electrodes. It is found that there is a mismatch in the optimum operational temperature of sensors prepared by CVD compared to those

prepared by screen-printing. Gallium oxide and antimony oxide sensors prepared by CVD have lower optimum temperatures than those prepared by screen-printing. This could be due to the island growth mechanism which may lead to grain boundaries and defects with a lower activation energy toward trap states and / or higher electron mobility. This is not the case with tin oxide samples; this may be because of the higher surface coverage and increased connectivity of the film. This indicates an advantage to CVD prepared sensors over screen-printed examples in terms of energy usage.

Previous work has examined the gas sensing properties of gallium and tin oxides prepared by PVD methods. PVD prepared gallium oxide films in the presence of gases such as methane and carbon monoxide [114,115] found that higher temperatures these gases are readily sensed. An example result indicates that the R/R_0 value for a sensor prepared by sputtering to 5000 ppm methane in dry air is 40 at 700 °C. This decreases dramatically at 600 °C to a R/R_0 of only 5. APCVD produced films had R/R_0 values between 1 and 2.84 for gas concentrations between 1 and 100 ppm, similarly screen printed sensors had responses between 1 and 2.12 under the same conditions. The optimum response temperature was found to be 400 °C for CVD prepared sensors and 500 °C for screen-printed sensors. These are significantly lower than the PVD prepared material (700 °C). Lowering the optimum operational temperature in sensor devices is desirable as this results in the consumption of less energy. Screen-printed tin oxide sensors give high responses to hydrocarbon gases at low temperature (400 °C). Typically these responses are in the order of 20 – 50.[177] Much work has been undertaken to improve the selectivity and stability of these sensors. Metals such as antimony or platinum are routinely doped into the sensors to help achieve this.[176] PVD routes have been used to deposit SnO_2 films for gas sensor applications. [121] These

sensors have optimum response while operating at 350 °C.[180] The sensors prepared by CVD give optimum responses at elevated temperature (600 °C), though this response is small (1.86) compared to the optimum response given by the screen-printed sensors investigate here (15.70 at 500 °C or 15.20 at 450 °C).

5.4 Conclusion

The response to reducing gas (ethanol) by APCVD and screen print prepared metal oxide sensors was evaluated. It was found that of the four materials prepared by APCVD evaluated here the gallium oxide sensors gave the greatest response of 2.83 at an operating temperature of 400 °C. The screen-printed samples gave better responses, with the exception of the gallium oxide sample. The best of these responses was by the tin oxide sensor of 15.7 at an operating temperature of 500 °C. It is likely that the more open morphology of the APCVD prepared gallium oxide sensor is responsible for increasing the sensitivity of this sensor versus the screen-printed gallium oxide sensor. APCVD prepared dense thin films of metal oxides have been shown to provide measurable responses to a reducing gas.

Chapter 6 - Aerosol Assisted Chemical Vapour Deposition

In the previous chapter we saw metal oxide films being evaluated as gas sensors. In this chapter we change tack and examine the versatility of aerosol assisted chemical vapour deposition in the deposition of ionic films from simple ionic precursors and as a novel way to dope materials.

6.1 Introduction

In recent years there has been much interest in the development of new precursors for the chemical vapour deposition of inorganic materials. In general, such precursors must be volatile, have sufficient stability to transport to the deposition site and decompose cleanly to give the desired material.[172]

Aerosol assisted chemical vapour deposition (AACVD) is a technique that is potentially an extremely valuable tool. It has been demonstrated that functionalised films can be deposited from traditional single source precursors [181] or grown using unconventional polyoxometelate precursors.[5]

Alkali fluoride films have received some interest in recent years since their characteristics suggest possible applications in the generation of light and as wave-guide devices.[182,183] For instance sodium fluoride film deposition has been observed from the single source CVD of sodium fluoralkoxides.[184,185] Alkali fluoride thin films have been deposited using β – diketonates [186] and alkoxide based precursors.[187-189] Optical and structural properties of sodium fluoride thin films deposited by physical vapour deposition methods have been investigated.[190]

6.2 Results

Deposition of metal fluoride films was achieved on glass substrates from the AACVD of metal fluoride powder dissolved in water. The process was studied at different substrate temperatures and carrier gas flow conditions (examples for NaF in table 6.1). We believe that this process is an actual CVD reaction rather than an aerosol spray type delivery because the hot zone of the reactor used was at a sufficiently high temperature to vaporise all of the aerosol solvent. Further, the NaF precursor would be expected to be in the form of dissolved and separated ions within the aerosol – rather than as a discrete molecule in conventional molecular based CVD processes.

There appeared to be no limit to deposition temperature as films were deposited at all temperatures investigated. All of the films were uniform; and all of the films had a white opaque appearance; as such they were unreflective and appeared powdery. They all failed the Scotch tape test, could be marked by a brass stylus and could be wiped from the substrate using a dry cloth. No optical change was apparent in the films over the course of three months.

Table 6.1. Experimental Conditions and micro-analytical results for NaF thin films.

Substrate Temperature / °C	Nitrogen Gas Flow Through Aerosol Mist l/min.	Elemental Composition As Determined By EDAX
600	2.0	NaF
600	1.0	NaF
600	0.5	NaF
600	0.3	NaF
600	0.1	NaF
550	1.0	NaF
500	1.0	NaF
450	1.0	NaF
400	1.0	NaF
350	1.0	NaF
300	1.0	NaF
250	1.0	NaF
200	1.0	NaF

Compositional analysis of the films was determined by EDXA. In all cases some breakthrough to the underlying glass substrate was observed. This was corrected for based on a sample of plain glass. The results indicate that the films have the same

elemental ratio as a pellet of the starting material, which was also examined (Table 6.1.).

SEM analysis of the films highlighted that films grew via island growth mechanism. A representative sample is shown in figure 6.1.

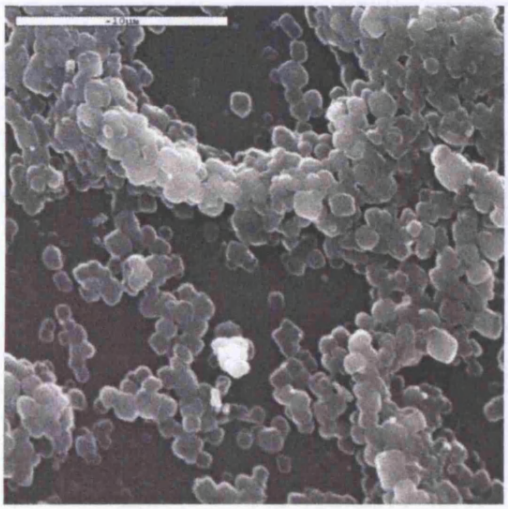

Figure 6.1. A Representative SEM photograph of AACVD prepared sodium fluoride thin film.

The optical properties of the films (Table 6.2.) were investigated using transmission / reflectance measurements and UV absorption between 1100 nm and 400 nm. All samples showed a shift in absorption edge relative to plain glass. The films showed minimal reflectivity (2%) and transmission (5-10%) between 1100 nm and 400 nm. The transmission spectra indicated high levels of hazing; indeed haze measurements gave values between 5 and 90.

Table 6.2. Optical properties and microanalytical results.

Sample	EDXA Analysis	Optical Properties	Haze
LiF	LiF	11% Transmission 3% Reflectance	18.2
NaF	NaF	10% Transmission 2% Reflectance	77.5
KF	KF	10% Transmission 3% reflectance	30.4
RbF	RbF	7% Transmission 4% Reflectance	15.2
MgF_2	MgF_2	12% Transmission 1% Reflectance	87.1
CaF_2	CaF_2	5% Transmission 1% Reflectance	5.1
SrF_2	SrF_2	9% Transmission 1% Reflectance	16.7

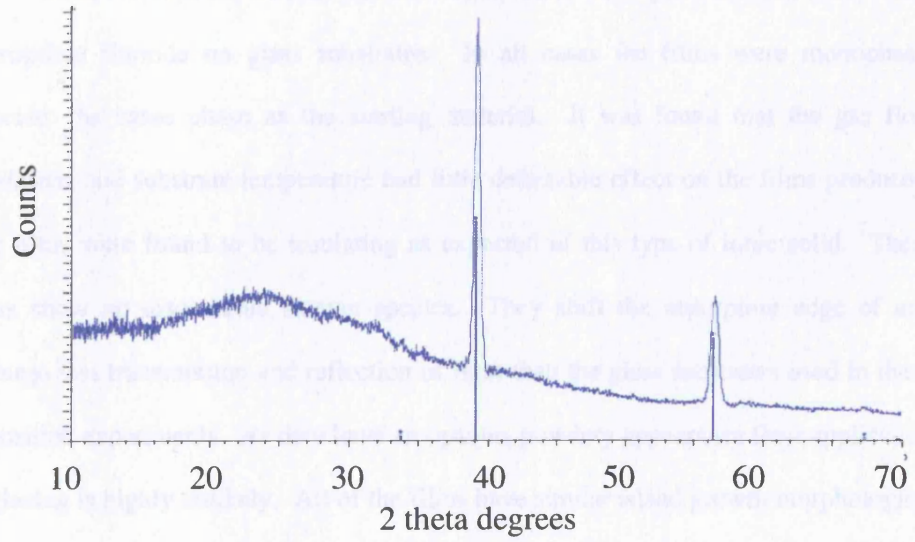

Figure 6.2. The X-ray diffraction pattern given by an AACVD prepared sodium fluoride thin film. The stick pattern is that of bulk sodium fluoride obtained from the database. Indexing indicated a face centred cubic lattice with lattice parameter a = 4.5777(1) Å.[99]

Metal fluoride films were examined by X-ray diffraction conditions and returned XRD patterns akin to those produced by powder XRD of the applicable metal fluoride powder (Figure 6.2.). [99] However, analysis of the same films a week later did not show the powder pattern seen before. There was evidence of a hydrate being produced.

XPS measurements on a sample of NaF revealed binding energies of 684.4 eV and 1071.0 eV for F 1s and Na 1s, respectively. These are comparable to previous literature values of 684.5 eV and 1071.2 eV.[95] The XPS peak profiles are consistent with one environment each for sodium and fluorine (figure 6.3.). Elemental quantification suggests a 1:1 ratio of metal to fluorine.

6.3 Discussion

AACVD of metal fluoride powders dissolved in water produces thin films of the appropriate fluoride on glass substrates. In all cases the films were monophasic fluoride: the same phase as the starting material. It was found that the gas flow conditions and substrate temperature had little detectable effect on the films produced. The films were found to be insulating as expected of this type of ionic solid. These films show no discernable Raman spectra. They shift the absorption edge of and undergo less transmission and reflection of light than the glass substrates used in these deposition experiments. As they have an opaque, powdery appearance their application in glazing is highly unlikely. All of the films have similar island growth morphologies. Subsequent reanalysis by EDXA in the light of the XRD results produced near identical elemental ratios to those from samples examined soon after production. It would appear

that these films absorb water from the air to form the hydrated metal fluoride. This might be expected, as the films are porous.

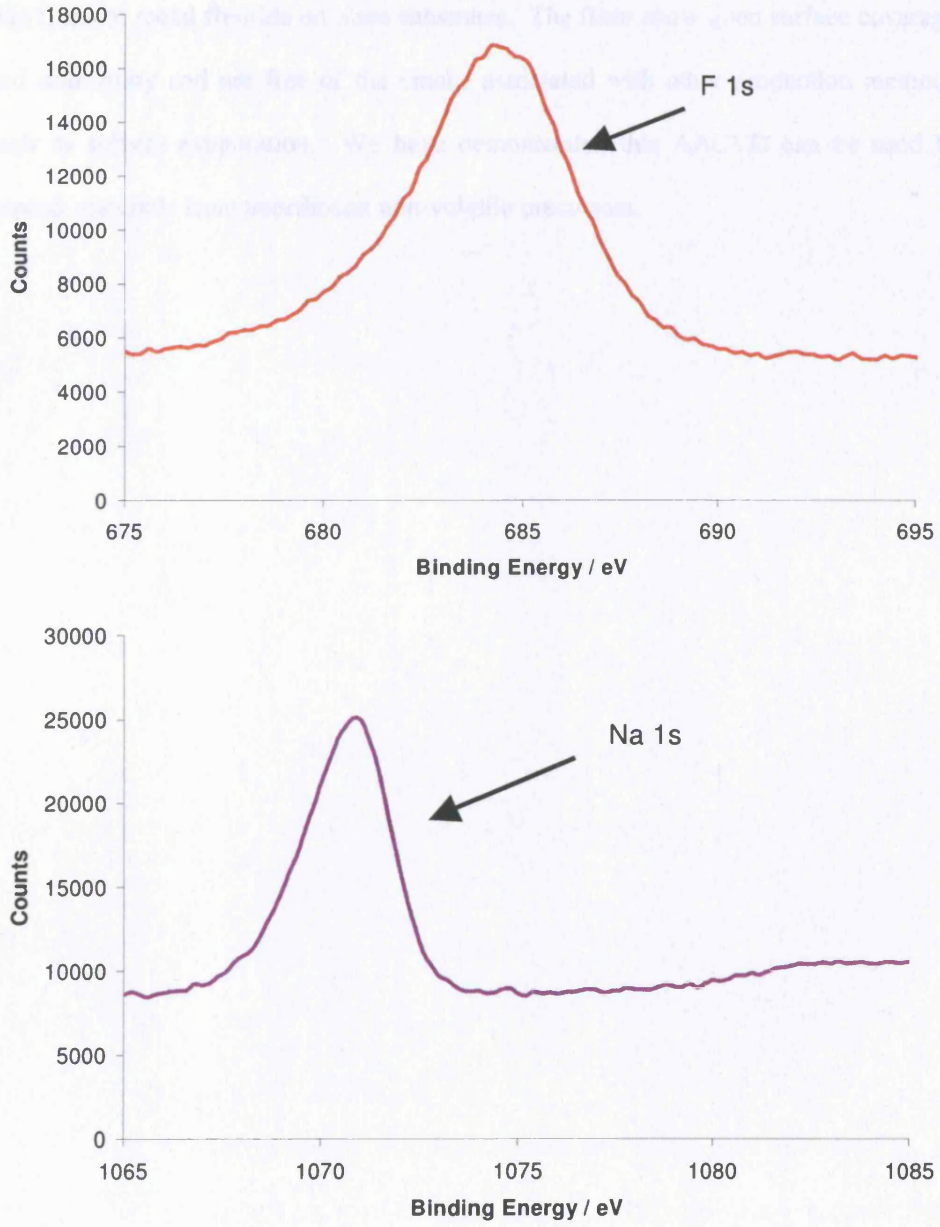

Figure 6.3. XPS binding energy shifts for F 1s and Na 1s respectively.

6.4 Conclusion

AACVD reaction of metal fluoride powders dissolved in water affords opaque thin films of metal fluoride on glass substrates. The films show good surface coverage and uniformity and are free of the cracks associated with other production methods such as solvent evaporation. We have demonstrated that AACVD can be used to deposit materials from unorthodox non-volatile precursors.

Chapter 7 AACVD + APCVD

Aerosol assisted chemical vapour deposition may also be used in conjunction with atmospheric pressure chemical vapour deposition as a way to dope materials, by diverting the plain flow of the atmospheric pressure chemical vapour deposition rig through the aerosol assisted chemical vapour deposition rig (both described in chapter 2, see figure 7.1).

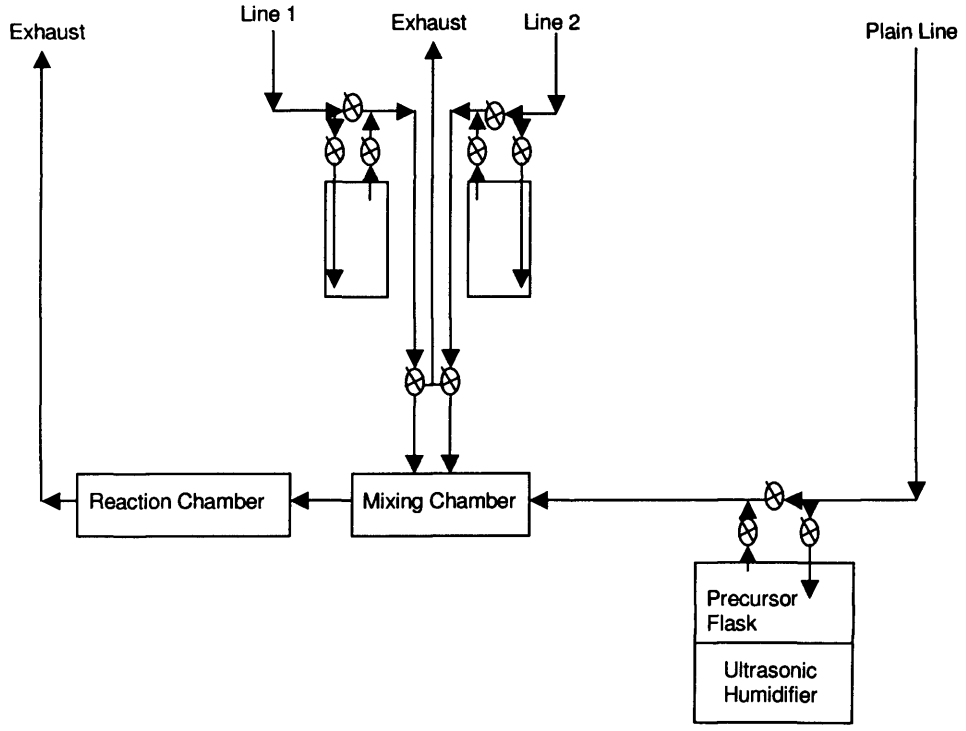

Figure 7.1. Schematic of AACVD / APCVD rig

Aerosol generated precursors can be introduced into the APCVD reaction. In test runs well known reactions were considered. For the atmospheric pressure reaction, the reaction of tin tetrachloride and ethyl acetate to form tin oxide was chosen because both of these precursors provide high enough vapour pressures to be used at room temperature and the formation of tin oxide by APCVD is relatively facile. The aerosol

precursor chosen was the tungsten polyoxometalate salt $[^{n}Bu_4N]_2[W_6O_{19}]$ dissolved in acetone Figure 7.2 is a structural representation of the anion $[W_6O_{19}]^{2-}$.

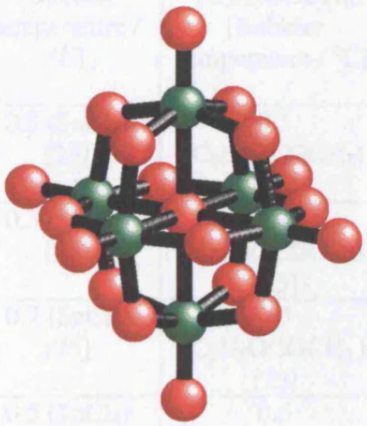

Figure 7.2. Structural representation of the anion of $[^{n}Bu_4N]_2[W_6O_{19}]$, $[W_6O_{19}]^{2-}$. Tungsten atoms are shown in green and oxygen atoms in red.

In the instance of this reaction the APCVD rig bubblers were not heated and neither was the incoming nitrogen gas flow as it was felt this would even out the reaction time scale of the two systems.

7.1 Results and Discussion

Compositional analysis of the films was determined by EDXA. In all cases some breakthrough to the underlying glass substrate was observed, this was corrected for based on a sample of plain glass. The results indicate that the films contained high amounts of tin and oxygen and smaller amounts of tungsten, though it is difficult to discern from the EDXA analysis the phases present in the film.

Table 7.1. Table of reaction conditions and microanalytical results for the mixed AA/AP CVD system.

Substrate Temperature / °C	Nitrogen Flow through $SnCl_4$ bubbler l/min ($SnCl_4$) [Bubbler temperature / °C]	Nitrogen Flow through Ethyl acetate bubbler l/min (C_2H_5OCOH) [Bubbler temperature / °C]	Nitrogen Flow of make up gas (flow through AA delivery system) l/min.	EDAX and Electron Probe analysis
550	0.5 ($SnCl_4$) [25]	0.5 ($C_2H_5OCOCH_3$) [25]	1.0	Sn 32% O 65% W 3%
600	0.3 ($SnCl_4$) [25]	0.7 ($C_2H_5OCOCH_3$) [25]	1.0	Sn 32% O 65% W 3%
600	0.7 ($SnCl_4$) [25]	0.3 ($C_2H_5OCOCH_3$) [25]	1.0	Sn 32% O 65% W 3%
600	0.5 ($SnCl_4$) [25]	0.5 ($C_2H_5OCOCH_3$) [25]	1.0	Sn 31% O 64% W 5%
600	0.5 ($SnCl_4$) [25]	0.5 ($C_2H_5OCOCH_3$) [25]	1.5	Sn 31% O 64% W 5%
600	0.5 ($SnCl_4$) [25]	0.5 ($C_2H_5OCOCH_3$) [25]	2.0	Sn 30% O 64% W 6%

SEM analysis of the films highlighted that films grew via island growth mechanism. A representative sample is shown in figure 7.3.

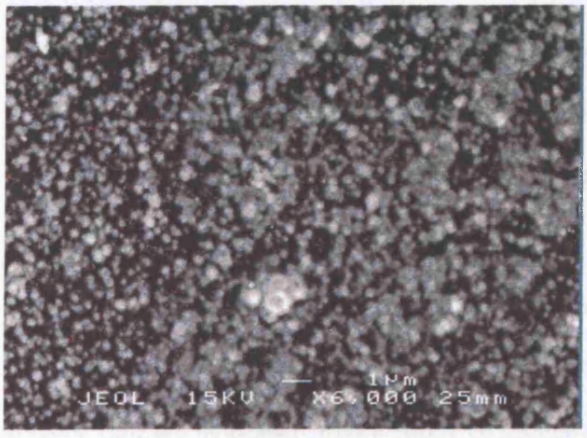

Figure 7.3. SEM picture of a film made from the combined AA / AP CVD system.

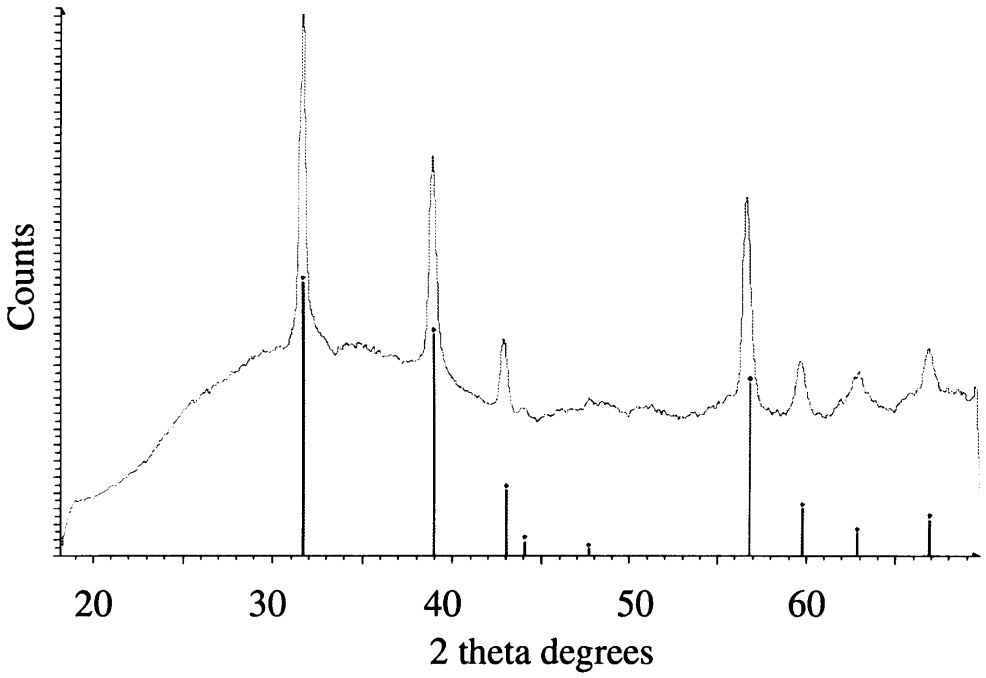

Figure 7.4. XRD pattern of a film made from the combined AA / AP CVD system. The pattern is that of SnO_2.[99]

X-ray diffraction indicated a pattern which matched a reference pattern of SnO_2 [99] (Figure 7.4.). Indexing this pattern indicated the presence of a tetragonal lattice with lattice parameters of a = 4.7688(6) and c = 3.2045(4) similar to previously published values.[99] These lattice parameters are larger than those found for the films of tin oxide in chapter 4. This is probably because tungsten is doped into the lattice. However, the ionic radius of 6 coordinate W^{4+} (0.66 Å) is actually slightly smaller than that of 6 coordinate Sn^{4+} (0.69 Å) [12] although perturbations of electron density may lead to a larger unit cell. X-ray photoelectron spectroscopy revealed binding energy shifts of 530.6 eV for O 1s and 487.2 eV for Sn 3d5/2 respectively. The XPS peak profiles (Figure 7.5.) are consistent with a single environment for tin and oxygen. The binding

energy shifts are in agreement with previous literature values of 487.3 eV for Sn 3d5/2 and 530.5 eV for O 1s.[95] Compositional analysis reveals that 6% of the material is tungsten. The tungsten 4f peak is asymmetrical suggesting that tungsten resides in a variety of oxidation states. This is a possibility as tungsten oxide is likely to be formed during the course of the reaction from the polyoxometalate precursor.[5] Unfortunately the oxygen 1s peak does not provide any information. Indeed the binding energy shift for oxygen in tin oxide and tungsten oxide is similar.[95]

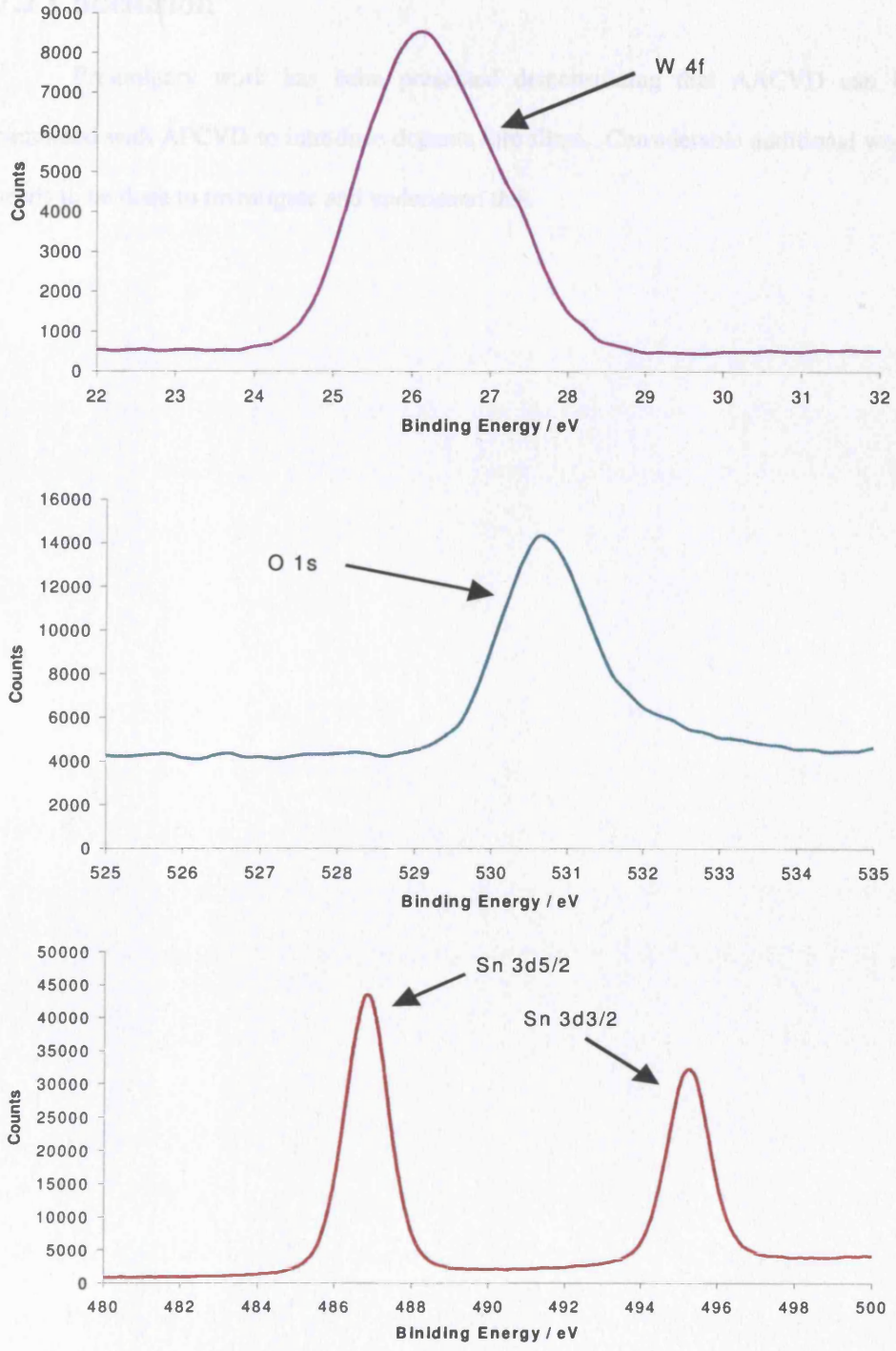

Figure 7.5. XPS peaks from a sample of tungsten doped tin oxide.

7.2 Conclusion

Preliminary work has been presented demonstrating that AACVD can be combined with APCVD to introduce dopants into films. Considerable additional work needs to be done to investigate and understand this.

Chapter 8 – Conclusions

8.1 Overall Conclusions

This thesis has examined the production of thin films of some novel main group metal phosphide and oxide thin films using dual source atmospheric pressure chemical vapour deposition. The main group metal oxides were deposited onto gas sensor substrates, and their response to ethanol, a reducing gas, was evaluated. The production of alkali metal and alkaline earth metal fluorides using aerosol assisted chemical vapour deposition is investigated. Atmospheric pressure and aerosol-assisted methodologies have been combined for what we believe is the first time and the resulting products examined.

Tin phosphide films could be made with a variety of stoichiometries. Tin phosphide has been found to have an indirect band gap of 2.2 eV. These films had an island growth mechanism with an interesting surface morphology of spherical particles. According to the experimental conditions the size, distribution and number of these particles could be controlled. In certain cases exotic web like structures were observed on the surface.

Films of germanium phosphide were produced via an island growth mechanism from the APCVD reaction of germanium chloride or bromide and $PCyc^{hex}H_2$. A variety of film stiochiometries could be prepared depending on the experimental conditions. The morphology of these films was fairly flat and featureless. Germanium monophosphide films were found to have a band gap of 1.1 eV.

Reaction of a copper metal substrate and $PCyc^{hex}H_2$ under APCVD conditions affords thin films of copper phosphide (Cu_3P). The use of a co-reactant produces thicker, more crystalline films. The films show excellent surface coverage, uniformity and good adhesion properties. Copper phosphide films (Cu_3P) could be obtained; these were grey in appearance and electrical insulators.

An attempt to make a thin film of silicon phosphide from the APCVD reaction of silicon tetrabromide and $PCyc^{hex}H_2$ was made. Grey, almost metal-like films were produced on glass substrates. Analysis proved inconclusive; XRD indicates that it is likely that a film with a variety of phases and compositions has been produced. In some samples phosphorous could be detected in the film using both XPS and EDAX along with a significant amount of oxygen. It is however, unclear as to if this oxygen originates as part of the film or from the glass substrate.

The APCVD reaction of antimony pentachloride and $PCyc^{hex}H_2$ led to the production of metallic films. XRD indicated that this film was of antimony metal. Examination by SEM and EDAX confirmed that antimony metal crystallites had grown on the surface of the glass substrate. EDAX conducted on areas free from metal crystallites indicated a very thin film containing antimony and phosphorous was present, although the quantities detected are near the limit of detection for the instrument and so are viewed as not 100% reliable.

Attempts to make boron phosphide films seemed to be beyond the limits of the CVD apparatus used. The maximum substrate temperature was 600 °C; boron phosphide has in the past been deposited at temperatures in the region of 1000 °C.[81-84]

The reaction of gallium trichloride with methanol under APCVD conditions affords clear films of gallium oxide on a variety of substrates. The films show good surface coverage, adhesion and uniformity. Gallium oxide films of a single phase were obtained. These were colourless in appearance and had low electrical conductivity at room temperature. The response to reducing gas (ethanol) by APCVD prepared gallium oxide gas sensors was evaluated. For the APCVD produced gas sensor it was found that there was a significant gas sensing response, which was most pronounced at 450 °C (3.29). The response was greater than that of a gallium oxide sensor prepared by screen-printing (2.07). This is most likely to be because of the high surface area afforded by the spherical particle morphology of APCVD produced gas sensors.

The APCVD reaction of tin tetrachloride with ethyl acetate leads to the production of clear films of tin oxide on a variety of substrates. The films show good adhesion, uniformity and surface coverage. Single-phase films of tin oxide were obtained. The gas sensor response to ethanol reducing gas was evaluated for both APCVD produced and screen-printed materials. The APCVD produced sensors' whose most pronounced response was at 600 °C (1.86), whereas the screen-printed sensors optimum temperature was 500 °C (15.7). The screen-printed sensor gave a response an order of magnitude greater than the APCVD prepared material. This is because of the open, porous morphology seen with screen-printing, versus the relatively closed, fine-grained, columnar structure of APCVD produced tin oxide.

Transparent, single-phase films of antimony oxide were produced from the APCVD reaction of antimony pentachloride and ethyl acetate. The films show good

adhesion, uniformity and surface coverage on a variety of substrates. The response to reducing gas (ethanol) by screen-printed and APCVD prepared antimony oxide gas sensors was evaluated. The screen-printed sensor gave the most significant response at 500 °C (1.47). The largest response afforded by the APCVD prepared sensor occurred at 400 °C (2.17).

The APCVD reaction of niobium pentachloride with ethyl acetate leads to the production of clear films of niobium oxide on a range of substrates. The films show good adhesion and uniformity. Surface coverage whilst complete to the naked eye was relatively poor when examined using an electron microscope. Single-phase films of niobium oxide were obtained. The response to reducing gas (ethanol) by APCVD prepared gallium oxide gas sensors was evaluated but no response could be elucidated. This is because there is a lack of physical connectivity over the surface of the gas sensor between the electrodes making the material appear as an insulator. It was, however, found that the screen-printed sensor gave a good gas sensing response (10.13) which was most pronounced at 600 °C.

AACVD reaction of alkali metal and alkaline earth metal fluorides in water affords opaque thin films of metal fluoride on glass substrates. The films show good surface coverage and uniformity and are free of the cracks associated with other production methods such as solvent evaporation. XRD suggests that the deposited materials are very similar to the starting materials, though hydrolysis occurs over the course of a week or so. It has been demonstrated that AACVD can be used to deposit materials from unorthodox non-volatile precursors.

Combination of aerosol assisted and atmospheric pressure CVD methodologies leads to the production of thin films where the aerosol-assisted precursor is doped into the film created from the APCVD reaction. More work needs to be conducted in order to understand this process better.

8.2 Future Work

The work described in this thesis has demonstrated that APCVD can be used in the production of novel metal phosphide thin films from metal halides and substituted phosphines. A broader assessment of their structure, properties and semiconductor qualities may prove useful.

Metal oxide semiconductor gas sensors are traditionally not produced via CVD routes though it has been shown in this thesis that devices with a measurable response can be created by such methodologies. CVD routes may have an advantage over traditional routes (such as screen-printing) in terms of time and cost. However, the magnitude of response would need to be comparable if not better than the traditionally produced sensors if they were to compete in the market place. More work to improve the film morphologies and optimise film thickness could be done to see if this can be achieved. Aerosol assisted routes have potential in this sphere as films tend to be much more porous than films produced by atmospheric pressure chemical vapour deposition and the choice of precursor is much less constrained.

Preliminary work is presented here on the combination of atmospheric and aerosol routes to produce a doped film. It may be that this is a convenient way to dope unusual and interesting materials into target films. More work needs to be done to understand the interaction of the two processes and possibly exploit it.

Bibliography

1 M. Ohring, The Materials Science of Thin Films, Academic Press, London, 1992.

2 M.L. Hitchman, K.F. Jensen (Editors), Chemical Vapour Deposition Principles and Applications, Academic Press, London, 1993.

3 P.W. Atkins, Physical Chemistry, 3rd Edition, Oxford University Press, Oxford, 1988.

4 O. Kubaschewski, C.B. Alcock, P.J. Spencer, Materials Thermochemistry, 6th Edition, Pergamon Press, Oxford, 1993.

5 A.R. West, Basic Solid State Chemistry, 2nd Edition, Wiley, New York, 2001.

6 G. Attard, C. Barnes, Surfaces, Oxford Chemistry Primer #59, Oxford University Press, Oxford, 1998.

7 J. Loader, Basic Laser Raman Spectroscopy, Heyden & Son Ltd, London, 1970.

8 P.J. Goodhew, J. Humphreys, R. Beanland, Electron Microscopy and Analysis, 3rd Edition, Taylor & Francis, London, 2001.

9 R.B. Alder, A.C. Smith, R.L. Longini, Introduction to Semiconductor Physics, Wiley, New York, 1964.

10 M.J. Morant, Introduction to Semiconductor Devices, 2nd Edition, Harrap & Co Ltd, London, 1970.

11 D. Briggs, M.P. Seah, (Editors), Practical Surface Analysis, 2nd Edition, Volume Auger and X-ray Photoelectron Spectroscopy, Wiley, (1990).

12 N. N. Greenwood, A. Earnshaw, Chemistry Of The Elements, Pergamon, Oxford, 1984.

13 J.R. Van Wazer, Phosphorous and its Compounds, Vol 1, Interscience, New York, 1958.

14 D.E.C. Corbridge, The Structural chemistry of Phosphorus, Elsievier, New York, 1974.

15 J.C. Bailer, H.J. Emeleus, R. Nyholm, A.F. Trotman-Dickenson, Comprehensive Inorganic Chemistry, Volume 2, Pergamon Press, Oxford, 1973.

16 P.T. Moseley, J.O.W. Norris, D.E. Williams (Eds), Techniques and Mechanisms in Gas Sensing, Adam Hilger, New York, 1991.

References

1 I. Lakatos, A. Musgrave Eds. Criticism and the Growth of Human Knowledge, Proceedings of the International Colloquium in the Philosophy of Science, London, 1965, Volume 4, P148.

2 P.W. Atkins Physical Chemistry, 3rd Edition, Oxford University Press, Oxford, 1988.

3 M. Ohring, The Materials Science of Thin Films, Academic Press, London, 1992.

4 M.L. Hitchman, K.F. Jensen Eds. Chemical Vapour Deposition Principles and Applications, Academic Press, London, 1993.

5 W.B. Cross, I.P. Parkin Chem. Comm. 14 (2003) 1696.

6 P.T. Moseley, J.O.W. Norris, D.E. Williams Eds. Techniques and Mechanisms in Gas Sensing, Adam Hilger, Bristol, 1991.

7 D. Niemeyer, D.E. Williams, P. Smith, K.F.E. Pratt, B. Slater, C.R.C.A. Catlow, A.M. Stoneham J. Mater. Chem. 12 (2002) 667.

8 D.E. Williams, K.F.E. Pratt Sens. And Actuators B 70 (2000) 214.

9 R.C. Weast Ed. Handbook of Chemistry and Physics, 55th Edition, Chemical Rubber Publishing Company, USA, 1975.

10 J. Tauc Ed. Proceedings of the International School of Physics, Enrico Fermi, Course XXXIV, The Optical Properties of Solids, 1966.

11 G.S. Henshaw, D.H. Dawson, D.E. Williams J. Mater. Chem. 5 (1995) 1791.

12 N. N. Greenwood, A. Earnshaw Chemistry Of The Elements, Pergamon, Oxford, 1984.

13 J.R. Van Wazer Phosphorous and its Compounds, Vol 1, Interscience, New York, 1958.

14 D.E.C. Corbridge The Structural chemistry of Phosphorus, Elsievier, New York, 1974.

15 L.L. Vereikina, G. Samsanov V. Zh. Neorgkhim 5 (1960) 1888.

16 N. Schonberg Acta Chem. Scand. 8 (1954) 226.

17 T. Ludstrom, P.O. Snell Acta Chem. Scad. 21 (1967) 1343.

18 R.B. Kaner, R.E. Treece, J.A. Conklin Inorg. Chem. 33 (1994) 5701.

19 R.B. Kaner, R.M. Jacubinas, R.J. Jarvis Inorg. Chem. 39 (2000) 3242.

20 I.P. Parkin, A.L. Hector J. Mater. Chem. 4 (1994) 229.

21 I.P. Parkin, A.L. Hector Z. Naturforsch Teil B 49 (1994) 477.

22 I.P. Parkin, J.C. Fitzmaurice, A.T. Rowley J. Mater. Chem. 4 (1994) 285.

23 I.P. Parkin, A.T. Rowley J. Mater. Chem. 3 (1993) 689.

24 J.D. Sweet, D.J. Casadonte Jr. Ultrasonics Sonochemistry 8 (2001) 97.

25 O. Olofsson Acta Chem. Scand. 24, (1970) 1153.

26 T. Wadsten Acta Chem. Scand. 21, (1967) 593.

27 T. Wadsten Acta Chem. Scand. 19, (1965) 1232.

28 P.C. Donohue, H.S. Young J. Solid State Chem. 1 (1970) 143.

29 J. Osagi, R. Namikawa, Y. Tanaka Rev. Phys. Chem. Japan 37 (1967) 81.

30 K.A. Gingerich Nature 200 (1963) 877.

31 S. Motojima, T. Wakamatsu, K. Sugiyama Less Common Metals 82 (1981) 379.

32 K. Komaki Japan Koka Tokkyo Kokon JP02150067

33 H. Su, Y. Xie, B. Li, X. Liu, Y. Qian J. Solid State Chem. 146 (1999) 110.

34 J.C. Bailer, H.J. Emeleus, R. Nyholm, A.F. Trotman-Dickenson Comprehensive Inorganic Chemistry, Volume 2, Pergamon Press, Oxford, 1973.

35 G.R. Gordon, S.R. Kurtz Thin Solid Films 140 (1986) 277.

36 A.N. Gleizes Chemical Vapour Deposition 6 (2000) 155.

37 Y. Kumashiro, K.Salo, S. Chiba, S. Yamada, D. Tanaka, K. Hyodo, T. Yokoyama, K. Hiata J. Solid State Chem. 154 (2000) 39.

38 K.L. Lewis, A.M. Pitt, D.R. Desmond, E.M. Waddell Nato ASI Series, Series 3: High Technology (1997), 21(Protective Coatings and Thin Films), 553-564.

39 Y. Kumashiro, T. Yokoyama, A. Sato, Y. Ando J. Solid State Chem. 133 (1997) 314.

40 Y. Kumashiro, H. Yoshizawa, T. Yokoyama J. Solid State Chem. 133 (1997) 104.

41 K. Kumashiro, K.Hirata, K. Sato, T. Yokoyama, T. Aisu, T.Ikeda, M. Minaguchi J. Solid State Chem. 154 (2000) 26.

42 E. Schroten, A. Goossens, J. Schoonman J. Appl. Phys. 79 (1996) 4465.

43 S. Varanas, M.B. Purvis, P.L. Higby, K.V. Goodwin, G.A. Young Us Patent 6,001,753.

44 A. Nocera, H.W. Levitin, J.M.N. Hilton Med. J. Australia, 173 (2000) 133.

45 O. Kumar, K. Sugendran, S.C. Pant, R. Singh, P.M.R. Reedy, R. Vijayaraghavan Biomed. Environ. Sci. 11, (1998), 179.

46 S. Shadnia, M. Rahimi, A. Pajoumand, M-H. Rasouli, M. Abdollahi Human and Exp. Toxi. 24(4) (2005) 215.

47 A.C. Vivian J. Inst. Met., 23 (1920) 325.

48 Ya.A. Ugai, L.I. Sokolov, E.G. Goncharov, A.N.Lukin, I.V. Vavresyuk Poluprovodn. Materially I ikh primenenie (1974) 104.

49 E.P. Domashevskaya, L.N. Terekhov, Ya.A. Ugai IZV Akad. Navk SSSR Serziz 38 (1974) 562.

50 G. Katz, J.A. Kohn, J.D. Broder Acta Crystallogr. 10 (1957) 607.

51 O. Olofsson Acta Chem. Scand. 21 (1967) 1659.

52 P.C. Donohue Inorg. Chem. 9 (1970) 335.

53 O. Olofsson Acta Chem. Scand. 24 (1970) 1153.

54 J. Gullman, O. Olofsson J. Solid State Chem. 5 (1972) 441.

55 Yu.B. Kuz'ma, S.I. Chikhrii, V.N. Davydov Inorg. Mater. 35 (1999) 10.

56 J. Gullman J. Solid State Chem. 87 (1990) 202.

57 Y. Xie, H. Su, B. Li, Y. Qian Mater Res. Bull. 35 (2000) 675.

58 A.M. Rao, E. Richter, S. Bandow, B. Chase, P.C. Eklund, K.A. Williams, S. Fang, K.R. Subbaswamy, M. Menon, A. Thess, R.E. Smalley, G Dresselhaus, M.S. Dresselhaus Science 275 (1997) 187.

59 R.L. Halm, K.M. Chadwick, B.R. Keyes U.S. Patent 4,946,980.

60 Z.M. Heimbrecht, M.B. Wilhelm Z. Anorg. Allgem. Chem. 242 (1939) 237.

61 T.B. Massalski Ed. Binary Alloys Phase Diagrams, 2nd Edition, ASM International, Materials Park, OH, 1990.

62 T. Wadsten Acta Chem. Scand. 21 (1967) 593.

63 T. Wadsten Acta Chem. Scand. 19 (1965) 1232.

64 O. Olofsson Acta Chem. Scand. 21 (1967) 1153.

65 P.C. Donohue, H.J.S. Young J. Solid State Chem. 1 (1970) 143.

66 J. Osagi, R. Namikawa, Y. Tanaka Rev. Phys. Chem. Japan 37 (1967) 81.

67 Y.A. Ugai, A.F. Demidenko, V.I. Koshchenko, V.E. Yachmenev, L.I. Sokolov, E.G. Goncharnov Inorg. Mat. (USSR) Eng. Trans. 15 (1979) 578.

68 D.J. Bottomley, M. Iwami, Y. Uehara, S. Ushioda J. Vac. Sci. Technol. A 17 (1999) 698.

69 O. Olofsson Acta Chem. Scand. 26 (1972) 2777.

70 H. Schlenger, H. Jacobs, R. Juza Z. Anorg. Allgem. Chem. 385 (1971) 177.

71 M.H. Moeller, W. Jeitschko Z. Anorg. Allgem. Chem. 491 (1982) 225.

72 R. Juza, K. Bar Z. Anorg. Chem. 283 (1956) 230.

73 J.A. Glass, J.T. Spencer Thin Solid Films 322 (1998) 138.

74 M.M. Oliveira, J.D. Bolton J. Mater. Procs. Tech. 92-93 (1999) 15.

75 J.R.A. Carlsson, J.E. Sundgren, L.D. Madsen, X.H. Li Thin Solid Films 300 (1997) 51.

76 Y. Huang, Y. Ding, Z. Li, C. Sun J. Phys. Chem. A. 104 (2000) 8765.

77 G.C. Allen, C.J. Carmalt, A.H. Cowley, A.L. Hector, S. Kamepalli, Y.G. Lawson, N.C. Norman, I.P. Parkin, L.K. Pickard Chem. Mater. 9(6) (1997) 1385.

78 J Kordis, K.A. Gingerich J. Chem. Phys. 58(11) (1973) 5141.

79 M.A. Besson, M. Troost C.R. Acad. Sci. 117 (1891) 78.

80 H. Moissan C.R. Acad. Sci. 113 (1891) 726.

81 K.Kumashiro, K. Hirata, K. Sato, T. Yokoyama, T. Aisu, T. Ikelda, M. Minaguchi, J. solid state chem. 154 (2000) 26.

82 E. Schroten, A Goossens, J. Schoonman, J. Appl. Phys. 79 (8) (1996) 4465.

83 T. Nishinaga, H Ogawa, H. Watanabe, T. Arizumi, J. Cryst. Growth 13/14 (1972) 346.

84 K. Shohno, H. Ohtake, J. Bloem, J. Cryst. Growth 45 (1978) 187.

85 Y. Kumasiro, T. Yokoyama, T. Sakamoto, T. Fujita J. Solid State Chem. 133 (1997) 269.

86 T.Takenaka, M. Takigawa, K. Shohno Japan J. Appl. Phys. 15 (1976) 2235.

87 M. Zhou, M. Nose, K. Nogi Surf. And Coat. Tech. 183(1) (2004) 45.

88 J. Smeets, V. Van Den Bergh, J Meneve, E. Dekempeneer, L. De Wilde Thin Solid Films 228(1-2) (1993) 272.

89 M. Durant, G. Merienne, D. Valette Eur. Pat. Appl. EP623,564.

90 E. R. T. Tiekink Appl. Oranomet. Chem. 5 (1991) 1.

91 P.R. Moses, L.M. Weir, J.C. Lennox, H.O. Finkelea, F.R. Lenhard, R.W. Murray Anal. Chem. 50 (1978) 576.

92 C.O. Wagner, D.A. Zatko, R.H. Raymond Anal. Chem. 52 (1980) 1445.

93 R. Riga, J.J. Verbist J. Chem. Soc. Perkin Trans. II (1983) 1545.

94 R.S. Wagner, W.C. Ellis J. Appl. Phys. 44 (1964) 502.

95 D. Briggs, M.P. Seah Eds. Practical Surface Analysis, 2nd Edition, Volume 1 – Auger and X-ray Photoelectron Spectroscopy, Wiley, (1990).

96 J.T. Scheper, K.C. Jayaratne, L.M. Liable-Sands, G.P.A Yap, A.L. Rheingold, C.H. Winter Inorg. Chem. 38 (1999) 4354.

97 T.S. Lewkebandara, J.W. Prosica, C.H. Winter Chem. Mater. 7 (1995) 1053.

98 C.S. Blackman, C.J. Carmalt, S.A. O'Neill, I.P. Parkin, L. Apostilco, K.C. Molloy J. Mater. Chem. 11 (2000) 2408.

99 The United Kingdom Chemical Database Service, D.A. Fletcher, R.F. McMeeking, D.J. Parkin J. Chem. Inf. Comuput. Sci. 36, (1996), 746.

100 Z. Z. Hajanal, J. Miro, G. Kiss, F. Reti, P. Deak, R.C. Herndon, J.M. Kuperberg J. Appl. Phys. 86 (1999) 3792.

101 H.G. Kim, W.T. Kim J. Appl. Phys. 62 (1987) 2000.

102 J. Passlack, Appl. Phys. 77 (1995) 686.

103 T. Miyata, T. Nakatkani, T. Minami Thin Solid Films 373 (2000) 145.

104 J. Hao, M. Cocivera J. Phys. D: Appl. Phys. 35 (2002) 433.

105 L. Binet, D. Gourier J. Phys. Chem. Solids 59 (1998) 1241.

106 M. Orita, H. Hiramatsu, H. Ohta, M. Hirano, H. Hosono Thin Solid Films 411 (2002) 134.

107 G.S. Park, W.B. Choi, J.M. Kim, Y.C. Choi, Y.H. Lee, C.B. Lim J. Cryst. Growth 220 (2000) 494.

108 Z.R. Dai, W. Pan, Z.L. Wang J. Phys. Chem. B 106 (2002) 902.

109 S. Sharma, M.K. Sunkara JACS 2002, 124, 12288.

110 A.L. Petre, J.A. Perdigón-Melón, A. Grvasini, A. Auroux Topics in Catalysis 19 (2002) 271.

111 A.L Petre, A. Auroux, P. Gélin, M. Caldararu, N.I. Ionescu Thermochimica Acta 379 (2001) 177.

112 C.O. Areán, A.L. Bellan, M.P. Menruit, M.R. Delagdo, G.T. Palomino Microporus and Mesoporus Materials 40 (2000) 35.

113 M. Ogita, K. Higo, Y. Nakanishi, Y. Hatanaka Appl. Surface Sci. 175-176 (2001) 721.

114 T. Schwebel, M. Fleischer, H. Meixner, C.D. Kohl Sens. And Actuators B 49 (1998) 46.

115 M. Fleischer, H. Meixner Sens. And Actuators B 26-27 (1995) 81.

116 N.C. Oldham, C.M. Garland, T.C. McGill J. Vac. Sci. Technol. A 20 (2002) 809.

117 A. Oritz, J.C. Alonso, E. Andrade, C. Urbiola J. Electro. Soc. 148 (2001) F26.

118 L. Mîinea, S. Suh, S.G. Bott, J.R. Liu, W.K. Chu, D.M. Hoffman J. Mater. Chem. 9 (1999) 929.

119 M. Valet, D.M. Hoffman Chem. Mater. 13 (2001) 2135.

120 G.A. Battiston, R. Gerbasi, M. Porchia, R. Bertoncello, F. Caccavale Thin Solid Films 279 (1996) 115.

121 C.A. Papadopoulos, J.N. Avaritsiotis Sens. And Actutors B 28 (1995) 201.

122 S.S. Park, J.D. Mackenzie Thin Solid Films 274 (1996) 154.

123 W. Göpel, K.D. Schierbaum Sens. And Actuators B 26-27 (1995) 1.

124 V.Lantto, P. Romppainen, S. Leppavuori Sens. And Actuators B 14 (1988) 149.

125 M. Ono Kokai Tokkyo Koho JP2005149742.

126 S. De Monredon, A. Cellot, F. Ribot, C. Sanchez, L. Armelao, L. Gueneau, L. Delattre J. Mater. Chem. 12(8) (2002) 2396.

127 D.W. Lane, J.A. Coath, H.S. Beldon Thin Solid Films 221 (1992) 262.

128 J.C. Manifacier, L. Szepessy, R. Stuck Mater. Res. Bull. 14 (1979) 163.

129 S.W. Lee, C. Yoon Bull. Korean Chem. Soc. 20(9) (1999) 1031.

130 J.R. Brown, M.T. Cheney, P.W. Haycock, D.J. Houlton, A.C. Jones, E.W. Williams J. Electrochem. Soc. 144(1) (1997) 295.

131 D. Davazoglou Thin Solid Films 302(1-2) (1997) 204.

132 R. Gordon J. Non Cryst. Solids 218 (1997) 81.

133 G. Centi, S. Perathoner S. Appl. Catal. 124A (1995) 317.

134 D.Z. Dzmitrowice, J.B. Goodenough, P.J. Wiseman Mater. Res. Bull. 17 (1982) 971.

135 S. Tanabe Ceramic Transitions 163 (2005) 1.

136 K. Kleveland, M.A. Einarsrud, T. Grande J. Am. Ceram. Soc. 83 (2000) 315.

137 Zhang, L. Feng, F. Qiu, B. lin Huaxue Jinzhan 16(4) (2004) 508.

138 Y. Zhang, G. Li, J. Zhang, L. Zhang Nanotechnology 15(7) (2004) 762.

139 Y. F. Liu Dianci Bileiqi 192 (2003) 36.

140 C.C. Wang, S.A. Akbar, M.J. Madou J. Electroceramics 2(4) (1998) 273.

141 P.W. Haycock, G.A. Horley, K.C. Molloy, C.P. Myers, S.A. Rushworth, L.M. Smith CVD 7(5) (2001) 191.

142 N. Tigau, V. Ciupina, G. Prodan J. Cryst. Growth 277 (2005) 529.

143 N. Tigau, V. Ciupina, G. Prodan, G.L. Rusu, E. Vasile J. Cryst. Growth 269 (2004) 392.

144 M. Fang, Q. Li, F. Gan, Cailiao Yanjiu Xuebao 18(1) (2004) 1.

145 W.A. Badawy, E.A. El-Taher Thin Solid Films 158 (1988) 277.

146 W.A. Badawy Thin Solid Films 186 (1990) 59.

147 S. K. Deb Sol. Energy Mater. 25 (1992) 327.

148 M.A. Aegerter Sol. Energy Met. Sol. Cells 68 (2001) 401.

149 N. Kumagai, T. Tanno, T. Nakajima, N. Watanabe Electrochim. Acta 28 (1983) 17.

150 N. Kumagai, S. Komba Proc. MRS (2000) 39.

151 M. Schmitt, M.A. Aegerter Electrochim. Acta 46 (2001) 2105.

152 K. Sayama, H. Sugihara, H. Arakawa Chem. Mater. 10 (1998) 3825.

153 P. Guo, M.A. Aegerter Thin Solid Films 351 (1999) 290.

154 M. Paulis, M. Martin, D.B. Soria, A. Diaz, J.A. Ordiozola, M. Montes Appl. Catal. A 180 (1999) 411.

155 G.J. Hutchings, S.H. Taylor Catal. Today 49 (1999) 105.

156 C.O. Park, S.A. Akbar Mater. Chem. Phys. 75 (2002) 56.

157 M.E. Gimon-Kinsel, K.J. Balkus Jr. Microporous Mesoporous Mater. 28 (1999) 113.

158 K. Yoshimura, T. Miki, S. Iwama, S. Tanemura Thin Solid Films 281 (1996) 235.

159 R. Cabanel, J. Chaussy, J. Mazuer, G. Delabouglise, J.C. Joubert J. Electrochem. Soc. 137 (1990) 1444.

160 M. Ozer, M.D. Rubin, C.M. Rubin Sol. Energy Mater. Sol. Cells 40 (1996) 285.

161 M.A.B. Jones, L.O.S. Bulhoes, S.C. Castro, A.J. Damiao J. Electrochem. Soc. 137 (1990) 3067.

162 A. Nagahori, R. Raj J. Am, Ceram. Soc. 78 (1995) 1585.

163 X. Li, M.L. Hitchman, S.H. Shamlian Electrohem. Soc. Proc. 97 (1997) 1246.

164 K. Kukli, M. Ritala, M. Leskela, R. Lappalainen CVD 4 (1998) 29.

165 S. Lim, J.C. Lee, D.S. Sohn, W.I. Lee, I.M. Lee Chem. Mater. 14 (2002) 1548.

166 C. Alquier, M.T. Vandenborre, M. Henry J. Non-Cryst. Solids 1 (1986) 28.

167 C.O. Avellaneda, A. Pawlicka, A. Aegerter J. Mater. Sci. 33 (1998) 2181.

168 M. Macek, B. Orel Sol. Energy Mater. Sol. Cells 54 (1998) 121.

169 J.T. Scheper, K.C. Jayaratne, L.M. Liable-Sands, G.P.A. Yap, A.L. Rheingold, C.H. Winter Inorg. Chem. 38 (1999) 4354.

170 C.S. Blackman, C.J. Carmalt, S.A. O'Neill, I.P. Parkin, L. Apostilco, K.C. Molloy J. Mater. Chem. 11 (2001) 2408.

171 S.A. O'Neill, I.P. Parkin, R.J.H. Clark, A. Mills, N. Elliot J. Mater. Chem. 13(12) (2003) 2952.

172 F. Maury CVD 2 (1996) 113.

173 K.D. Sanderson, A. Simpson, S. Hurst, T. McKittrick, D. Rimmer, L. Ye, D. Strickler, M. Soubeyrand Glass Processing Days (2001) Session 32 762.

174 D.W. Sheel, M.E. Pemble CVD Coatings on Glass ICCG4 (2002).

175 P.W. Haycock, G.A. Horley, K. Molloy, C.P. Myers, S.A. Rushworth, L.M. Smith Journal de Physique IV Proc. (2001) 11.

176 J.S. Bae, D.H. Yun, C.O. Park, J.S. Hwang Sens. And Actuators B 75(3) (2001) 160.

177 K. Wada, M. Egashira Chem. Sens. 15B (1999) 109.

178 D. Kohl Sens. And Actuators B 1 (1990) 158.

179 J.F. McAleer, P.T. Moseley, J.O.W. Norris, D.E. Williams J. Chem. Soc. Faraday Trans. 1 83 (1987) 1323.

180 S. Gupta, R.K. Roy, M.P. Chowdhury, A.K. Pal Vacuum 75 (2004) 111.

181 W.B. Cross, I.P. Parkin, S.A. O'Neill, P.A. Williams, M.F. Mahon, K.C. Molloy Chem Mater. 15 (2003) 2786.

182 M. Cremona, M.H.P. Mauricio, L.V. Fehlberg, R.A. Nunes, L.C. Scavarda do Carmo, R.R. de Avillez, A.O. Caride Thin Solid Films, 333 (1998) 157.

183 A. Buzulutskov, A. Breskin, R. Chechik J. Appl. Phys. 81 (1997) 466.

184 G. Baldacchini, M. Cremona, S. Martelli, R.M. Montereali, L.C. Scavarda de Carmo Phys. Stat. Sol. (a) 151 (1995) 319.

185 M. Cremona, A.P. Sotero, R.A. Nunes Radiat. Eff. Def. Solids, 136 (1995) 163.

186 J.A. Samuels, W. Chiang, C. Yu, E. Apen, D.C. Smith, D.V. Baxter, K.G. Caulton Chem. Mater. 6 (1994) 1684.

187 A.P. Purdy, A.D. Berry, R.T. Holm, M. Fatemi, D.K. Gaskill Inorg.Chem. 28 (1989) 2799.

188 J. Zhao, K. Dahmen, H.O. Marcy, L.M. Tonge, T.J. Marks, B.M. Wessels, C.R. Kannewurf Appl. Phys. Lett. 53 (1989) 1750.

189 D.L. Larkin, L.V. Interrante, A.J. Bose J. Mater. Res. 5 (1990) 2706.

190 L.J. Lingg, A.D. Berry, A.P. Purdy, K.J. Ewing Thin Solid Films, 209 (1992) 9.